# INVESTIGATION INTO YIELD PILLAR BEHAVIOR AND DESIGN CONSIDERATIONS

by

Gang Chen

Dissertation submitted to the Faculty of the
Virginia Polytechnic Institute and State University
in partial fulfillment of the requirements for the degree of
Doctor of Philosophy
in
Mining and Minerals Engineering

APPROVED:

M. Karmis, Chairman & Department Head

G. J. Faulkner

C. Haycocks

M. Karfakis

J. R. Lucas

Feburary, 1989

Blacksburg, Virginia

# INVESTIGATION INTO YIELD PILLAR BEHAVIOR AND DESIGN CONSIDERATIONS

by

Gang Chen

M. Karmis, Chairman & Department Head

Mining and Minerals Engineering

(ABSTRACT)

Adopting yield pillars has been considered an effective way of alleviating ground control problems and increasing production. The purpose of this research was to study the behavior of yield pillars and to develop the design criteria.

After a literature review, two 2-D finite element models were developed, each following a different non-linear approach. The first model adopted the successive iteration technique incorporated with the Mohr-Coulomb yield criterion. The second followed the elastic-plastic approach, implementing a generalized Von Mises yield criterion. Extensive underground monitoring was conducted and the finite element models were compared with the field data, both yielding promising results.

Three different longwall entry layouts were investigated. The yield-stable-yield pillar system was considered to be the best design. A parametric analysis was also performed. The triaxial factor and Poisson's ratio were found to be the most important material properties affecting pillar yielding.

The progressive failure hypothesis for pillar design was critically examined. The analysis suggested that the formulation defining the stress distribution in the yield zone under

this hypothesis may be satisfied only in extreme cases and, therefore, the actual distribution can be different. An improved equation, describing the stress distribution in the yield zone, was derived by statistically analyzing the results of finite element simulations. The latter equation fitted the observed field data better than did the original equation, and it was further developed for estimation of yield zone width.

Consideration was also given to yield pillar design. Three possible yield pillar sizes were proposed in this paper. The maximum yield pillar size was considered to be twice the width of the yield zone. Based on the pressure arch concept, the minimum yield pillar size was determined by accepting that yield pillars were only supporting the rock strata under this pressure arch. A suggested yield pillar size was obtained by selecting a size which would force the peak stress at the center of the yield pillar to equal the average tributary stress. The case studies conducted in this research indicated that the predicted yield pillar sizes were reasonably accurate.

# Acknowledgements

Grateful acknowledgement is due to Dr. Michael Karmis, dissertation advisor, for his guidance, encouragement and support throughout the investigation; and to Dr. Gavin J. Faulkner, Dr. Christopher Haycocks, Dr. Mario Karfakis, and Dr. Richard J. Lucas, dissertation committee members, for their review and criticism of this dissertation.

Sincere appreciation is expressed to Dr. Andrzej Jarosz, whose constructive suggestions and generous help during the course of this research were extremely valuable. Appreciation is also extended to for her help in editing this dissertation.

Sincere thanks go to the author's mother for her love and endless encouragement throughout the study. And finally, thanks are gratefully expressed to the author's wife. Without her support, patience and love, the completion of this dissertation would not have been possible.

# Table of Contents

# List of Illustrations

# List of Tables

# CHAPTER 1: INTRODUCTION

Pillar stability is a major concern in underground coal mines. Since such pillars will provide protection around the underground production area for mining personnel and equipment to work safely and efficiently, the determination of proper pillar sizes appears to be one of the main tasks in mine system planning. Conventionally, the pillars have been considered to support the weight of all overlying rock strata and the load has often been assumed to be evenly distributed on the pillars. As coal mining becomes more complex, a number of ground control problems are encountered, such as coal bumps, floor heaves, multiple seam interactions, surface subsidences and so on. The traditional pillar design concept has, therefore, been challenged. Coal mining is being conducted today at depths well below 2,000 feet. At such great depth, large pillar sizes must be adopted if pillars are considered to support all the overburden strata, therefore, a low production efficiency and low recovery rate will result. In addition, a pillar design based on this concept will frequently cause high stress concentration in the pillars and, in turn, induce coal bumps and various ground control problems at great mining depths. Practice and theoretical analysis have proven that coal pillars do not necessarily have to support all the overlying strata up to the surface, nor must they be rigid. In many cases, properly

designed yield pillars will produce a higher degree of ground stability in underground coal mines. The concept of the yield pillar has, therefore, been introduced into pillar design and mine layout planning.

A yield pillar is defined as one which yields upon isolation. The concept of yield pillars in longwall and room-and-pillar mines has been discussed for a number of years. In general, it is suggested that yield pillars can:

- Increase production
- Improve ground control conditions
- Minimize the potential of bumps
- Reduce subsidence effects on the surface

Despite these advantages, few applications can be found over the years utilizing this concept, due to the difficulties in the trial-and-error procedures required to develop appropriate yield pillar design criteria. In other words, the behavior of yield pillars are still not well understood.

The objectives of this research were, therefore, as follows:

- To achieve better understanding of yield pillar behavior
- To identify and evaluate the most influential parameters affecting pillar yielding
- To develop general design criteria on the basis of a better comprehension of pillar yielding mechanism.

A comprehensive literature review was carried out in this research. The review covered different aspects of coal pillar design theories. Following the literature review, computer

modeling of yield pillars was conducted. Two different non-linear finite element models were developed in this study. The first was a model utilizing the successive iteration technique incorporated with the Mohr-Column failure criterion. The second was an elastic-plastic model, in which a generalized Von Mises failure criterion and the Prandtl-Reuss flow rule were applied. Computer programs were specifically coded for both models. In order to validate the models established, extensive underground monitoring was conducted. The monitoring program included the monitoring of pillar stress, roof-floor convergence, pillar horizontal dilation and roof sag. Following the model validation, several different longwall entry layouts were investigated with the elastic-plastic finite element model, and a comprehensive parametric study was also performed. Based on the modeling results, the progressive failure theory for pillar design was critically examined. An improved equation describing the stress distribution in the yield zone was derived by statistically analyzing the results of a series of non-linear finite element simulations. Finally, consideration was given to yield pillar design. The pressure arch theory was utilized and a design procedure was introduced.

# CHAPTER 2: LITERATURE REVIEW

## 2.1 Introduction

Yield pillar design, similar to conventional pillar design, involves the calculation of pillar load, the determination of in-situ pillar strength, and considerations of factors such as the confinement of roof and floor on pillars, the bearing capacities of roof and floor, and the probabilities of pillar instability. These fundamental principles have been studied for decades for pillar design. A review of the basic pillar design principles would provide a solid basis for further studies on pillar yielding mechanism and yield pillar behavior. In this chapter, a comprehensive literature review is presented on the theories concerning pillar design as well as the state-of-the-art on yield pillars. In addition, some successful yield pillar applications are also discussed.

## 2.2 Pillar Design Concepts

### *2.2.1 Pillar Load*

A common practice for estimating pillar load is by applying the tributary area loading method. In this method, the area supported by a pillar is assumed to cover the area above it and the neighboring area tributary to it (Obert and Duvall, 1967). In other words, a pillar supports uniformly the weight of the rock overlying the pillar as well as one-half the width of rooms or entries surrounding the pillar. Thus, for a typical rectangular pillar, the average stress can be expressed as:

$$\sigma_a = \frac{(L_p + W_o)(W_p + W_o)\gamma h}{W_p L_p} \tag{2.1}$$

where:

$\sigma_a$ = average pillar stress;

$L_p$ = pillar length;

$W_p$ = pillar width;

$W_o$ = opening width;

$\gamma$ = average overburden density; and

h = mining depth.

This method is extensively used because of its simplicity. However, the tributary area loading method ignores the relative extent of the mined area, the horizontal stress component, the relative deformation properties of pillar, roof and floor rocks, and the positions of the pillars in the mining zone. Taking some of these factors into account, Coates (1981) developed a formulation for pillar load estimation, principally applicable to long pillars in deep mines, which is:

$$\frac{\Delta\sigma_p}{\sigma_z} = \frac{2R(1+M) - KM(1-W+W_p n)}{Mn + 2(1-R)(1+M) + \frac{2RB}{\pi}(1-W)} \tag{2.2}$$

where:

$\Delta\sigma_p$ = the stress increase in the pillar above the virgin stress;

$\sigma_z$ = vertical virgin stress;

R = extraction ratio;

K = horizontal to vertical stress ratio;

M = ratio of mining height to the extent of the mined area;

$W = \mu/(1-\mu)$;

$\mu$ = Poisson's ratio for the roof and floor rock;

$W_p = \mu_p/(1-\mu_p)$;

$\mu_p$ = Poisson's ratio for pillar;

$n = [E/(1-\mu^2)]/[E_p(1-\mu_p^2)]$;

E = elastic modulus for country rock;

$E_p$ = elastic modulus for pillar; and

B = ratio of pillar width to the extent of the mined area.

This equation may lead to a more accurate prediction of pillar load than the tributary area loading method. However, since it is complicated and requires more input parameters, this equation has not been widely tested and used.

### *2.2.2 Pressure Arch*

As soon as an opening is made, the vertical load directly above the opening shifts towards the ribs of the excavation, leaving a destressed or relaxed zone in the roof strata. The shape of the destressed zone is considered to resemble an arch and thus it is called

a pressure arch. Different theories exist concerning the size and shape of the pressure arch.

Holland (1963) recommended that the minimum width of the maximum pressure arch was influenced mainly by the depth. The minimum width may be computed by the following equation:

$$W = 3(\frac{h}{20} + 20) \tag{2.3}$$

where:

W = minimum width of the maximum pressure arch (ft.); and

h = mining depth (ft.).

Observations have also indicated that the height of the maximum pressure arch extends a distance about equal to twice its width above and below the seam in which the excavation is located (Figure 2.1).

Denkhaus (1964) suggested that the shape and size of the pressure arch be considered under two different conditions, namely, sufficiently cohesive rock and insufficiently cohesive rock. If the rock is sufficiently cohesive, the relationship between span and height of the arch is given by:

$$W = \sqrt{\frac{8\sigma_c d}{\gamma}\,(1 - d/h)} \tag{2.4a}$$

where:

W = span of the pressure arch;

$\sigma_c$ = uniaxial compressive strength of the rock;

$\gamma$ = specific weight of the rock;

d = height of the arch; and

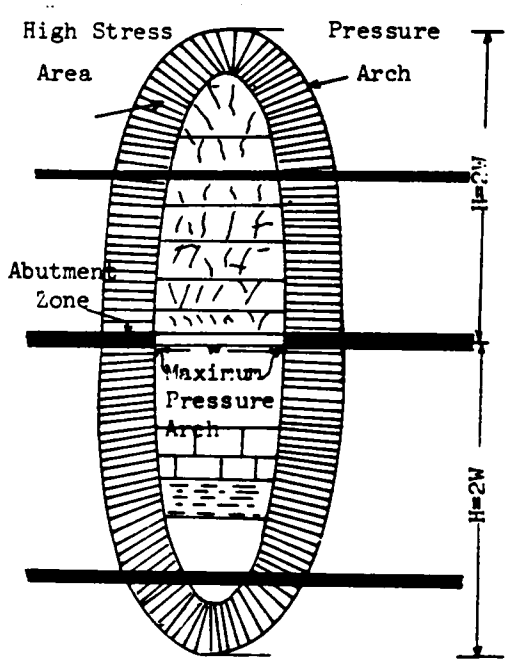


**Figure 2.1 Pressure Arch (After SME, 1973)**

h = mining depth.

The largest possible height at which the arch remains stable and the corresponding span are given by:

$$d_{max} = 0.5h \tag{2.4b}$$

$$W_{max} = \sqrt{\frac{2\sigma_c h}{\gamma}} \tag{2.4c}$$

If the rock is insufficiently cohesive, the corresponding formulae read:

$$W = \sqrt{\frac{8\sigma_c h}{\gamma}(1 - d/h)\ \log(1 - d/h)} \tag{2.5a}$$

$$d_{max} = 0.63h \tag{2.5b}$$

$$W_{max} = \sqrt{\frac{2.96\sigma_c h}{\gamma}} \tag{2.5c}$$

Another concept in pressure arch theory is the load transfer distance. Due to underground excavations, the virgin stress is redistributed. The maximum range in which the virgin stress is affected is called the load transfer distance. Observations have revealed that the load transfer distance increases with depth such that (Abel, 1982):

$$LTD = -31.44 + 0.349h - 0.0000723h^2 \tag{2.6}$$

where:

LTD = load transfer distance (ft.); and

h = depth (ft.).

If the pressure arch is assumed to have a parabolic shape, the height may be computed as (Figure 2.2):

$$d = l_2 h(2l - l_2)/l \tag{2.7}$$

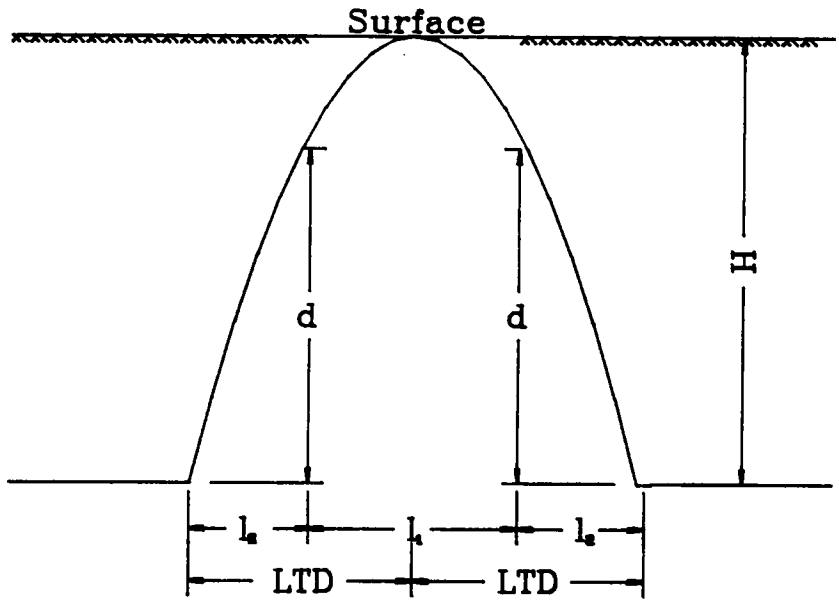


**Figure 2.2 Pressure Arch Height Calculation (After Abel, 1981)**

where:

d = arch height at $l_2$ distance away from the barrier pillar rib;

$l_2$ = distance to the barrier pillar rib;

l = width of the arch, $l = 2 \times LTD$; and

h = mining depth.

The pressure arch concept is particularly useful in yield pillar design. When the pillar yields, a destressed zone similar to that formed over an opening will occur above the yield zone. The load on yield pillars may be estimated, therefore, by using the pressure arch theory.

### *2.2.3 Size and Shape Effects on Coal Strength*

Coal strength can be determined by laboratory and in-situ tests. Coal strength obtained from laboratory tests is usually greater due to the smaller size of the specimens. This is generally attributed to the fact that the larger the specimen size, the more cracks and fractures it contains, reducing its bearing strength. In-situ strength tests of underground pillars, however, can eliminate or reduce the size problems and produce more representative results. On the other hand, they can be expensive and time-consuming. It is common, therefore, to predict the in-situ pillar strength from small-scale laboratory test results. Evans et al. (1960) generalized the relationship between the size and the strength of the specimen by the equation:

$$\sigma_1 = k_1 d^{-a} \tag{2.8}$$

where:

$\sigma_1$ = uniaxial compressive strength of the cubical pillars;

a = constant ranging from 0.38 to 0.66;

$k_1 = \sigma_c\sqrt{D}$ ;

$\sigma_c$ = uniaxial compressive strength of specimen; and

D = diameter or cube size dimension of specimen.

Tests performed by Greenwald (1941) and Bieniawski (1968) found that coal strength decreased with increasing specimen size, reaching a constant value at a certain specimen size. These results are illustrated in Figure 2.3.

The in-situ coal strength may also be extrapolated from the laboratory strength by the following equation (Hustrulid, 1976):

$$\sigma_1 = \frac{k_1}{\sqrt{H}} \tag{2.9}$$

where:

H = mining height, using 36 when H > 36 in.

Wilson (1981) suggested that a strength-reduction factor, f, be applied on the laboratory value to obtain in-situ rock strength, that is:

f = 1 for strong, massive unjointed rock

f = 1/2 for widely spaced joints or bedding planes

f = 1/3 for more jointed but still massive rock

f = 1/4 for well-jointed and weaker rocks

f = 1/5 for coal and unstable seatearths

f = 1/6 and 1/7 for fault zone

In addition to the size effect, coal strength is also found to depend on specimen geometry or the shape effect, that is, the ratio of the diameter or the width to the height of the specimens. Most empirical pillar design formulas take the shape effect into consideration.

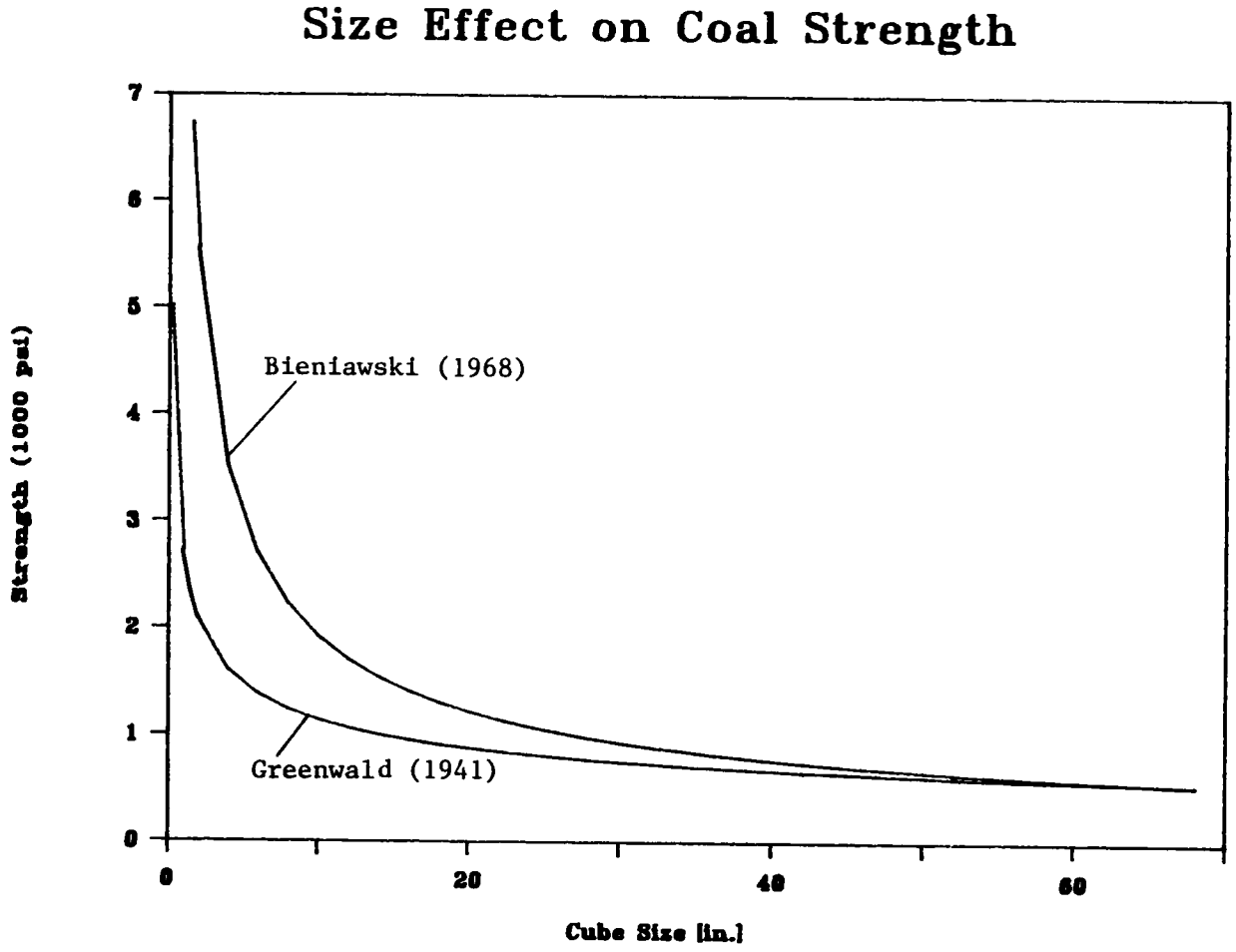


**Figure 2.3 Size Effect on Coal Strength (After Peng, 1978)**

### *2.2.4 Interaction of Pillar, Floor and Roof*

The properties of the contact planes at the ends of a pillar affect the stress distribution within the pillar. This is especially true in coal pillars, where contacts are made with completely different materials. Due to frictional restraint, lateral expansion in the vicinity of the contact planes can be either smaller or greater than in the rest of the area, causing non-uniform stress distribution within the pillar. Experiments performed by Peng (1978) showed that different deformation may occur for rock specimens in contact with various materials, as shown in Figure 2.4. With perfect confinement, no lateral expansion is allowed at the ends. Direct contact represents most laboratory testing conditions. Uniform deformation occurs when loading platens expand as much as the specimen, and with teflon or neoprene inserts the specimens expand much more at the ends than in the middle. Deformation with shale or sandstone roof or floor is generally between perfect confinement and uniform loading, whereas with soft clay roof and floor it may resemble those between uniform loading and the type identified with teflon or neoprene inserts.

The coal pillar and the immediate floor and roof rock strata are components of a complete structure. Failure of any component may cause the whole structure to collapse. Hence the bearing capacity of floor and roof also plays an important role in pillar stability. The ultimate bearing capacity for a rectangular footing or a pillar can be calculated by the following equation (SME, 1973):

$$q_u = cN_c(1 + 0.3W_p/L) + \gamma hN_g + (1 - 0.2W_p/L)\,\gamma\frac{W_p}{2}N_\gamma \qquad (2.10)$$

where:

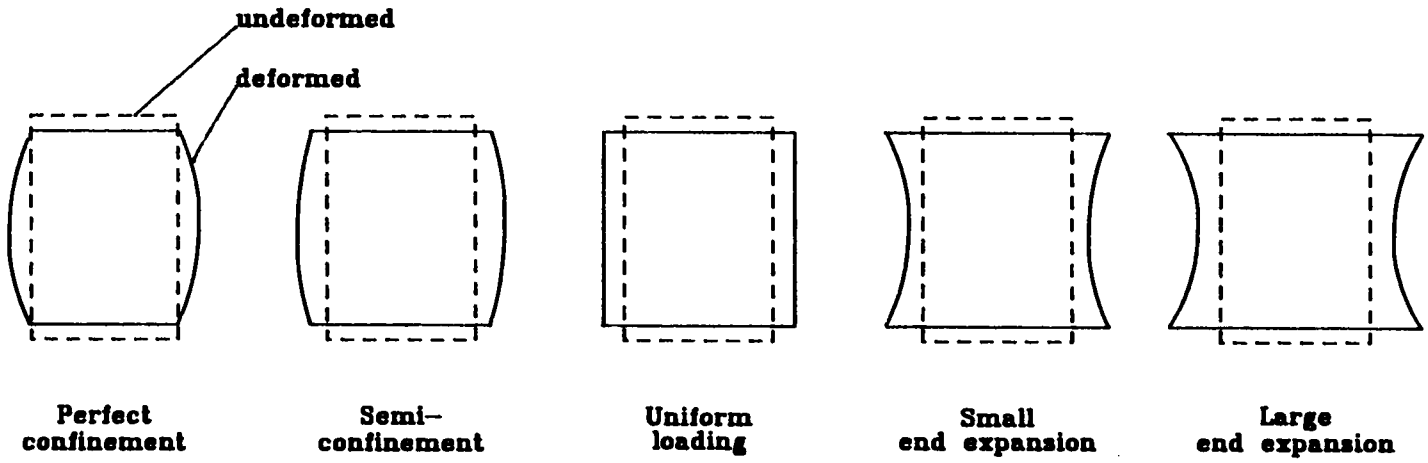


Figure 2.4 Different Confinements on Coal (After Peng, 1978)

$q_u$ = ultimate bearing capacity;

c = cohesion;

$W_p$ = pillar width;

L = pillar length;

h = depth of surcharge;

$\gamma$ = rock density;

$N_c = (N_q - 1) \cot \phi$ ;

$N_\gamma = 1.5(N_q + 1) \tan \phi$ ;

$N_q = e^{\pi \tan \phi} \tan^2(\frac{\pi}{4} + \frac{\phi}{2})$ ; and

$\phi$ = internal frictional angle.

For mine design the following expression was also derived for a cohesive, frictional material such as soft rock (Bieniawski, 1987):

$$q_u = \frac{1}{2} \gamma W_p N_\gamma S_\gamma + c \cot \phi \, N_q S_q - c \cot \phi \qquad (2.11)$$

where:

$S_\gamma = 1.0 - 0.4 (W_p/L)$ ; and

$S_q = 1.0 + \sin \phi \, (W_p/L)$ .

Bieniawski (1987) suggested that the factor of safety against bearing capacity failure should be greater than 2.0 in view of the uncertainty of assuming that the average pillar stress is applied as a uniformly distributed load.

### *2.2.5 Probability of Pillar Instability*

Because of the complex underground conditions and the difficulties in testing rock mass properties, a great amount of uncertainty is involved in pillar design. It is also uneco-

nomic and unnecessary to use large safety factors to guarantee pillar stability. A probability analysis is, therefore, useful.

Coates (1981) studied the dispersions of pillar load and pillar strength. Assuming normal distributions of load and strength as shown in Figure 2.5, Coates suggested that the probability of pillar failure be estimated in the following way.

If both functions in Figure 2.5 are standard normal distributions, their difference is also a standard normal curve, i.e. $Q_p - \sigma_p$ in Figure 2.5, where $Q_p$ is the distribution of pillar strength and $\sigma_p$ is the distribution of pillar load. The area under the difference curve represents either the frequency or probability of failure. The following equations describe characteristics of this curve:

$$m = Q_{pm} - \sigma_{pm} \tag{2.12}$$

where:

m = mean of the difference curve;

$Q_{pm}$ = mean of pillar strength; and

$\sigma_{pm}$ = mean of pillar load.

and,

$$S = (S_q^2 + S_s^2)^{1/2} \tag{2.13}$$

where:

S = standard deviation of the difference curve;

$S_q$ = standard deviation of the $Q_p$ curve; and

$S_s$ = standard deviation of the $\sigma_p$ curve.

Finally, the variable Z obtained from the following equation can be used to obtain the probability of instability from any standard normal distribution table:

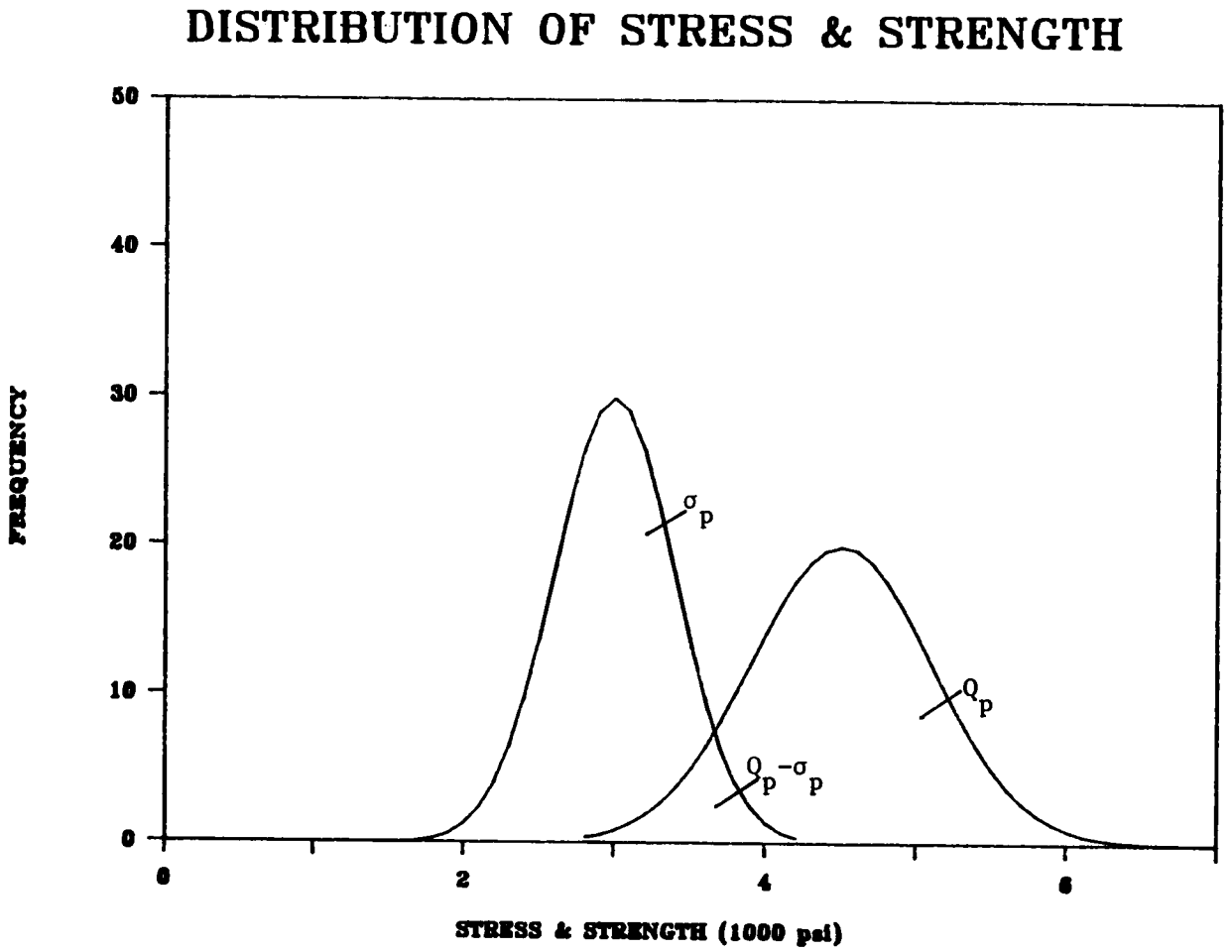


**Figure 2.5 Distributions of Pillar Load and Strength (After Coates, 1981)**

$$Z = m/S \tag{2.14}$$

Variables used in the above analysis can be obtained from laboratory tests and previous experience. However, the pillar load distribution is difficult to determine and a large number of tests must be carried out in order to achieve a reasonable estimation of the probability. These factors limit the use of the probability of pillar instability.

## 2.3 Pillar Design Formulas

### *2.3.1 Empirical Formulas*

Many mine pillar design equations have been proposed in the literature. Most of them have two basic components in common. These are a size effect and a shape effect component. These components are utilized to interpolate from the strength of laboratory or large-scale in-situ rock test samples to mine pillars which have various heights, widths, and lengths.

A widely used rule of thumb for pillar design in England is that the width of a coal pillar is one tenth of the depth plus fifteen yards. This has, however, proven to be suitable only for depths of less than 2,000 feet. At greater depths, this rule of thumb overestimates the pillar size (Wilson, 1980).

Obert and Duvall (1967) recommended that the following equation be utilized for the design of mine pillars:

$$\sigma_p = \sigma_1[0.778 + 0.222\frac{W}{H}] \quad (2.15)$$

where:

$\sigma_p$ = pillar strength;

$\sigma_1$ = uniaxial compressive strength of a cubical pillar (Equation 2.9);

W = pillar width; and

H = pillar height.

A factor of safety of 2 to 4 was recommended by the Bureau of Mines for this equation.

Holland (1964) developed a pillar design formula based on the results of tests on thin prisms of coal. The equation is suitable for coal pillars having width-to-height ratios from unity to 10, which is expressed as:

$$\sigma_p = \frac{k_1\sqrt{W}}{H} \quad (2.16)$$

where:

$k_1$ = a constant defined in Equation 2.8.

This formula calls for a factor of safety between 1.8 to 2.2.

Bieniawski (1981) reported the results of a Pennsylvania State University survey of room and pillar dimensions and design practice in U. S. coal mines. Based on this survey, he recommended a design formula as follows:

$$\sigma_p = \sigma_1[0.64 + 0.36\frac{W}{H}]^{\alpha} \quad (2.17)$$

where:

$\alpha$ = 1.4 for $\frac{W}{H} > 5$;

$\alpha$ = 1.0 for $\frac{W}{H} < 5$; and

$\sigma_1$ = compressive strength of a 60-inch cube or larger.

This equation results in a significant step increase of strength at a width to height ratio of 5. As a consequence of this step, uncertainty exists regarding which curve to use as the width-to-height ratio of 5 is approached.

Salamon and Munro (1987) compiled a list of 98 stable and 27 collapsed coal mine pillar histories. These data were statistically analyzed and mine pillar design equations developed, which is:

$$\sigma_p = \sigma_1 \left( \frac{W^{0.46}}{H^{0.66}} \right) \tag{2.18}$$

where:

$\sigma_1$ = uniaxial compressive strength of one-foot cube of coal.

Where strength data is not available for one-foot cubical samples of coal, the following modification of the formula has been recommended:

$$\sigma_p = \sigma_s \left[ \frac{(W/W_s)^{0.46}}{(H/H_s)^{0.66}} \right] \tag{2.19}$$

where:

$W_s$ = sample width;

$H_s$ = sample height; and

$\sigma_s$ = uniaxial compressive strength of the sample.

For design purposes, a factor of safety of 1.6 has been recommended by Salamon when using this equation.

### *2.3.2 Progressive Failure Theory*

Empirical pillar design equations deal with the ultimate strength of coal pillars. Average pillar stress and average strength are considered in those equations. Practice and theoretical analysis have, however, determined that the stress in a pillar is distributed far from uniformly. Wilson (1972) put forward an hypothesis on pillar strength. He suggested that there should be basically two zones in a pillar: a yield zone at the rib sides and an elastic core in the center which is confined by the yield zone. Figure 2.6 shows the hypothetical stress distribution across a pillar. Vertical stress is very low at the ribs and increases rapidly to a maximum yield stress at certain distance from the ribs. Beyond this point in the center of the pillar is a relatively undisturbed intact zone called the pillar core. By contrast, the pillar edges covering the yield zone more or less fail and undergo a certain amount of flow. However, the strength of the pillar core increases because of confining constraints rendered by the yield zone.

Wilson (1977, 1981) later concluded that for wide excavations the stress conditions in the yield zone might be under two different conditions. When the coal seam is sandwiched between a relatively strong roof and floor, the stress distribution from the ribside into the yield zone can be approximated by:

$$\sigma_v = p\,q\,\exp\{\frac{X}{H}[\frac{q-1}{\sqrt{q}} + \frac{(q-1)^2}{q}\,\tan^{-1}\sqrt{q}\,]\} \tag{2.20}$$

$$\sigma_h = \frac{1}{q}\,\sigma_v \tag{2.21}$$

where:

$\sigma_v$ = vertical stress;

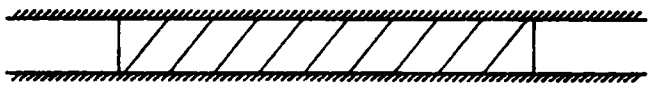

a. Pillar cross section

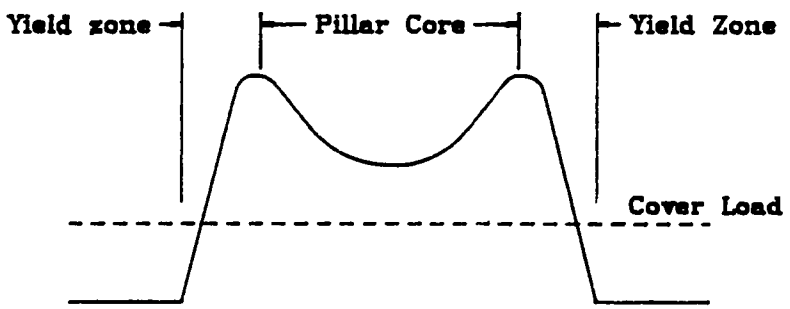


b. Probable stress distribution

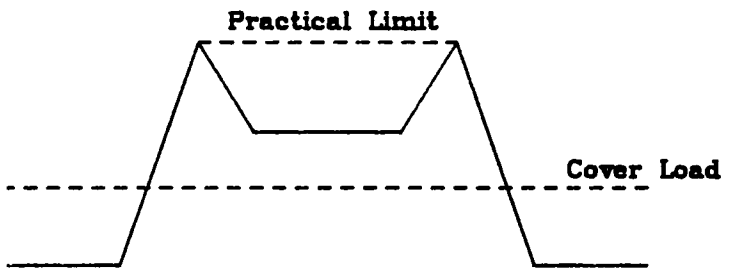


c. Hypothetical stress distribution

**Figure 2.6 Stress Distribution in a Pillar (After Wilson, 1972)**

$\sigma_h$ = horizontal stress in the pillar;

X = distance from the ribside;

q = triaxial factor;

p = horizontal constraint at the ribside, assumed to be 0.1 MPa; and

H = pillar height.

When the roof and floor are relatively soft, that is, as soft as the coal seam, the stresses in the yield zone can be expressed as:

$$\sigma_v = p\,q\,(\frac{X + X_0}{X_0})^{q-1} \tag{2.22}$$

$$\sigma_h = p\,(\frac{X + X_0}{X_0})^{q-1} \tag{2.23}$$

where:

$$X_0 = \frac{H}{2}.$$

The stress conditions at the yield-elastic boundary, according to Wilson (1977), are:

$$\sigma_h = \gamma h \tag{2.24}$$

$$\sigma_{vy} = q\gamma h \tag{2.25}$$

$$\sigma_{ve} = q\gamma h + \sigma_0 \tag{2.26}$$

where:

$\gamma$ = average overburden density;

h = overburden thickness;

$\sigma_{vy}$ = vertical stress at yield side of the yield zone boundary;

$\sigma_{ve}$ = vertical stress at elastic side of the yield zone boundary; and

$\sigma_0$ = uniaxial strength of coal.

Knowing the state of stresses in the yield zone and at the boundary, the width of the yield zone can be determined. When a weak coal is sandwiched between strong roof and floor, the width of the yield zone $X_b$ is:

$$X_b = \frac{H}{F} \ln \frac{\gamma h}{p} \tag{2.27}$$

where F is a function of the triaxial factor, which is expressed as:

$$F = \frac{q-1}{\sqrt{q}} + \frac{(q-1)^2}{q} \tan^{-1}\sqrt{q} \tag{2.28}$$

When the roof and floor rocks are as soft as the coal, the width of the yield zone is:

$$X_b = \frac{H}{2}\left[\left(\frac{\gamma h}{p}\right)^{1/(q-1)} - 1\right] \tag{2.29}$$

The bearing capacity of a square pillar then can be determined by integrating the vertical stresses over the pillar as follows:

$$P_b = \sigma_{ve}(W_p - 2X_b)^2 + 4\left(\int_0^{X_b} \sigma_v \, dx\right)(W_p - X_b) \tag{2.30}$$

where:

$P_b$ = pillar bearing capacity;

$\sigma_{ve}$ = pillar vertical stress at elastic side of the yield zone boundary;

$\sigma_v$ = pillar vertical stress in the yield zone; and

$W_p$ = pillar width.

When a weak coal is sandwiched between a strong roof and floor, the bearing capacity is:

$$P_b = \frac{4Hpq\,(W_p - X_b)}{F}\,[\exp(\frac{FX_b}{H}) - 1] +$$

$$+ (q\gamma h + \sigma_0)\,(W_p - 2X_b)^2 \qquad (2.31)$$

When the roof and floor is as soft as the coal:

$$P_b = \frac{4pX_b^q\,(W_p - X_b)}{(H/2)^{q-1}} + (q\gamma h + \sigma_0)\,(W_p - 2X_b)^2 \qquad (2.32)$$

The progressive failure theory provides some insight into the pillar yielding mechanism, and allows for the estimation of the yield zone width. It is, therefore, very useful for the study of pillar yielding behavior and for yield pillar design.

## 2.4 Yield Pillar Modeling

### *2.4.1 Numerical Modeling*

Numerical modeling techniques, especially the finite element method, have been extensively used to study the yield pillar behavior. The advantage of using the finite element method is its flexibility in dealing with inhomogeneous materials and complex boundary conditions. In addition, non-linear procedures may be introduced into the finite element model to cope with material or geometry non-linearity. This is especially useful for yield pillar modeling, since yield pillars work with the stress-strain conditions beyond the linear section of the material.

Several approaches have been suggested by various authors for the modeling of yield pillars. Kripakov (1981) developed a computer procedure to simulate progressive rock failure around coal mine entries. The ADINA code was used in his computer simulation. Three failure modes were allowed in the model: tension, compression, or shear. The Mohr-Coulomb failure criteria was adopted; for shear strength, it is:

$$\tau_F = c_0 + \sigma_n \tan \phi \tag{2.33}$$

where:

$\tau_F$ = shear strength of coal;

$c_0$ = cohesion;

$\sigma_n$ = normal stress; and

$\phi$ = internal friction angle.

For compressive strength, it is:

$$\sigma_F = \sigma_0 + \sigma_3 \tan \beta \tag{2.34}$$

where:

$\sigma_F$ = compressive strength of coal;

$\sigma_0$ = uniaxial strength of coal;

$\sigma_3$ = confining pressure; and

$\tan \beta$ = triaxial factor.

In this model, the factor of safety of every element was computed after each iteration. Both shear and compression modes of failure were considered, utilizing the following relationships:

$$\text{Factor of Safety} = \frac{\text{Strength}}{\text{Applied Stress}} \tag{2.35a}$$

$$\text{(Shear) F.S.} = \frac{\tau_F}{\tau_n} = \frac{c_0 + \sigma_n \tan \phi}{\tau_n} \tag{2.35b}$$

$$\text{(Compression) F.S.} = \frac{\sigma_F}{\sigma_{max}} = \frac{\sigma_0 + \sigma_{min} \tan \beta}{\sigma_{max}} \tag{2.35c}$$

The calculated factors of safety were then selected by the following criteria:

| | |
|---|---|
| i) compressive or shear failure | F.S. = F.S. |
| ii) compression but not failed | F.S. = 1 |
| iii) tension | F.S. = 0 |

The computer procedure was set up to survey every element for failure and to automatically set up a new data input file, reducing the value of modulus of elasticity of the material by the inverse of the factor of safety, utilizing the following equation:

$$E_n = \text{F.S.} \times E_o \tag{2.36}$$

where:

$E_n$ = new modulus of elasticity; and

$E_o$ = original modulus of elasticity.

The finite element model was then rerun with new material properties. The procedure continued until no failure occurred at any point in the structure.

Adopting Kripakov's non-linear procedure, Park (1985) performed a stability analysis of entries for a deep coal mine. The stress distribution in yield pillars was studied and the computer output was compared with field measurements. The results were very promising. The finite element code, MSC/NASTRAN developed by NASA, was utilized in Park's study. A model with 984 elements and 1,158 nodes was constructed. The computer results for the yield pillar system and their comparison with field data are listed in

Table 2.1. It can be seen in Table 2.1 that the agreement between the modeling and field measurements is good.

In an effort to develop a chain pillar design formula under weak roof conditions, Hsiung and Peng (1985) conducted a 3-D finite element parametric analysis. The NASTRAN code was again used in the analysis. Similarly, the pillar yielding zone was simulated by reducing the elastic modulus of the pillar material. However, the reduction factors were fixed at specific levels of the original properties.

### *2.4.2 Physical Modeling*

Physical modeling has been widely performed in rock mechanics research. In the study of yield pillars, it has also proven useful. Kicker and Park (1986) built a physical model of an underground longwall panel. The model was 47.5 inches in length, 29.5 inches in width and 20 inches in height. The materials used in the model were various combinations of sand, cement and SAE 250 or SAE 90 oil in order to satisfy the similitude between the model and the prototype. Two different yield pillar layouts, namely yield-abutment-yield and yield-yield pillar systems, were investigated, and are shown in Figure 2.7. The tested stress distributions for both cases are shown in Figure 2.8. In their investigations, Kicker and Park found that a pillar 1 inch by 9 inches, or simulated 24 feet by 214 feet, was too large to yield in the yield-abutment-yield system, and that reducing the width to 20 feet did produce yielding. A yield pillar with the size of 24 feet by 95 feet showed a better stress reduction and stress transfer to the abutment pillar. Kicker and Park concluded that the model had demonstrated the use of yield pillars as an effective control of high stress concentrations.

**Table 2.1. Comparison of Yield Pillar Stresses**

| (MPa) Stage | Gage 18 Sim. | Act. | Gage 17 Sim. | Act. | Gage 14 Sim. | Act. |
|---|---|---|---|---|---|---|
| 1 | 48.28 | - | 31.04 | - | 20.68 | - |
| 2 | 22.07 | 20.68 | 20.68 | 20.68 | 27.59 | 27.59 |
| 3 | 18.62 | 13.80 | 33.10 | 31.04 | 28.97 | 34.48 |

Note: Sim. = Simulated; Act. = Actual.

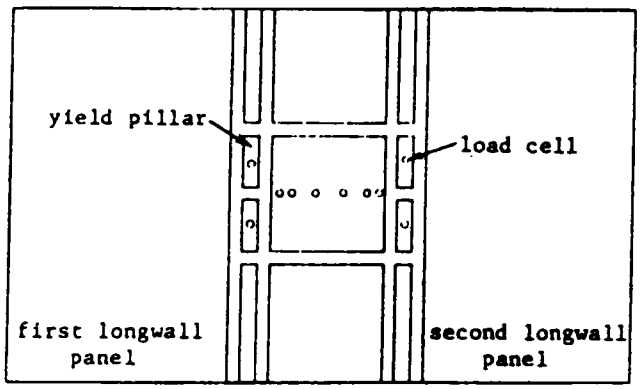


Yield-Abutment-Yield Model

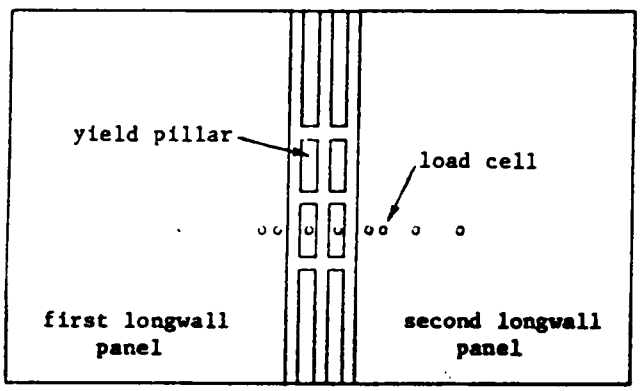


Yield-Yield Model

**Figure 2.7 Experimental Pillar Layouts (After Kicker & Park, 1986)**

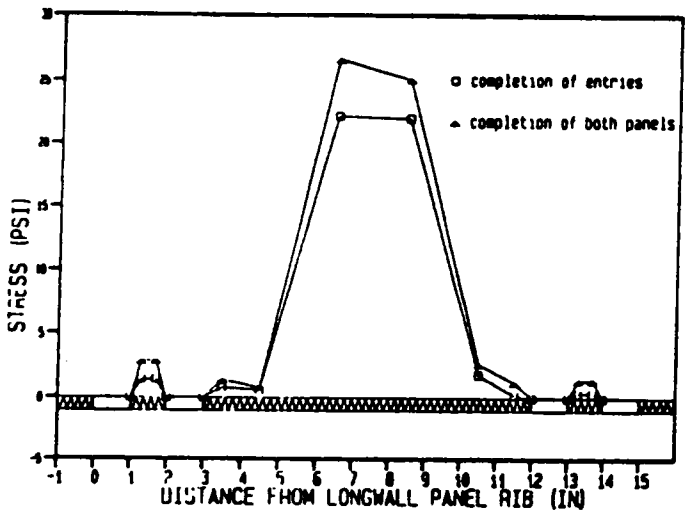


a. Stress Distribution on
Yield-Abutment-Yield Pillars

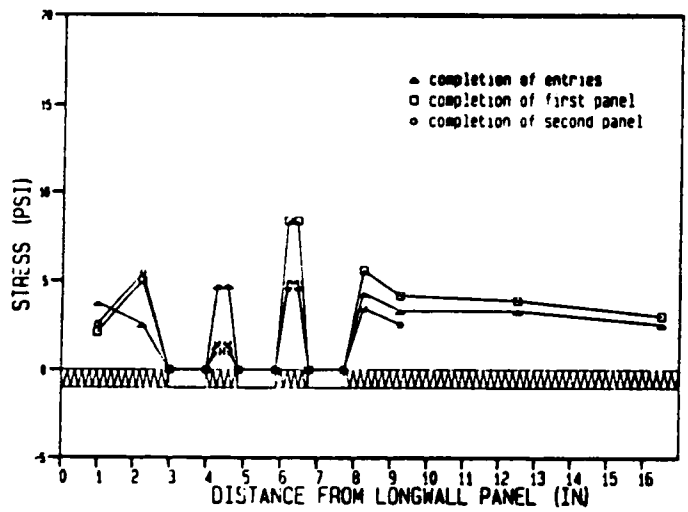


b. Stress Distribution on
Yield-Yield Pillars

**Figure 2.8 Tested Stress Distributions (After Kicker & Park, 1986)**

## 2.5 Yield Pillar Application

Successful application of yield pillars has been reported in the deep mines of Jim Walter Resources, Inc. (JWR) in Alabama. In a series of publications (Carr and Wilson, 1982; Martin and Care, 1984; Gauna et al., 1985; Martin et al., 1985), JWR has presented its design philosophy and success using yield pillars or combination of stable-yield pillars in deep and gassy longwall mines. Based on Wilson's progressive failure theory, JWR designed different yield pillar layouts both in the main entries and longwall gateways, which is illustrated in Figure 2.9. By this experience, it has been shown that the yield pillar allows a general lowering of the roof and transfer of load onto larger abutment pillars which flank the yield pillar development. The yield pillar design is critical in the sense that the load transferring is not unlimited. Excessive load transferring will cause instability of entries. Table 2.2 shows JWR's prediction regarding longwall tailgate entry stability.

Figure 2.10 shows the predicted stress profiles for a yield-abutment-yield pillar and a total yield pillar layout. It is clear that the stress concentration in yield pillar area is greatly reduced. As a result, it was concluded that:

- Applications of yield pillars offer production and ground control advantages when mining coal at great depth.
- The ground control advantages are most apparent when a yield-abutment-yield pillar design is applied for longwall panel development.
- The yield pillar in the yield-abutment-yield pillar design for longwall gateroads de-stresses the immediate roof and floor and serves as a "breaker line" for the waste and gateroad support during the longwall extraction phase.

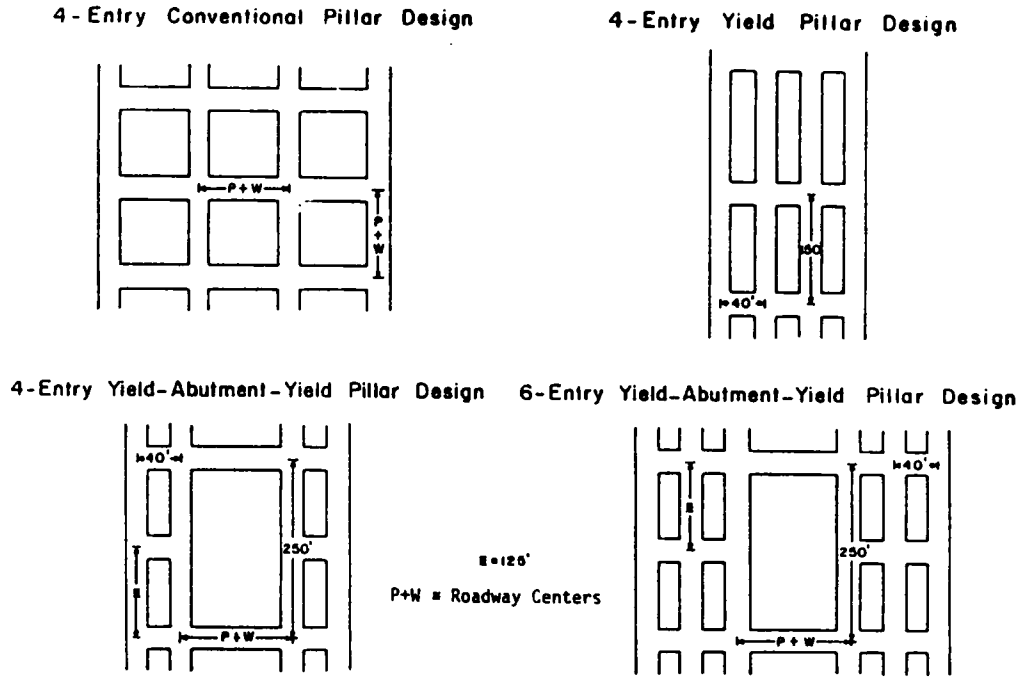


**Figure 2.9 Different Pillar Layout Designs (After Martin et al, 1985)**

**Table 2.2. Transferred Loads and Tailgate Conditions**

| Transferred load, tons/ft. | Condition in Tailgate |
|---|---|
| 0 | No damage attributable to longwall extraction. |
| 0 - 10,000 | Limited damage, some cribbing required. |
| 10,000 - 20,000 | Damage more severe. General cribbing required, condition still reasonable. |
| 20,000 - 30,000 | Damage severe, extensive cribbing required. Condition not considered good, but tolerable. |

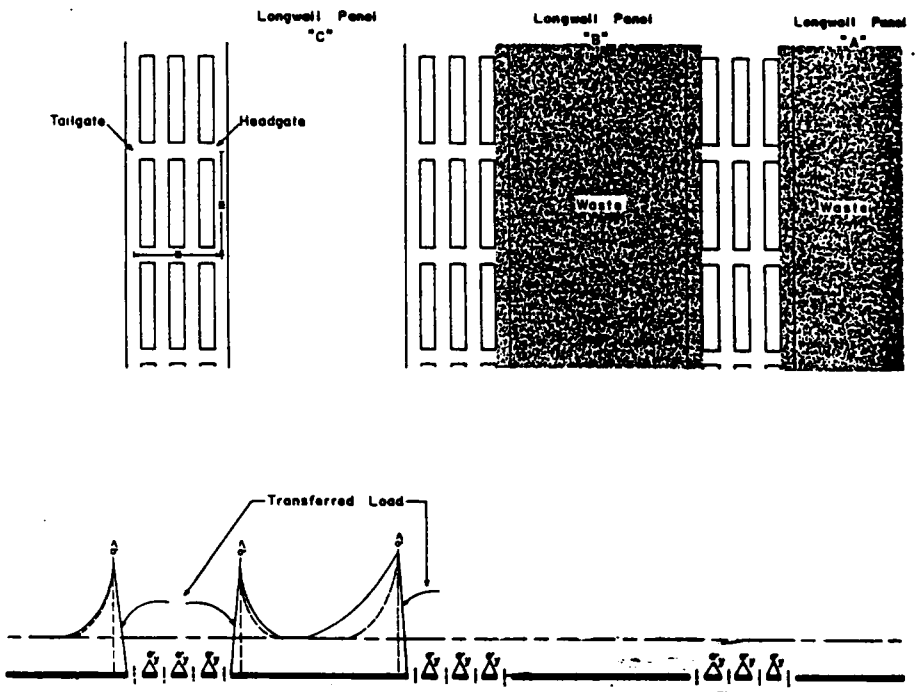


**Figure 2.10 Predicted Stress Profiles (After Martin et al, 1985)**

- The rate of development advance and reserve recovery are improved when mining using the yield-abutment-yield pillar design, but coal production is somewhat reduced.

Adopting yield pillars in underground coal mines may also reduce the effect of surface subsidence significantly. A study by Karmis and Jarosz (1985) revealed that yield pillars would produce a smoother surface subsidence profile and reduce both maximum tensile and compressive horizontal strain considerably. Figure 2.11 shows some results of their case studies. It can be seen that the maximum strain is reduced by a factor in excess of 4. The study concluded that designing mining panels using yield pillar principles could be of considerable interest for subsidence abatement.

## 2.6 Summary and Discussion

A review of the basic pillar design principles was conducted in this chapter. Most of them are applicable to the design of yield pillars. For a quick calculation of pillar load, the tributary area loading method may provide an acceptable estimation. The pressure arch theory is particularly convenient for designing yield pillars. A similar destressed zone may be formed above the yield pillar area as would occur above an opening. By following the pressure arch theory, the load and the displacement in and around the yield pillars may be analyzed. The size and shape effects of coal, as well as the interaction between coal and country rock, also provide useful information for the study of yield pillars.

Most empirical pillar design formulas have dealt only with the average stress and the ultimate strength of pillars. No yield zones have been considered. It is, therefore, difficult

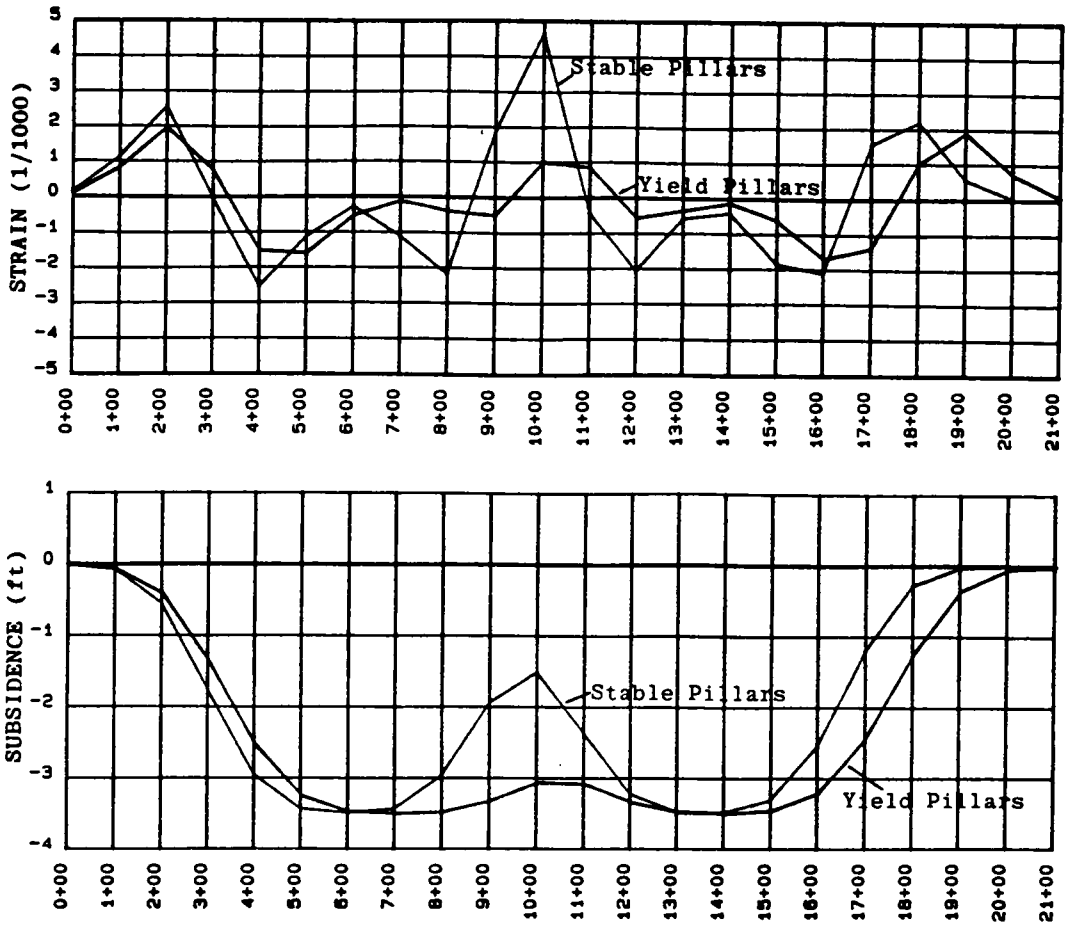


**Figure 2.11 Comparison of Subsidences and Strains (After Karmis & Jarosz, 1985)**

to use these formulas for yield pillar design. On the other hand, the progressive failure theory provides a possible explanation of pillar yielding phenomena. It may be further developed to estimate yield pillar sizes and to evaluate the stability of yield pillars.

The literature review also shows that numerical methods are capable of modeling yield pillar behaviors. Because of the non-linear nature of coal and coal measure rocks, however, especially the working conditions of yield pillars, linear models cannot be used to perform accurate anaylsis of yield pillars. In order to successfully simulate yield pillars, non-linear models must be introduced along with an appropriate yield criterion.

# CHAPTER 3: DEVELOPMENT OF FINITE ELEMENT MODELS

## 3.1 Introduction

Computer modeling of yield pillars must be capable of dealing with the non-linear behavior of coal and coal measure rocks. A good understanding of the characteristics of these types of materials is fundamental to the study of yield pillars. In order to simulate the inelastic behavior of yield pillars utilizing the finite element method, special non-linear techniques have to be developed. In this chapter, after a brief description of the mechanical properties of coal and coal measure rocks, two finite element models are presented, each following a different non-linear approach. Basic equations for the models are derived and detailed procedures in the simulations, including a computer flow chart for each model, are presented.

## 3.2 Mechanical Properties of Coal and Coal Measure Rocks

Laboratory experiments and in-situ tests have demonstrated that coal measure rock exhibits non-linear behavior. This is especially true when the rock materials are at yielding conditions. A typical complete stress-strain curve for coal samples is illustrated in Figure 3.1. The curve includes two sections: a section of approximately elastic stress-strain relationship before the stress reaches the ultimate strength of the material (Section AB), followed by a strain-softening deformation section (Section BC). In Section BC, although the coal has failed, it still holds some ability to support certain amount of load. A proper design of yield pillars allows the pillar to work at this section of the stress-strain curve.

Research has also revealed that coal strength increases with confining pressure. Figure 3.2 shows a set of typical test curves for coal. At different confining pressures, coal specimens fail at different peak stress. The higher the confining pressure, the higher the strength of coal. The strength of coal is, therefore, a function of the confining pressure. This function may be approximated by the following expression (Wilson, 1980):

$$\sigma = \sigma_0 + q\,\sigma_3 \tag{3.1}$$

where:

$\sigma$ = coal strength with confining pressure;

$\sigma_0$ = uniaxial strength of coal;

q = triaxial factor; and

$\sigma_3$ = confining pressure.

After failure, the rock will be in a fractured condition and $\sigma_0$ will be small. If movement occurs in the form of sliding along the fracture surface, the change in the triaxial stress

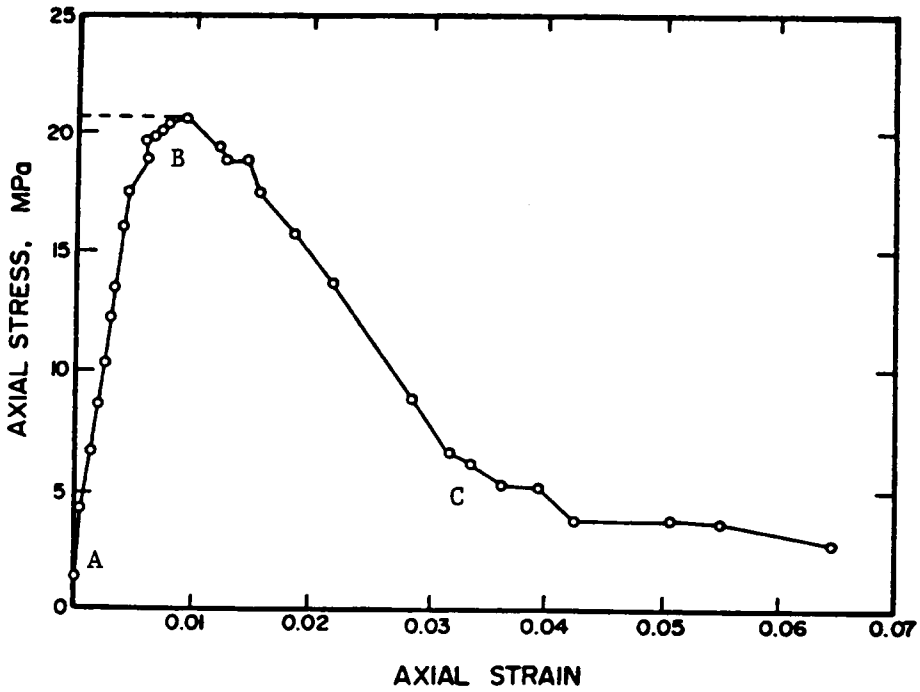


**Figure 3.1 A Typical Stress-Strain Curve of Coal (After Bieniawski, 1987)**

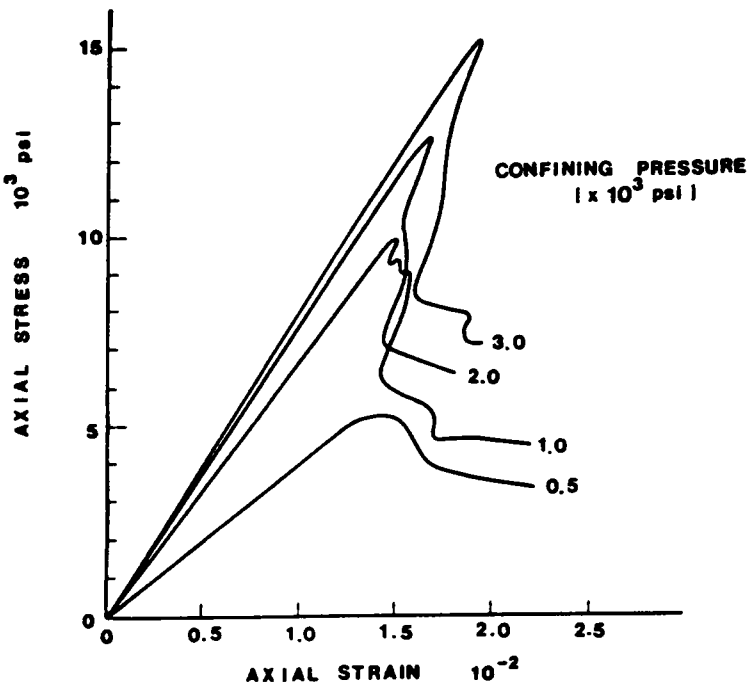


**Figure 3.2 Effect of Confining Pressure on Coal Strength (After Peng, 1986)**

factor q is small (Wilson, 1980). For the purposes of approximation, q can be considered unchanged. Hence the condition of the rock in the yield zone can be represented by the equation:

$$\sigma = q\,\sigma_3 \tag{3.2}$$

where $\sigma_0$ is assumed to be negligible.

The actual relation between the strength and the confining stress for both intact and yield coal is most probably non-linear, as illustrated in Figure 3.3 (Wilson, 1980). For practical applications, however, the linear simplification in Equations 3.1 and 3.2 will provide sufficient accuracy for most coal measure rocks under normal conditions. The linear relation was, therefore, adopted in this research.

Based on the above discussion it may be concluded that, to simulate coal and coal measure rocks with the finite element method, two major factors must be considered, namely the strain-softening behavior of the material and the triaxial loading effect. To deal with the former, a non-linear model must be introduced. For the triaxial loading effect, a proper yield criterion must be selected. In the following sections, two different non-linear models were developed, each using a different yield criterion.

## 3.3 Non-Linear Model with Successive Iterations

Finite element methods have been used extensively in solving rock mechanics problems. The flexibility of the finite element method in dealing with complex boundary conditions and non-uniform material properties makes this method a powerful tool for underground

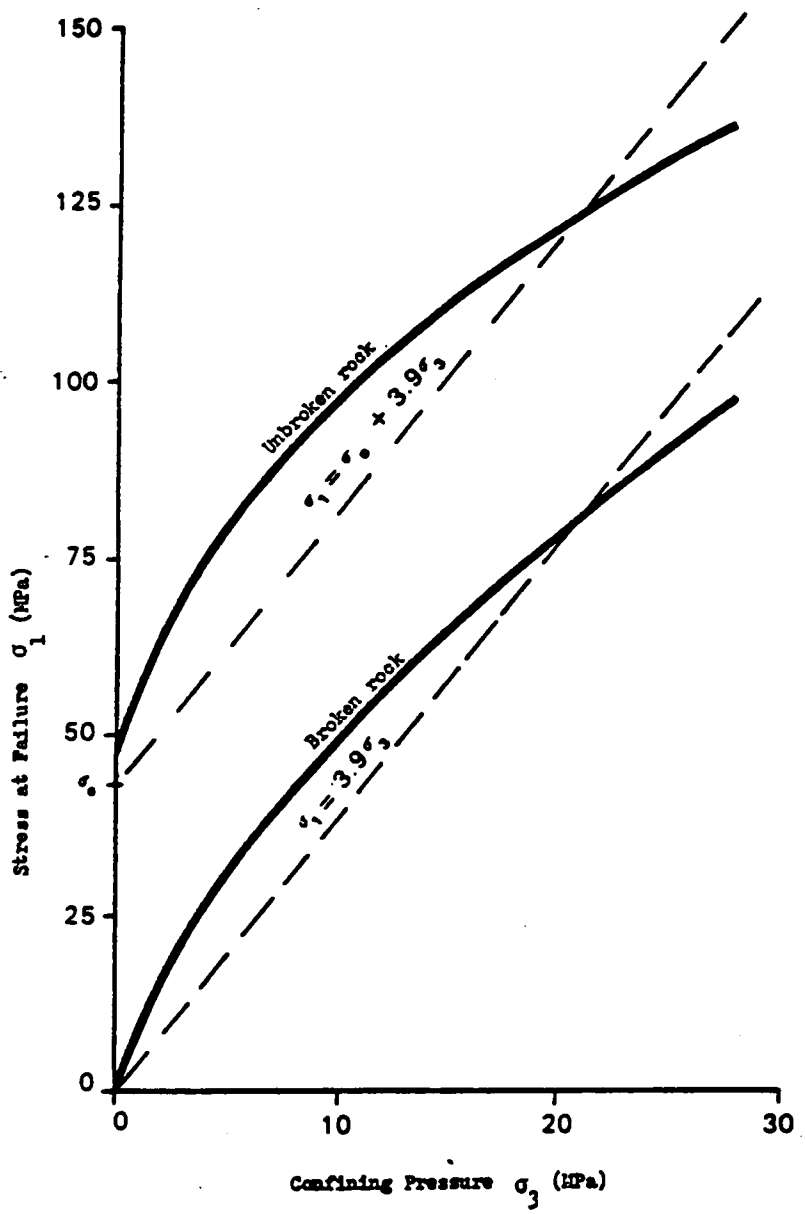


**Figure 3.3 Relation Between Confining Pressure and Strength (After Wilson, 1980)**

structure design. The basic steps involved in the finite element analysis are stated as follows:

**Step 1: Discretize and Select Element Configuration** In this step, the region to be studied is subdivided into a suitable number of small bodies, called finite elements. Two-dimensional models were established in this study and quadrilateral elements were used.

**Step 2: Select Approximation Function** A proper function is selected to interpolate the unknown displacement and stress from nodal point values in each element. Because of its simplicity, polynomials are widely used. The polynomial interpolation function used in this study can be expressed as:

$$u = N_1 u_1 + N_2 u_2 + N_3 u_3 + \cdots + N_m u_m \tag{3.3}$$

where:

$u$ = displacement in the element;

$u_i$ = displacement at nodal point; and

$N_i$ = interpolation function.

**Step 3: Define Strain-Displacement and Stress-Strain Relationships** The strain-displacement relation is defined as (for 2-D analysis):

$$\varepsilon_x = \frac{\partial u}{\partial x} \tag{3.4a}$$

$$\varepsilon_y = \frac{\partial v}{\partial y} \tag{3.4b}$$

$$\gamma_{xy} = \frac{\partial u}{\partial y} + \frac{\partial v}{\partial x} \tag{3.4c}$$

where:

$\varepsilon_x$ = strain in x direction;

$\varepsilon_y$ = strain in y direction;

$\gamma_{xy}$ = shear strain in x-y plane;

u = displacement in x direction; and

v = displacement in y direction.

Since a local coordinate system is usually used for simplification of the computation, a transformation is needed from the local coordinate to the global system, i.e.

$$\varepsilon_x = \frac{\partial u}{\partial x} = \frac{\partial u}{\partial s}\frac{\partial s}{\partial x} + \frac{\partial u}{\partial t}\frac{\partial t}{\partial x} \tag{3.5a}$$

$$\varepsilon_y = \frac{\partial v}{\partial y} = \frac{\partial v}{\partial s}\frac{\partial s}{\partial y} + \frac{\partial v}{\partial t}\frac{\partial t}{\partial y} \tag{3.5b}$$

$$\gamma_{xy} = \frac{\partial u}{\partial y} + \frac{\partial v}{\partial x} = \frac{\partial u}{\partial s}\frac{\partial s}{\partial y} + \frac{\partial u}{\partial t}\frac{\partial t}{\partial y} + \frac{\partial v}{\partial s}\frac{\partial s}{\partial x} + \frac{\partial v}{\partial t}\frac{\partial t}{\partial x} \tag{3.5c}$$

where:

s, t = local coordinates.

With certain mathematical manipulations, this is finally reduced to:

$$\{\varepsilon\} = [B]\{q\} \tag{3.6}$$

where:

$\{\varepsilon\}$ = a $3 \times 1$ vector of strains;

[B] = a $3 \times 8$ matrix relating the nodal point displacements to strain;

$\{q\}$ = a $8 \times 1$ vector of nodal point displacements.

The stress-strain relation or constitutive relation is expressed as:

$$\{\sigma\} = [C]\{\varepsilon\} \tag{3.7}$$

where:

$\{\sigma\}$ = a $3 \times 1$ matrix of stresses;

[C] = a $3 \times 3$ matrix of material properties relating strain to stress.

**Step 4: Derive Element Equations** By invoking available laws and principles, equations governing the behavior of the element are derived. A number of alternatives are possible for this derivation. The energy method was selected in this study. The element equation is expressed as:

$$[k]\{q\} = \{Q\} \tag{3.8}$$

where:

$\{Q\}$ = a $8 \times 1$ vector of applied forces at element nodal points; and

$\{k\} = \int\int [B]^T[C][B]dxdy$ .

**Step 5: Assemble Element Equations to Obtain Global Equations and Introduce Boundary Conditions** Based on the law of compatibility or continuity, the element equations established in Step 4 are assembled to produce global or assemblage equations in the following form:

$$[K]\{r\} = \{R\} \tag{3.9}$$

where:

[K] = global property matrix;

$\{r\}$ = global vector of nodal displacements; and

$\{R\}$ = global vector of applied forces at nodal points.

The boundary conditions are then introduced into the finite element model. To apply the boundary conditions, Equation 3.9, is modified with the constrain conditions at the geometric boundary. The final global equations are expressed as:

$$[K'] \{r'\} = \{R'\} \tag{3.10}$$

The primes in the variables indicate modification of those variables.

**Step 6: Solve for Primary Unknowns and Derived Quantities** Equation 3.10 is a set of linear simultaneous algebraic equations. The well-known Gaussian elimination method was used in this study to solve the equations. The primary unknowns in this case are the nodal displacements. After the nodal displacements are computed, the secondary or derived quantities such as strains and stresses can be obtained based on their relations as derived in Step 3.

**Step 7: Interpretation of Results** The final and the important aim is to obtain output from the finite element analysis. The output can be made in the form of printed results or plotted graphs, which can be readily used for analysis and design.

The finite element method was first introduced for linear elastic analysis of rock mechanics problems. Linear models, however, are very rough approximations of real conditions, especially of coal and coal measure rock strata. Qualitative analysis may be conducted with linear elastic models. Accurate quantitative results, however, appear to be difficult to achieve with these models. In order to simulate the actual behavior of coal and coal measure rock strata as described in Section 3.1, non-linear procedures must be introduced into the finite element models. Several techniques are available for non-linear finite element analysis, such as direct iterations, tangent iterations, incremental iterations, initial stress method and initial strain method. In order to be able to utilize a linear finite element program with minimum modifications to account for the non-linear behavior of rock, the successive iteration technique, which is basically a direct iteration method, was adopted in this study.

As shown in Figure 3.4, an idealized non-linear stress-strain curve was assumed in the finite element model. In this curve, the decreasing part, Section BC, was assumed to have a negative value of the initial elastic modulus, Section AB, that is:

$$E_{BC} = -E_{AB} \tag{3.11}$$

In addition, by examining a number of tested curves, the residual strength of yield material was assumed to be approximately 10% of the strength of intact coal. The non-linear behavior of the yielding material was then simulated by gradually altering the elastic modulus of the material (Figure 3.4). The model commenced with an elastic modulus for intact coal. After each computer iteration, every element was checked for failure against the following criteria.

a) For compressive failure:

$$\sigma = \sigma_0 + q\sigma_3 \tag{3.12}$$

where:

$\sigma$ = strength of coal;

$\sigma_0$ = uniaxial compressive strength of coal;

q = triaxial factor; and

$\sigma_3$ = confining pressure.

b) For tensile failure:

$$\sigma = \sigma_T \tag{3.13}$$

where:

$\sigma_T$ = tensile strength of coal.

If the tensile stress of an element exceeded the tensile strength, the element failed in tension. The modulus of this particular element was then reduced to a very small value,

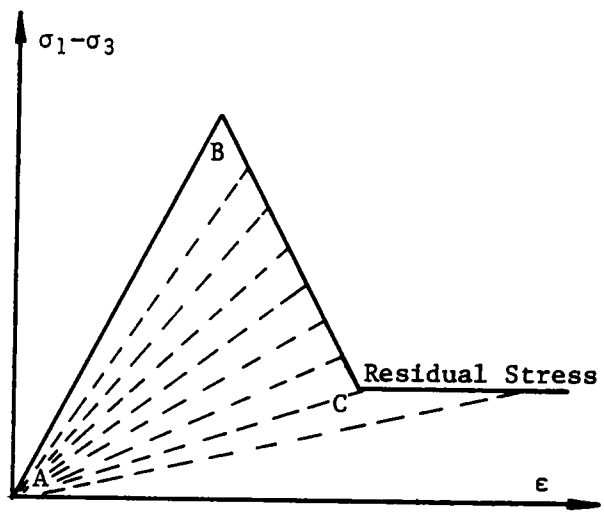


**Figure 3.4 Idealized Stress-Strain Curve**

approximately 1/1000 of the value for intact coal. If the compressive stress of an element exceeded the compressive strength, it failed in compression. The modulus of this element was then reduced by approximately 10%, and its uniaxial strength was reduced to a smaller value. This new value was the stress value indicated by the intersection point of the new stress-strain curve with the reduced elastic modulus and the original stress-strain curve, which is shown in Figure 3.4. When the survey in all elements had been completed, a new iteration commenced. The same procedure was repeated and iterations continued until no more elements failed. At this stage, the strength of some elements might have been gradually reduced to the residual strength and the elastic modulus of the elements reduced to a very small value, approximately 1/1000 of original value. The procedure stated above is illustrated in the flowchart shown in Figure 3.5.

The non-linear model established is basically a direct iteration type. It is similar to the model developed by Kripakov (1981) as described in Chapter 2. However, since the new model adopted a procedure of gradually reducing the elastic modulus of the yielding elements, i.e. 10% at a time, the stress-strain curve could be followed more closely.

## 3.4 Elastic-Plastic Finite Element Model

It is accepted by many authors that the pillar may be considered to behave plastically after yielding. In a small, localized region, this plastic deformation assumption may not be accurate. On a large scale, however, the resulting behavior of a pillar may be well simulated with elastic-plastic models. A finite element model was, therefore, developed in this study utilizing the Von Mises yielding criterion. The model simulated yield pillars

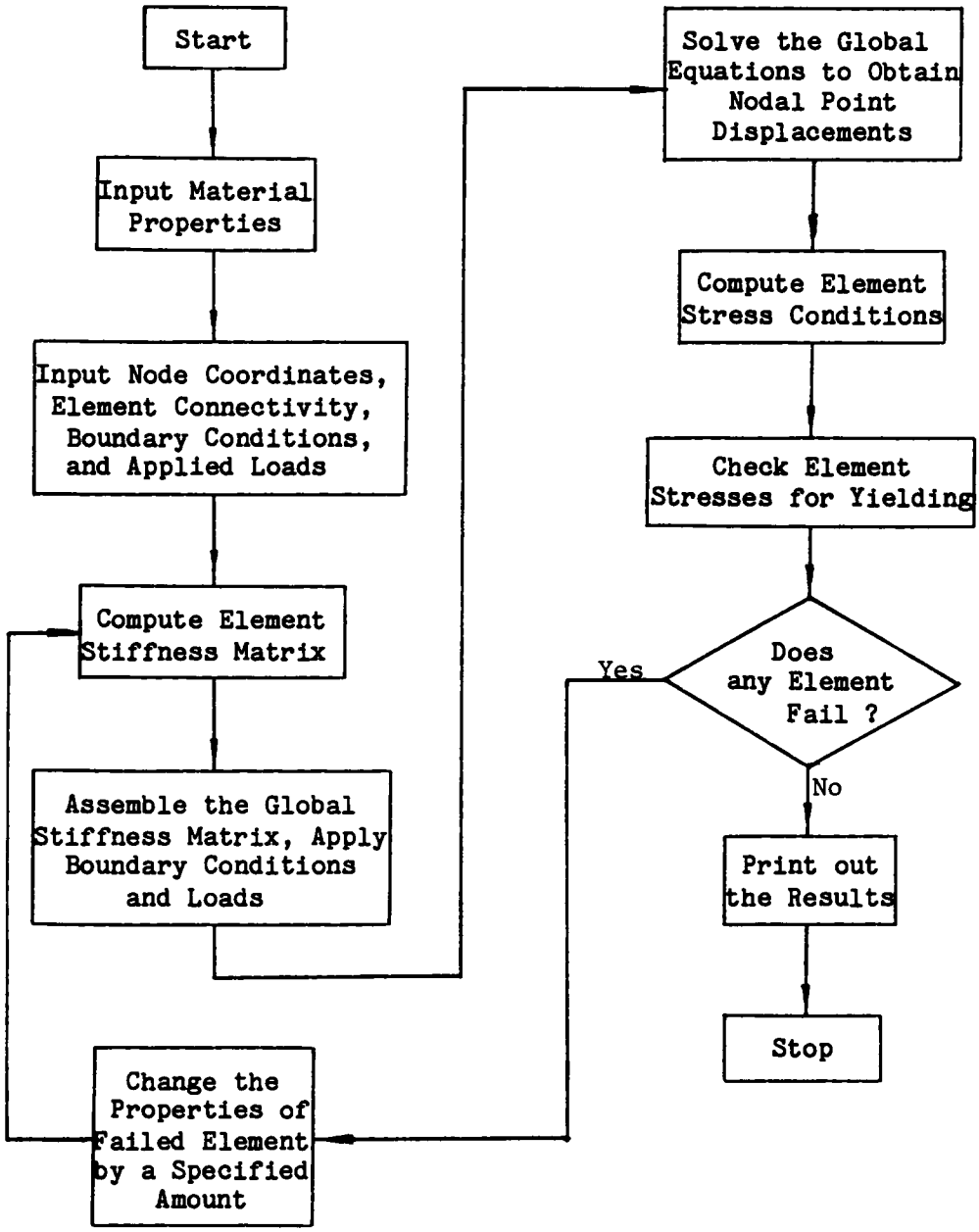


**Figure 3.5 Flowchart of Successive Iteration Model**

in two stages: an elastic stage prior to yielding, followed by a perfect-plastic stage. The model also simulated the strain-softening behavior of yielding coal.

During a complete loading cycle, a coal pillar will progress through two distinct stages: an elastic deformation stage, which will be maintained up to certain peak load, and the yielding stage that follows. During the yielding process, the pillar will lose some of its bearing ability and the load will be transferred elsewhere. A typical test curve is illustrated in Figure 3.6, and was simplified to simulate the progressive failure as shown in the same graph. This model was previously discussed by Gates (1972) and applied to clay shale for slope stability analysis. It was introduced for pillar yielding analysis in this research, with some modifications.

The basis of this model is a yield function, a generalized Von Mises criterion, which was first used by Drucker and Prager (1952) for soils. The yield function f is expressed as follows:

$$f = \alpha I_1 + (J_2)^{1/2} = k \tag{3.14}$$

where:

$\alpha$ , k = material constants;

$I_1$ = first invariant of stress tensor, $I_1 = \sigma_x + \sigma_y + \sigma_z$;

$J_2$ = second invariant of stress deviator tensor;

$$J_2 = \frac{1}{6}\left[(\sigma_x - \sigma_y)^2 + (\sigma_y - \sigma_z)^2 + (\sigma_z - \sigma_x)^2 + 6(\tau_{xy}^2 + \tau_{yz}^2 + \tau_{zx}^2)\right].$$

This function can be represented by a cone-shaped yield surface in the stress space. Different material constants will produce different shapes of cones. As shown in Figure 3.7, the large cone represents the yield surface at the peak strength of coal. Prior to yielding, any stress condition indicated by a point inside of the large cone, i.e. $f < k$, is in the elastic state. When the point representing the stress condition reaches the surface

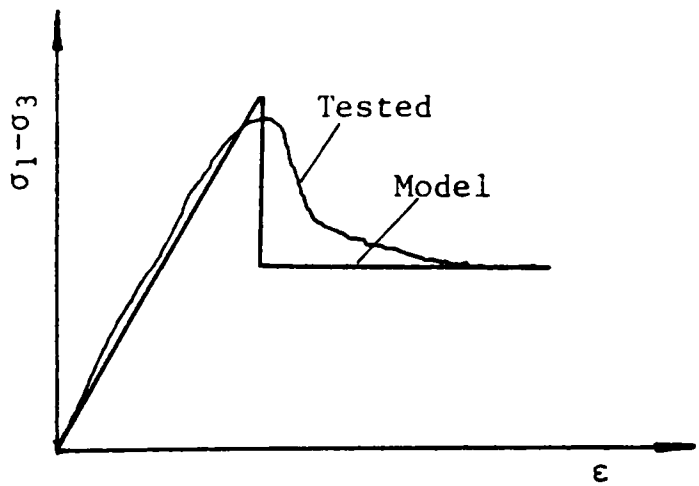


**Figure 3.6 Simplified Stress-Strain Curve**

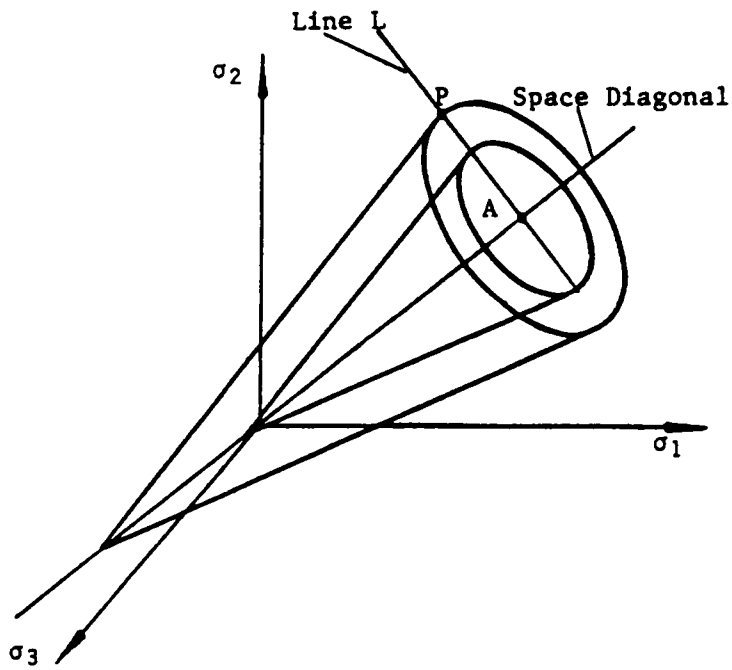


**Figure 3.7 Yield Surface in Stress Space**

of the large cone, the coal begins to yield. At this moment, some load is released and the stress drops to the surface of the small cone. The point representing the state of the stress subsequently slides on the surface of the small cone, indicating a perfect-plastic condition.

The material constants $\alpha$ and k may be obtained from the cohesion c and the internal frictional angle $\phi$. The relations between them have been derived by Drucker and Prager as follows:

$$\alpha = \frac{\tan \phi}{(9 + 12 \tan^2 \phi)^{1/2}} \tag{3.15a}$$

$$k = \frac{3c}{(9 + 12 \tan^2 \phi)^{1/2}} \tag{3.15b}$$

The cohesion c and the internal frictional angle $\phi$ are in turn related to the uniaxial compressive strength $\sigma_0$ and the triaxial factor q by the following equation:

$$c = \sigma_0 \frac{1 - \sin \phi}{2 \cos \phi} \tag{3.16a}$$

$$\phi = \sin^{-1} \frac{q - 1}{q + 1} \tag{3.16b}$$

As mentioned above, when the material yields, the stress moves from the large yield surface to the small one (Figure 3.7). Physically this corresponds to changing $\sigma_0$ and q. As discussed in Section 3.1, when coal yields, the change in q is small. The triaxial factor q was, therefore, assumed to be constant. Only the uniaxial compressive strength $\sigma_0$ was reduced. For simplicity, $\sigma_0$ was assumed to be zero for broken coal.

Since mathematically there are numerous ways of changing the stress condition from the peak yield surface to the residual, some assumptions must be made in order to single out a unique path of changing stress. It was assumed that the change in the material properties would not affect the material's ability to take hydrostatic stress, only deviatoric. Therefore, the new stress point remained on a plane of constant hydrostatic stress, and only decreased its deviatoric component. The direction of the principal stress was also assumed not to change. In order to establish a unique path and a unique point on the new yield surface, a line L was drawn from the initial yield point, $P_1$, to the point of intersection of the deviatoric plane and the space diagonal (point A, Figure 3.7). This line intersected the new yield surface at two points, and the point closer to the initial yield point was selected. Assuming that at stress ($\sigma_{x1}, \sigma_{y1}, \sigma_{z1}$) coal starts to yield, the equation representing Line L in Figure 3.7 is expressed as:

$$\frac{\sigma_x - \sigma_{x1}}{\sigma_m - \sigma_{x1}} = \frac{\sigma_y - \sigma_{y1}}{\sigma_m - \sigma_{y1}} = \frac{\sigma_z - \sigma_{z1}}{\sigma_m - \sigma_{z1}} \tag{3.17}$$

where:

$\sigma_m = (\sigma_{x1} + \sigma_{y1} + \sigma_{z1})/3$ , which is on the space diagonal line.

Since the uniaxial compressive strength was assumed to be zero for yield coal, the constant k in Equation 3.14 was also zero. The equation for the small cone-shaped yield surface in Figure 3.7, therefore, becomes:

$$\alpha I_1 + (J_2)^{1/2} = 0 \tag{3.18}$$

By combining Equations 3.17 and 3.18, and solving for $\sigma_x, \sigma_y$ and $\sigma_z$, the new stress condition was able to be determined. Detailed derivations were listed in Appendix B.

A yield element in the finite element model has to go through two stages: an elastic stage and a plastic stage. In the elastic range, the strain-stress relation or the constitutive relation follows Hook's law, that is:

$$\{\sigma\} = [C]\{\varepsilon\} \tag{3.19}$$

For plane strain problem models, which were primarily used in this study, the variables in Equation 3.19 are defined as:

$$\{\sigma\} = \begin{Bmatrix} \sigma_x \\ \sigma_y \\ \tau_{xy} \end{Bmatrix}$$

$$[C] = \frac{E}{2(1+\mu)(1-2\mu)} \begin{bmatrix} 2-2\mu & 2\mu & 0 \\ 2\mu & 2-2\mu & 0 \\ 0 & 0 & 1-2\mu \end{bmatrix}$$

$$\{\varepsilon\} = \begin{Bmatrix} \varepsilon_x \\ \varepsilon_y \\ \gamma_{xy} \end{Bmatrix}$$

For plastic deformation, the Prandtl-Reuss hypothesis of plastic incremental flow rule is applied. The hypothesis states that the plastic strain rate is proportional to the gradient of the yield function, i.e.:

$$d\{\varepsilon\}_p = \lambda \frac{\partial f}{\partial \{\sigma\}} \tag{3.20}$$

where:

$\{\varepsilon\}_p$ = the plastic strain component;

$f$ = the yield function;

$\{\sigma\}$ = the stress vector; and

$\lambda$ = a constant which can be determined from the yield function.

By incorporating Hook's law, the Prandtl-Reuss hypothesis, and the yield function, the function for the stress-strain relation in the plastic range, corresponding to the C matrix in Equation 3, was able to be derived (Reyes, 1966):

$$C_{11} = 2G\left[1 - h_2 - \sigma_x\left(2h_1 + \sigma_x h_3\right)\right]$$

$$C_{22} = 2G\left[1 - h_2 - \sigma_y\left(2h_1 + \sigma_y h_3\right)\right]$$

$$C_{33} = 2G\left(\frac{1}{2} - h_3\tau_{xy}^2\right)$$

$$C_{12} = C_{21} = 2G\left[-h_2 - h_1\left(\sigma_x + \sigma_y\right) - h_3\sigma_x\sigma_y\right]$$

$$C_{13} = C_{31} = 2G\left(-\tau_{xy}\right)\left(h_1 + \sigma_x h_3\right)$$

$$C_{23} = C_{32} = 2G\left(-\tau_{xy}\right)\left(h_1 + \sigma_y h_3\right)$$

where:

G = shearing modulus, and:

$$h_0 = 3\alpha\,\frac{1+\mu}{3-6\mu} - \frac{I_1}{6\left(J_2\right)^{1/2}}$$

$$h_1 = \frac{h_0}{\left(1 + 18\alpha^2\,\frac{1+\mu}{3-6\mu}\right)\left(J_2\right)^{1/2}}$$

$$h_2 = \frac{2h_0\left(\alpha - \frac{I_1}{6\left(J_2\right)^{1/2}}\right) - \frac{\mu k}{(1-2\mu)\left(J_2\right)^{1/2}}}{\left(1 + 18\alpha^2\,\frac{1+\mu}{3-6\mu}\right)}$$

$$h_3 = \frac{1}{2J_2\left(1 + 18\alpha^2\,\frac{1+\mu}{3-6\mu}\right)}$$

The principles discussed above were incorporated into a 2-D finite element program which was specifically coded in FORTRAN . The incremental loading procedure was applied in the program and the displacement formulation adopted. Since the C matrix is also a function of the current stress condition, the iteration technique was used to compute the new stresses. When a particular element yielded in a load increment, the calculated stresses were substituted back to the C matrix and the stresses recalculated. The process continued until a certain criterion was met or the number of interactions exceeded a preset value.

When an element yielded, its stresses dropped to a lower level and the load on the whole structure lost its balance. Re-establishing the load balance was accomplished by examining the difference between the applied force and the computed force at every node point of the finite element mesh. The differential force was applied back to each corresponding node and the stresses recalculated. Four node quadrilateral elements were used in this finite element model. In order to calculate the nodal forces of each element, the following integration was carried out:

$$\{F\}^e = \int\int [B]^t \{\sigma\}\, w\, dx\, dy \qquad (3.21)$$

where:

$\{F\}^e$ = the element nodal force vector;

$[B]$ = the element geometric matrix;

$\{\sigma\}$ = the stress vector; and

$w$ = the thickness of the element, taken as unity.

In order to evaluate this integration, the element stresses were computed at four Gauss points as shown in Figure 3.8 and the Gauss quadrature numerical integration method

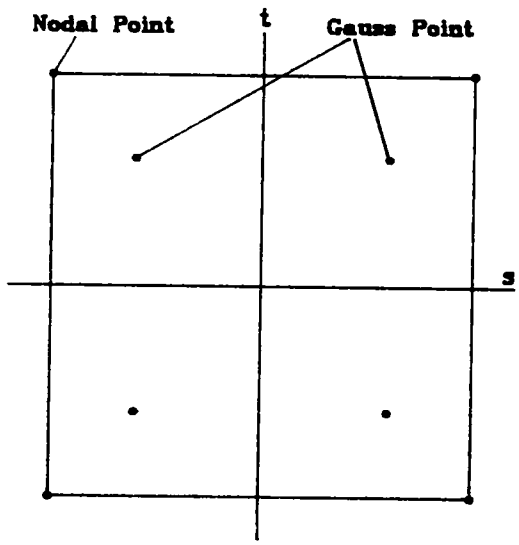


**Figure 3.8 Gauss Point in an Element**

used to carry out the computation. The output results, however, printed only the mean values of the stresses at the four Gauss points for each element. A flow chart of the computer program was constructed, as shown in Figure 3.9, which illustrates the internal logic of the elastic-plastic finite element model.

## 3.5 Summary and Discussion

Two finite element models were developed in this research, using different approaches to simulate the non-linear behavior of yield pillars. The first one adopted the successive iteration technique, and therefore, is a quasi-elastic model. The model was basically a linear-elastic one. The non-linear stress-strain behavior was simulated by altering the elastic modulus of the material with a number of iterations. The second model subdivided the non-linear deformation into two distinct portions: linear-elastic deformation prior to yielding, followed by perfect plastic deformation.

The first model can be easily realized with a linear finite element program, and requires minor modifications. The model, however, involved unloading and reloading of the applied forces whenever the elastic modulus was altered in any of the elements during the simulation process. This does not occur in reality. It is, therefore, difficult to simulate a continuous mining sequence with this model. In simulating a continuous mining sequence, unloading-reloading cycle may cause major errors. The elastic-plastic model, on the other hand, is constructed on a more solid mathematical base. While it requires more complicated computer programming, the load increment technique allows the model to simulate underground excavating activities more realistically.

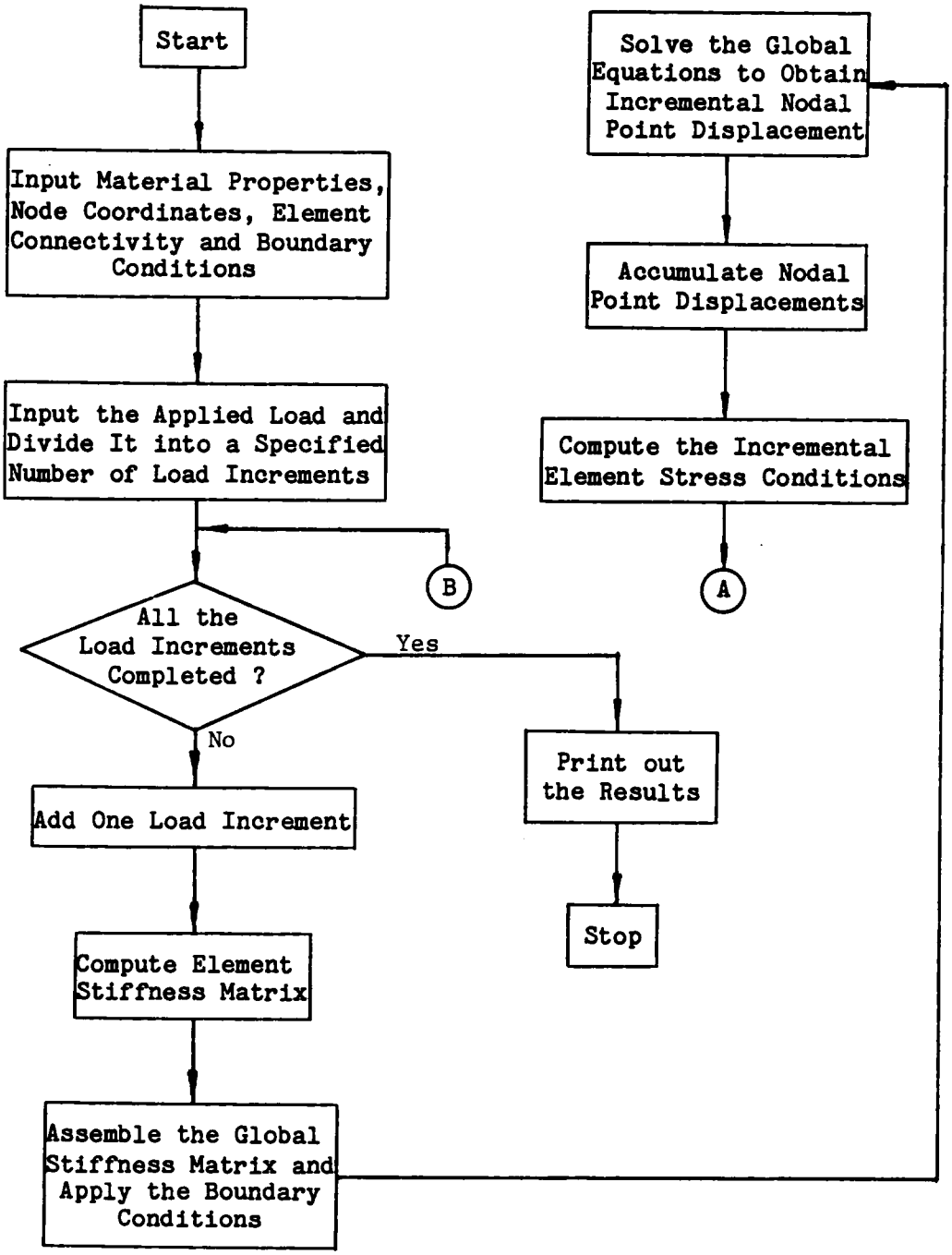


**Figure 3.9a Flowchart of the Elastic-Plastic Model**

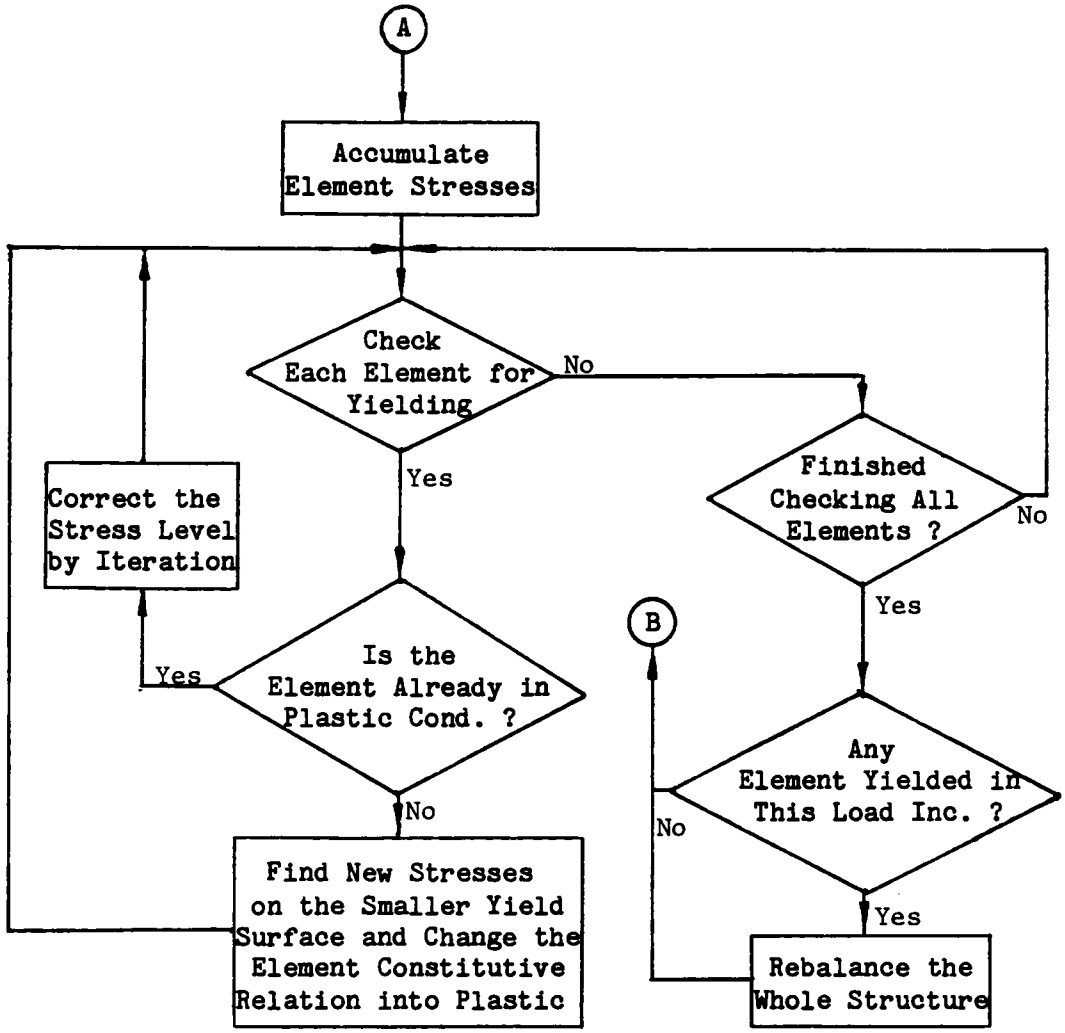


**Figure 3.9b Flowchart of the Elastic-Plastic Model (Continued)**

# CHAPTER 4: FIELD MONITORING AND MODEL VALIDATION

## 4.1 Field Monitoring

In order to validate the finite element models developed, an underground monitoring program was initiated in a longwall coal mine located in southwestern Virginia. This operation was at a depth of 1,500-1,600 feet with a mining height in the range of 5.0-6.0 feet. The yield-stable-yield pillar system had been adopted for the longwall entry and submain entry development to alleviate problems in strata control and to increase coal recovery. The instrumentation program included monitoring of pillar stresses, roof-to-floor convergences, roof sags, and horizontal pillar dilations.

### *4.1.1 Monitoring Site Selection*

The monitoring was carried out during the entry development period. In order to observe the pillar deformation and stress during the excavation of the entries, the monitoring stations were set up as close to the excavation face as possible. The monitoring continued until the face advanced a sufficient distance away from the monitoring stations and all related ground movement had been completed. In addition, simple geometry was preferred for the site selected in order to facilitate mathematical analysis and computer modeling.

Based on the above criteria, two monitoring sites were considered, as shown in Figure 4.1. Site 1 was at the intersection of the submain and the longwall gateway, and was close to the longwall panel. It was considered possible to detect some influence of the longwall face on the pillars at Site 1. This site, however, had a complex geometry, which made computer modeling difficult. This drawback was compensated for by adding a second monitoring station at Site 2, also shown in Figure 4.1. This location had a simple geometry and the pillar layout was in a regular yield-stable-yield pattern.

### *4.1.2 Monitoring Station Set-up and Operation*

The measurement of pillar stress was implemented by installing BPC hydraulic cells. The BPC's (Borehole Pressure Cells) were designed by the Bureau of Mines and furnished by MSHA in this research program. As shown in Figure 4.2, the basic component of a BPC is a flat cell made of mild steel. The flat cell is 8 inches long, 2 inches wide and 0.35 of an inch thick. It is covered with Portland Cement to form a cylindrical capsule having a diameter of 2.165 inches. This structure makes the cells sensitive to the applying load

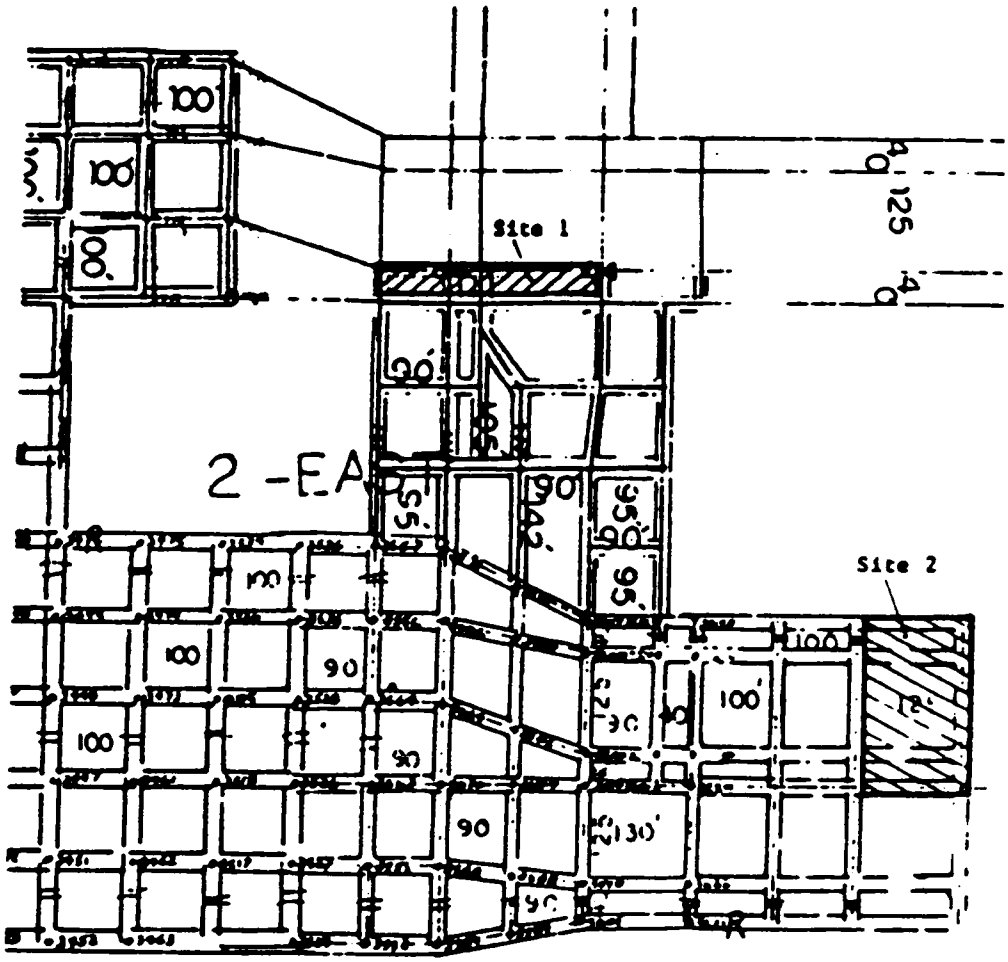


**Figure 4.1 Monitoring Sites**

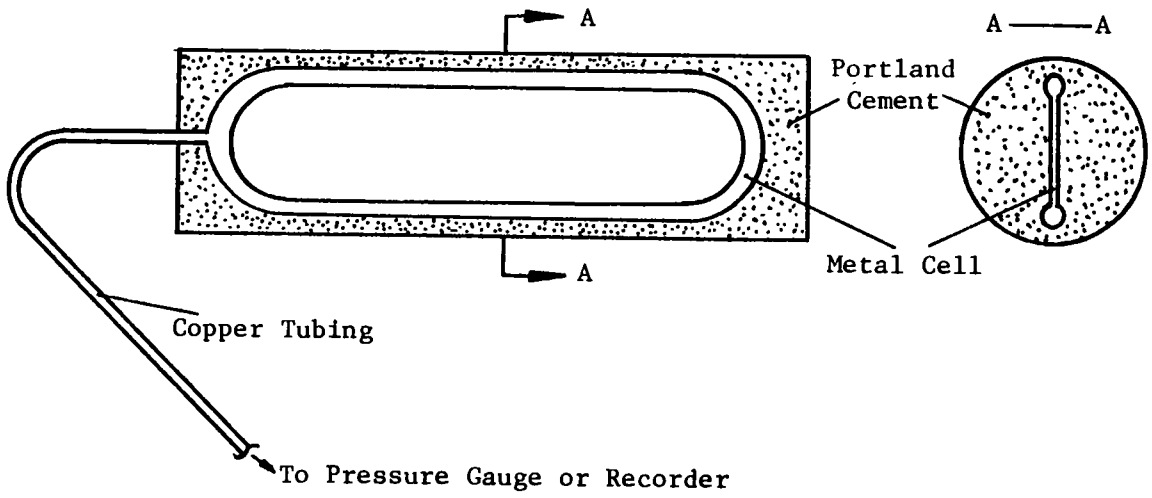


**Figure 4.2 Structure of a BPC Cell**

in one direction only, which is the direction perpendicular to the flat cell. The cells were then pressured up to approximately 3000 psi with a hand pump. The setting pressure was considered higher than estimated pillar loading pressure. With copper tubing, the cells were connected to automatic recorders, as shown in Figure 4.3, which could record up to seven days of data without interruption. Figure 4.4 shows a borehole into which a cell was inserted and connected to copper tubing leading to the recorder.

Roof-floor convergences, horizontal pillar dilations and roof sags were monitored by a number of monitoring stations. A typical set-up is diagrammed in Figure 4.5. Bolts of 7/16 of an inch by 1 inch were installed in the roof and the floor as convergence points. The convergences were measured with a convergence pole as shown in Figure 4.6. A dial-gauge, which could be read with an accuracy of 1/1000 of an inch, was installed on the convergence pole. Pins with a length of 1.5 feet were fixed on the pillar ribs as dilation points. A dilation station consisted three pins in a vertical line, as shown in Figure 4.5. The horizontal pillar dilations were monitored by hanging a plumb bob from the roof convergence point and measuring the horizontal distance between the plumb bob string and the dilation points. These readings were also taken weekly. Roof sags were inspected by leveling. The leveling was referenced to a monument point, which had a sufficient distance from the working face and was considered stable. The leveling was conducted bi-weekly.

A total of nineteen hydraulic cells, forty two pairs of convergence points (roof and floor points), and twenty four dilation stations were installed. Figure 4.7 shows the monitoring plan for Site 1 and Figure 4.8 for Site 2. The dotted line in both figures indicates entries to be excavated. The hydraulic cells were inserted into the coal seam before the

**Figure 4.3 Automatic Pressure Recorder**

**Figure 4.4 Pressure Cell Borehole**

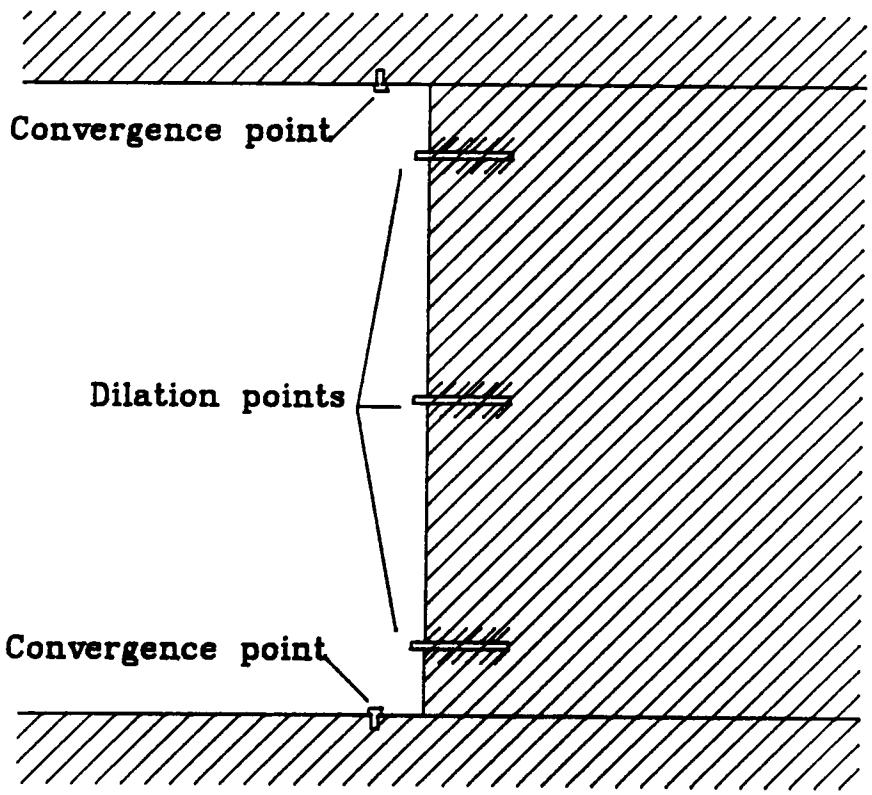


**Figure 4.5 Monitoring Sation Set-up**

**Figure 4.6 The Convergence Pole**

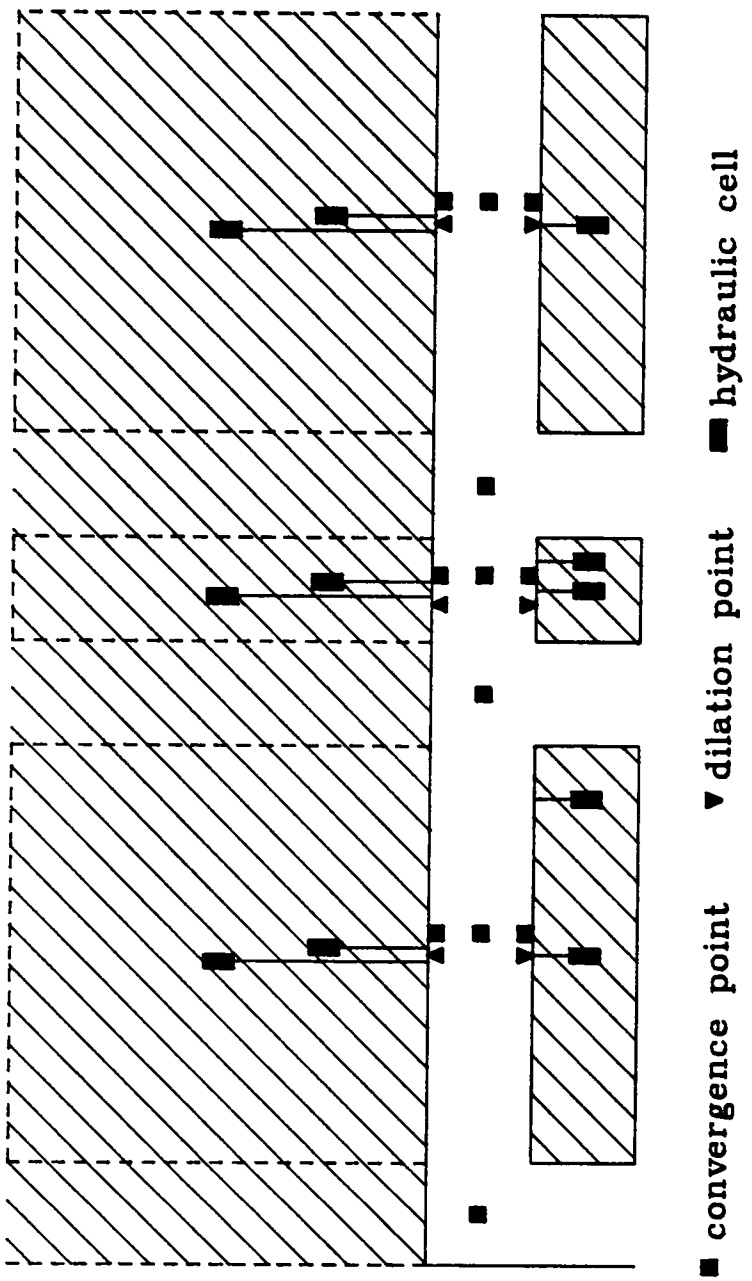


Figure 4.7 Monitoring Plan for Site 1

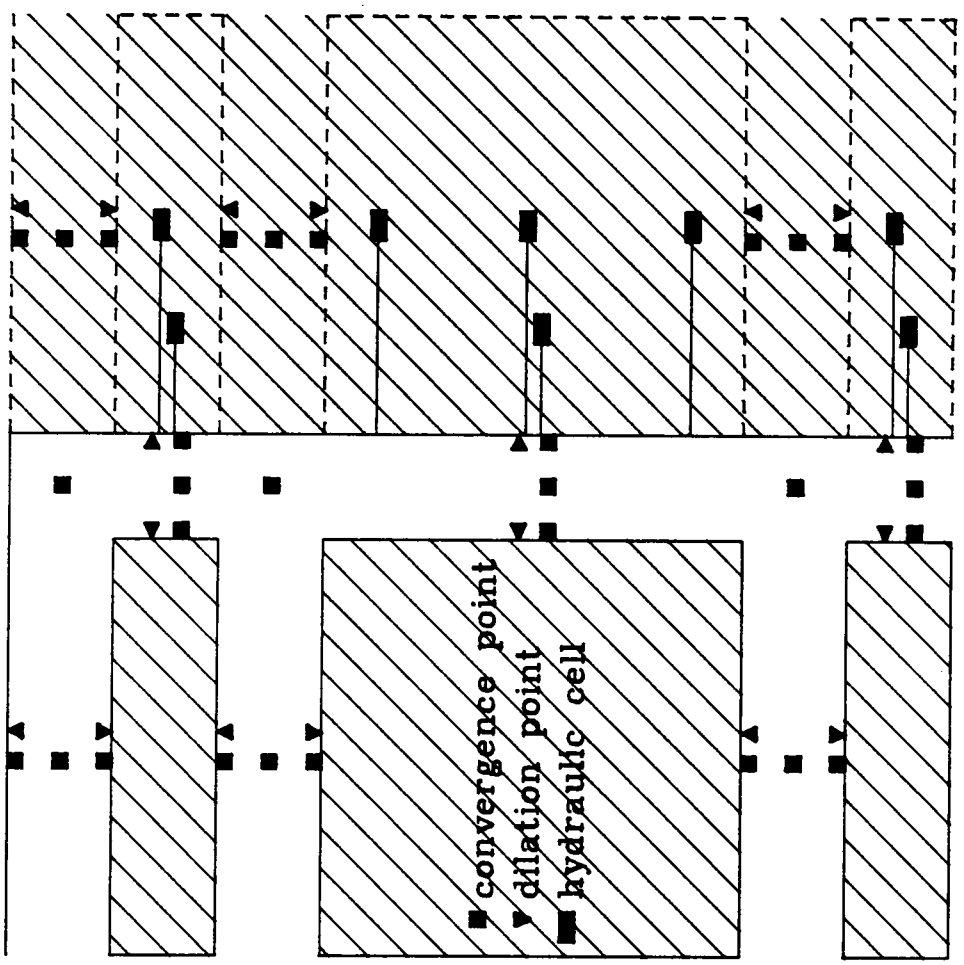


**Figure 4.8 Monitoring Plan for Site 2**

pillars were made so that the pillar stress distribution could be better observed during the excavation period.

### *4.1.3 Monitoring Results and Discussion*

The monitoring at Site 1 was not very successful. Some of the hydraulic cells failed. In addition, shortly after the measurement started, the mine unexpectedly cut an overcast through Site 1 and a few more hydraulic cells had to be removed, as well as some convergence points. The data obtained from Site 1 was incomplete and could not be used for any serious analysis. The following discussion will therefore focus only on Site 2.

Figures 4.9 through 4.14 show the hydraulic cell pressure readings. Cell No. 1 and Cell No. 7, which were installed at yield pillar centers, exhibited a pressure increase up to approximately 6,500 psi and then kept approximately constant at that level. It was noticed that the pressure in Cell No. 1 increased more rapidly than that in Cell No. 7. This was because Cell No. 1 was closer to the working face starting point and was affected earlier than Cell No. 7. The pressure patterns in Cell No. 1 and Cell No. 7 indicated that the two yield pillars did not yield completely. The high stress at the center of the pillar was not yet released. Cell No. 8 had a similar location in the yield pillar as Cell No. 1. However, Cell No. 8 displayed a different pressure pattern. It increased up to 6,000-7,000 psi before gradually dropping down to approximately 3,500 psi. This can possibly be accounted for by the fact that some coal spalling occurred on the yield pillar rib near the location of Cell No. 8. This spalling caused the yield zone to extend to the Cell No. 8 position. Since the cell was in the yield zone, the cell pressure showed a stress release pattern. The cell pressures in the stable pillar showed a symmetric pattern. Cell No. 3 and Cell No. 6, which were both located approximately 10 feet from the pillar rib, ex-

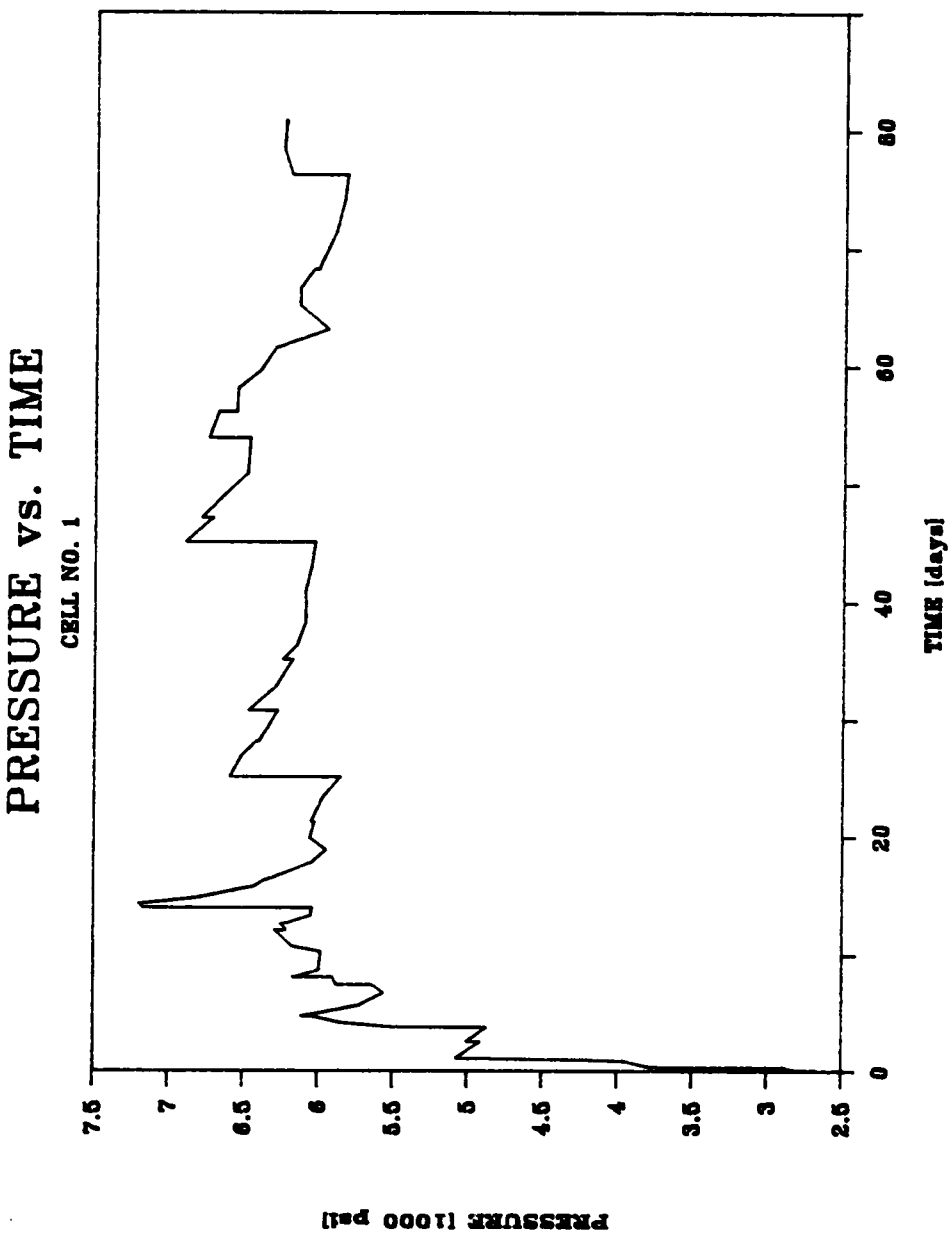


Figure 4.9 Pressure Curve of Cell No. 1

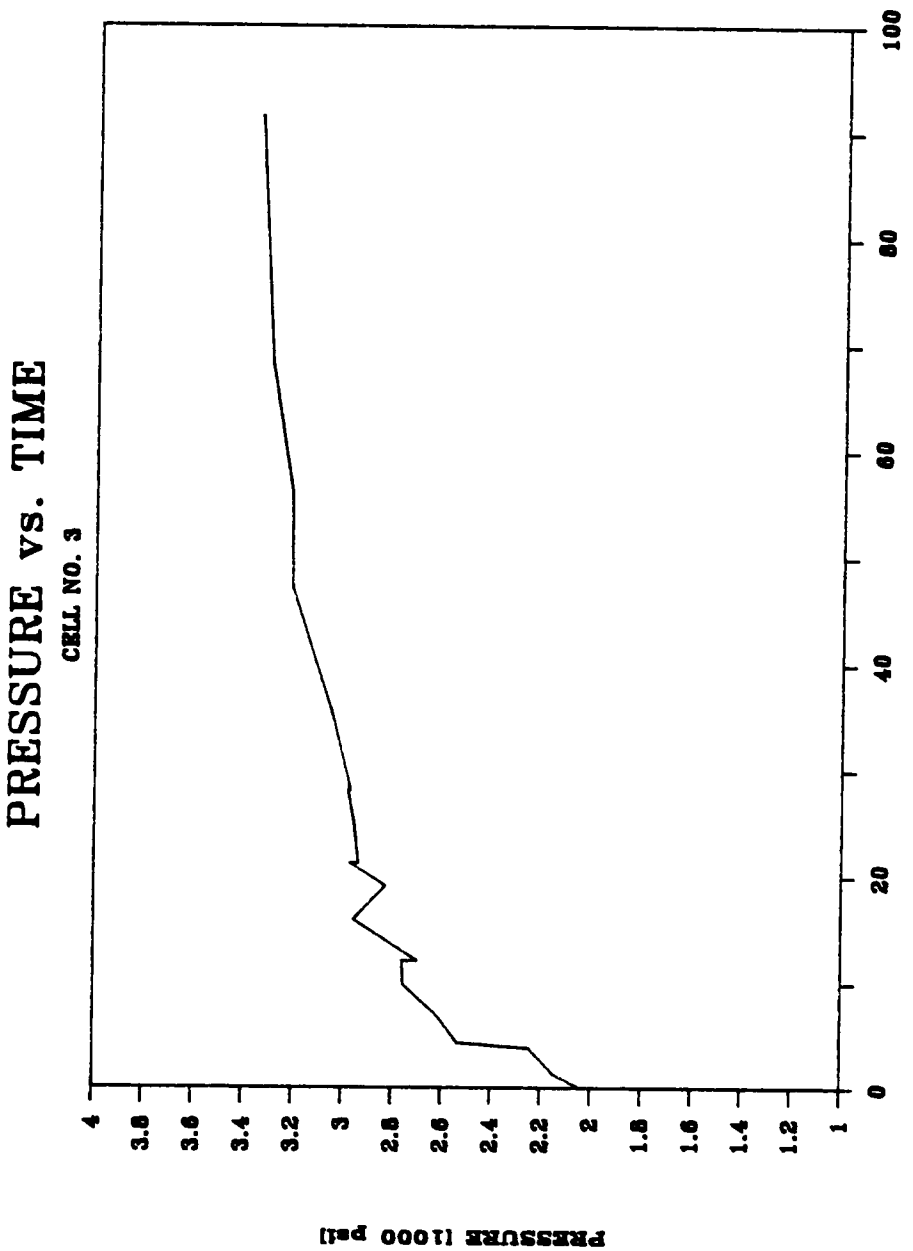


Figure 4.10 Pressure Curve of Cell No. 3

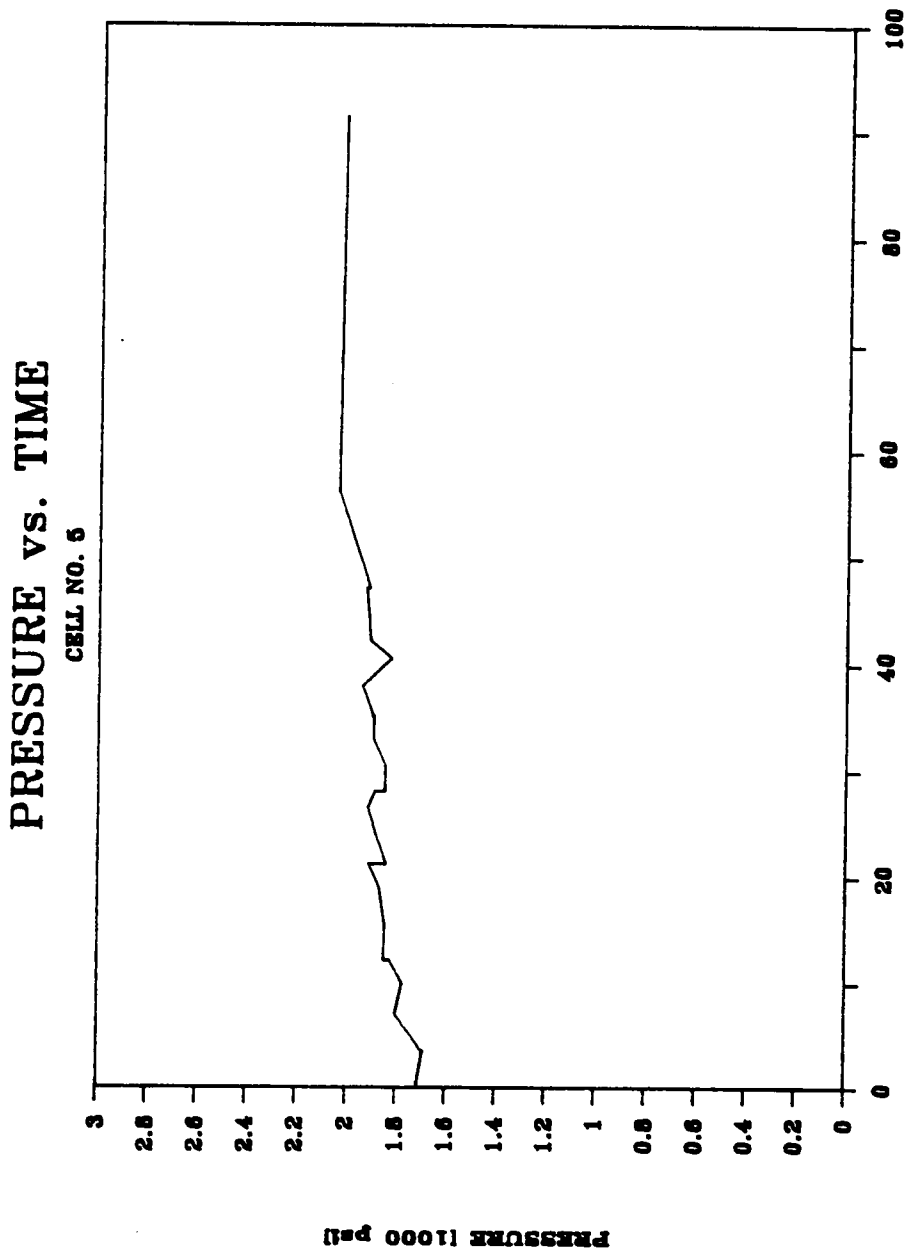


Figure 4.11 Pressure Curve of Cell No. 5

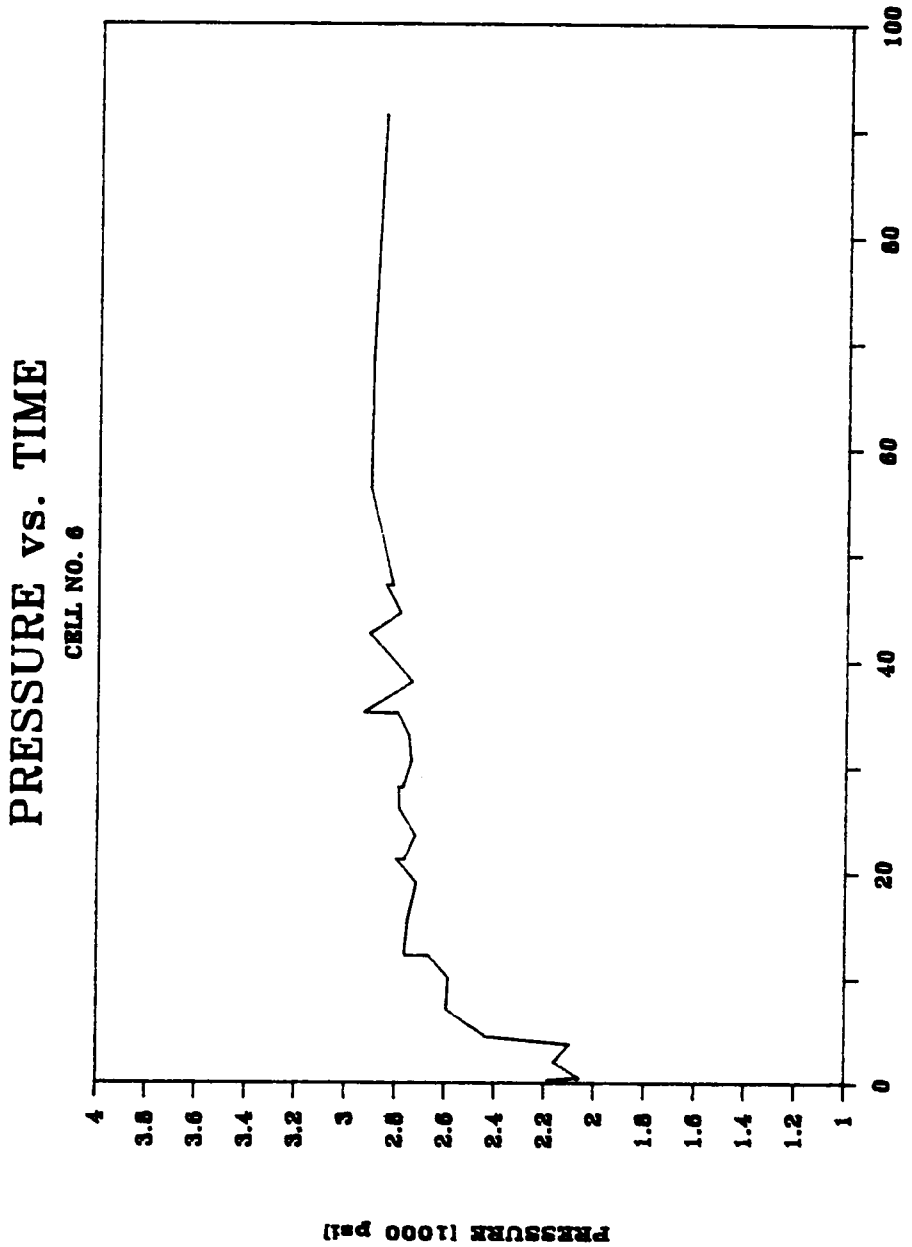


Figure 4.12 Pressure Curve of Cell No. 6

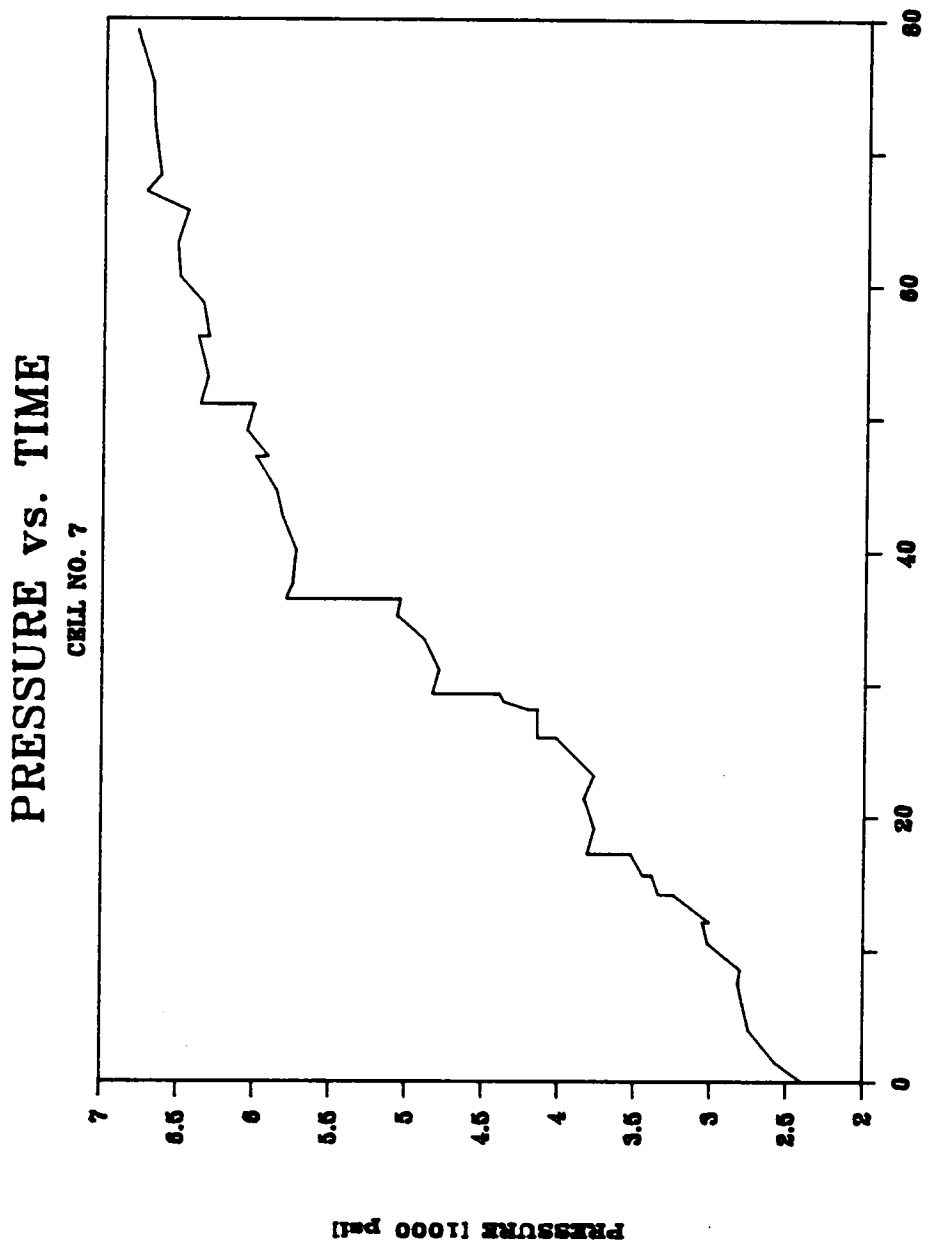


Figure 4.13 Pressure Curve of Cell No. 7

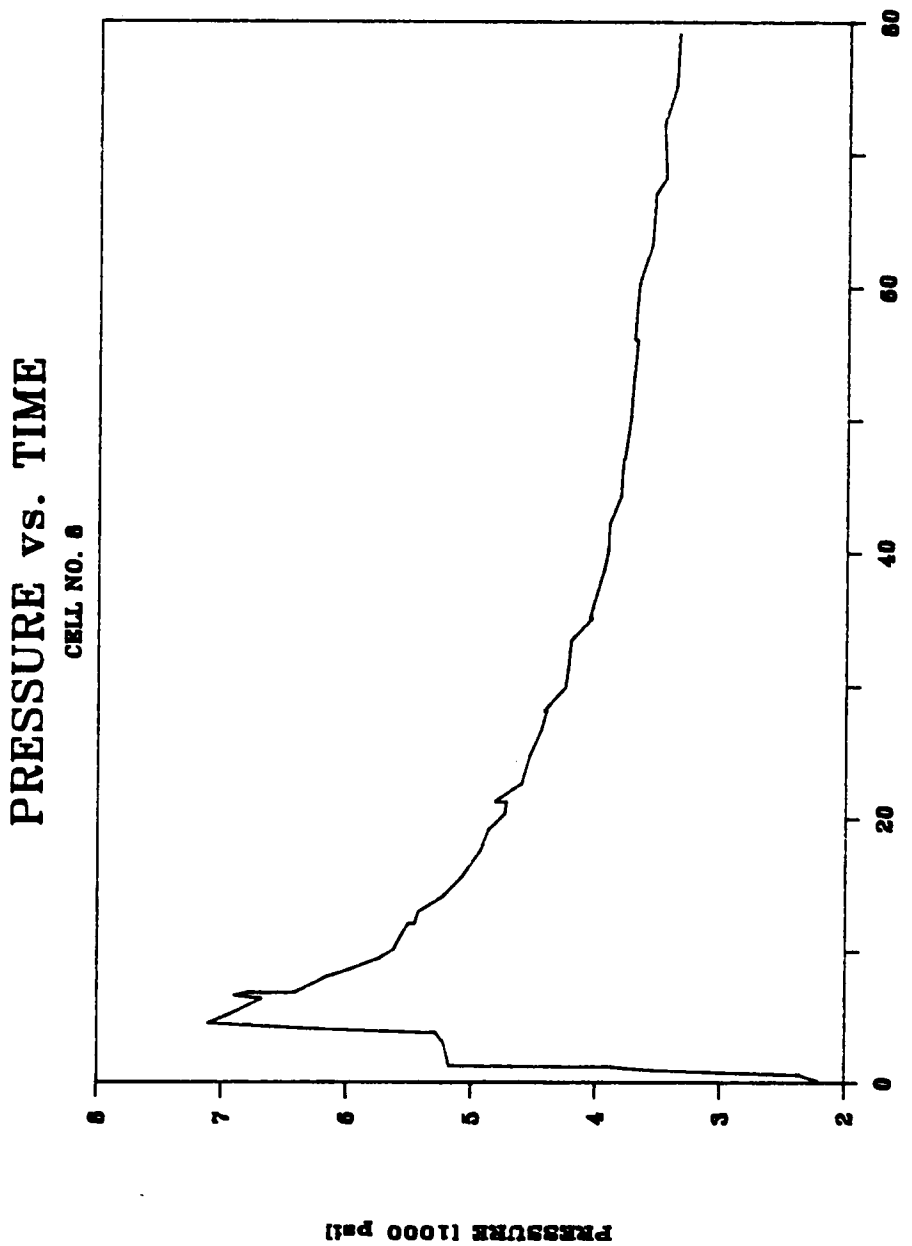


Figure 4.14 Pressure Curve of Cell No. 8

hibited similar pressures in the vicinity of 3,000 psi. By comparison, Cell No. 5, which was located in the center of the stable pillar, showed a relatively lower pressure of 2,000 psi. This pattern clearly indicated that the stable pillar center was in the intact condition and that no yielding occurred in the center part of the stable pillar.

Cells No. 2 and No. 4 failed shortly after the excavation started and no useful data were gained from these two cells.

The hydraulic cells had remained in the pillars for several months and had reached equilibrium pressures. These values, however, did not represent the true stresses in the pillars. Some transformation had to be performed to obtain valid pillar stress measurements. As suggested by Lu (1986), vertical pillar stress can be calculated by using the following equation:

$$F = \frac{P_e}{\sigma_v + S\,\sigma_h} \tag{4.1}$$

where:

F = a factor depending on the composite modulus of coal and cell material;

$P_e$ = cell equilibrium pressure;

$\sigma_v$ = vertical stress;

$\sigma_h$ = horizontal stress; and

S = a factor depending on the cell geometry.

Factors F and S were not tested in this study. However, Lu used the same type of hydraulic cells as used in this study and conducted underground instrumentation in a West Virginia coal mine. The values for the study were F=0.93 and S=0.185. Since the measurements in this monitoring program were performed in the same Appalachian coal

field, these two values were adopted as an approximation. In addition, the horizontal stress $\sigma_h$ was assumed to be:

$$\sigma_h = \frac{\mu}{1-\mu}\sigma_v \tag{4.2}$$

where $\mu$ is Poisson's ratio for coal.

By substituting the values of F and S into Equation 4.1 and considering Equation 4.2, the pillar vertical stresses were calculated as illustrated in Table 4.1.

Figures 4.15 and 4.16 present typical curves of the roof-floor convergence versus the face advance distance. As illustrated, the largest convergences in both cases occurred at the yield pillar side and the smallest at the stable pillar side. Further examination found that the value of the convergence at the entry center was closer to that at the yield pillar side than to that at the stable pillar side.

Some rock samples from the monitoring site were tested in the laboratory for mechanical properties. The roof and floor were tested previously by the mining company and found to have an average uniaxial strength of 19,800 psi (laboratory value) and a triaxial factor of 2.0. In this study, a number of coal specimens were taken from the mining site and triaxial tests were performed. Cylindrical specimens with a diameter of 2 inches were used. Tests were conducted at five different confining pressures, which were 300 psi, 500 psi, 900 psi, 1,500 psi and 2,000 psi respectively. Since the specimens were not cut with an exact length-to-diameter ratio of 2, the following well-accepted converting equation was used to convert the tested values to the standard values of two-to-one ratio samples:

**Table 4.1. Pillar Vertical Stresses**

| Location | Yield Pillar Center (No.1) | Yield Pillar Center (No.7) | Stable Pillar Center (No.5) | 10′ from Rib (No.3) | 10′ from Rib (No.6) |
|---|---|---|---|---|---|
| Stress | 6100 psi | 6600 psi | 2050 psi | 3300 psi | 2820 psi |

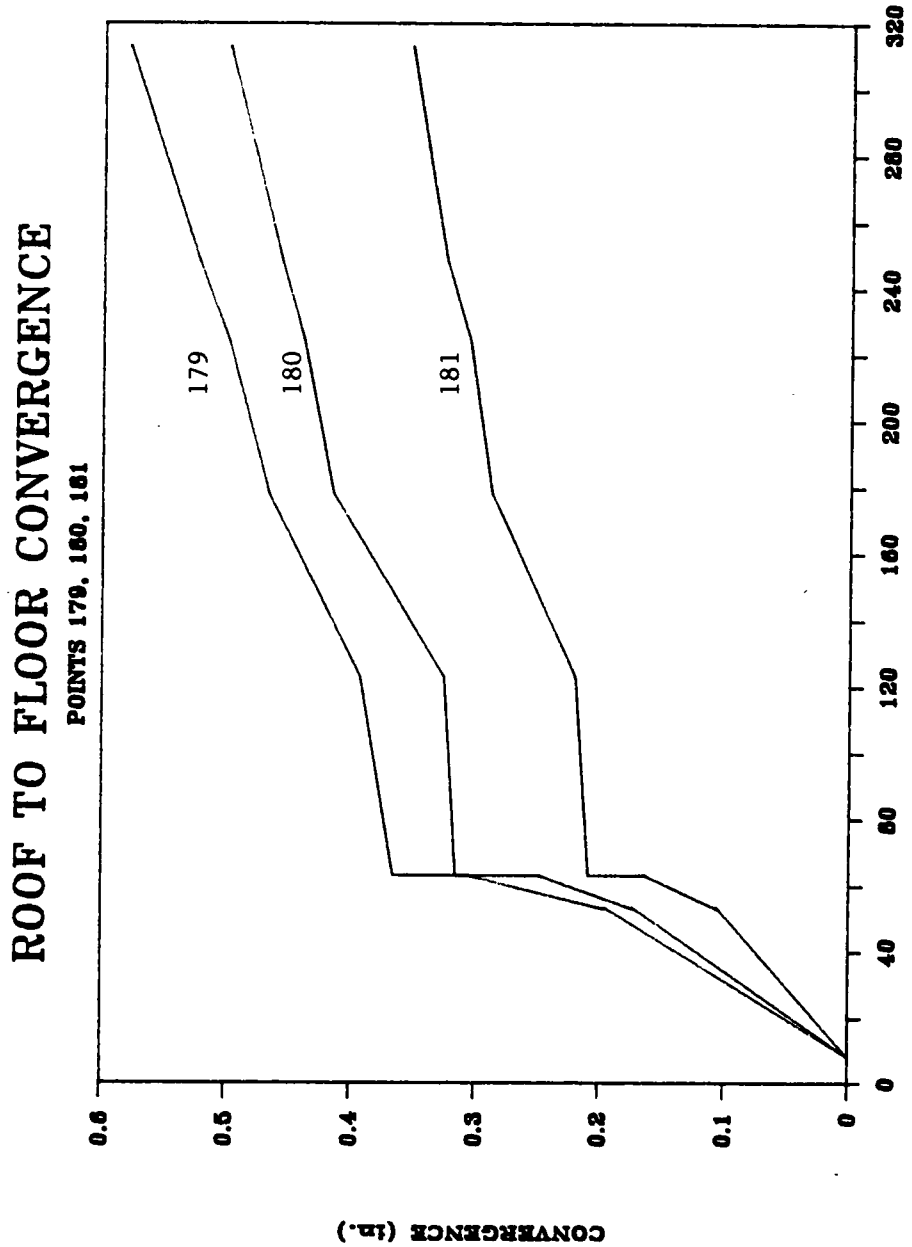


Figure 4.15 Roof-Floor Convergence Curve I

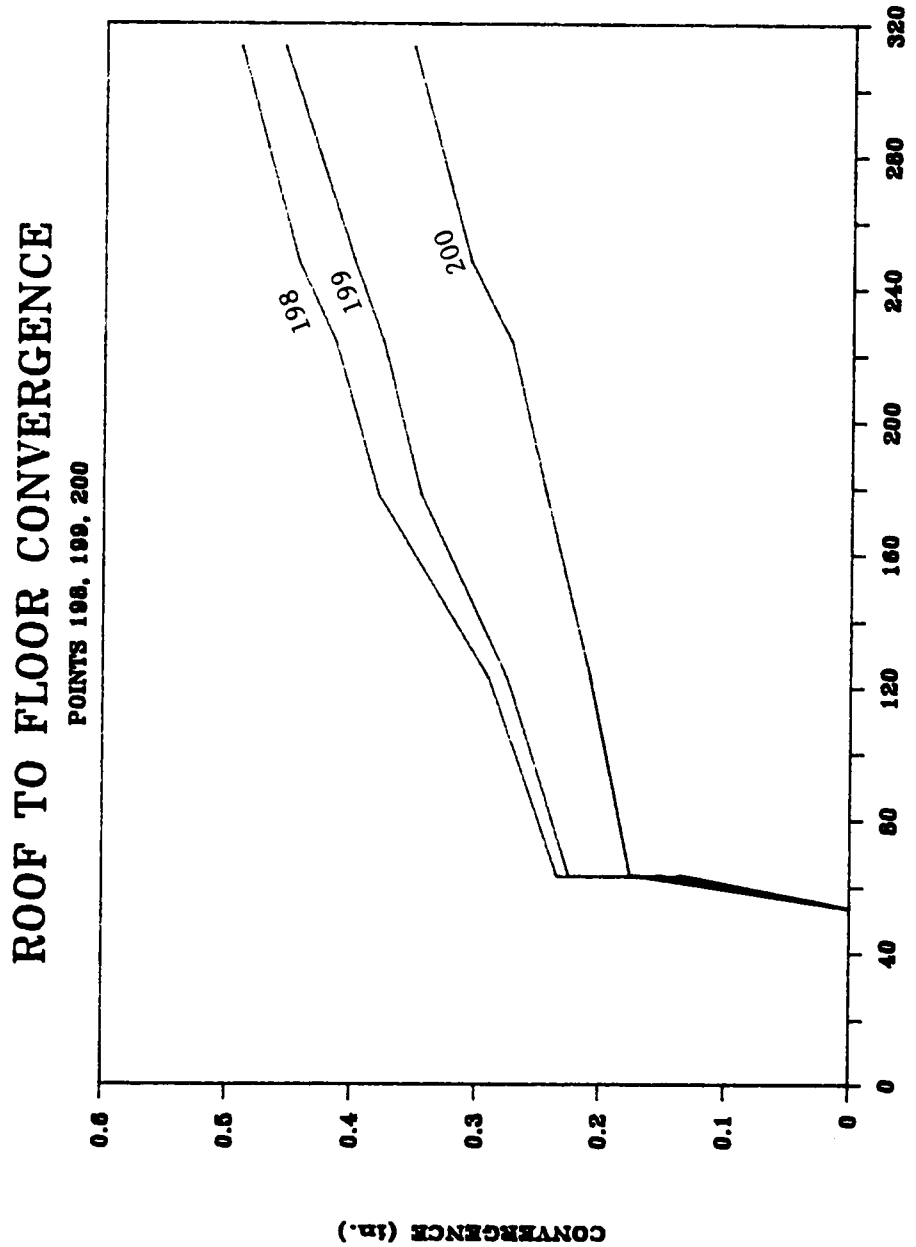


Figure 4.16 Roof-Floor Convergence Curve II

$$\sigma_{1/2} = \frac{0.889 \times \sigma_{D/L}}{0.778 + 0.222 \frac{D}{L}} \tag{4.3}$$

where:

$\sigma_{1/2}$ = strength of two-to-one ratio specimen;

$\sigma_{D/L}$ = tested sample strength;

D = diameter of the specimen; and

L = length of the specimen.

The converted results are plotted in Figure 4.17. Linear regression analysis was performed on the data. As a result, the following equation was obtained with $R^2 = 0.869$:

$$\sigma = 1870 + 3.71 \times \sigma_3 \tag{4.4}$$

where:

$\sigma$ = coal strength (psi); and

$\sigma_3$ = confining pressure (psi).

## 4.2 Comparison of Field Data and Finite Element Models

In order to examine the applicability of the finite element models to the analysis of the load and displacement in coal pillars, the models were compared with the field-observed data. Two-dimensional analysis of Site 2 was conducted utilizing the finite element models developed above. Site 2 had a yield-stable-yield pillar pattern with three yield pillars, two stable pillars and six entries in a row, as shown in Figure 4.1. The yield pillars were 20 feet, the stable pillars 100 feet, and the entries 20 feet wide. Since the configuration was symmetrical, only half of it was modeled. A 2-D finite element mesh was

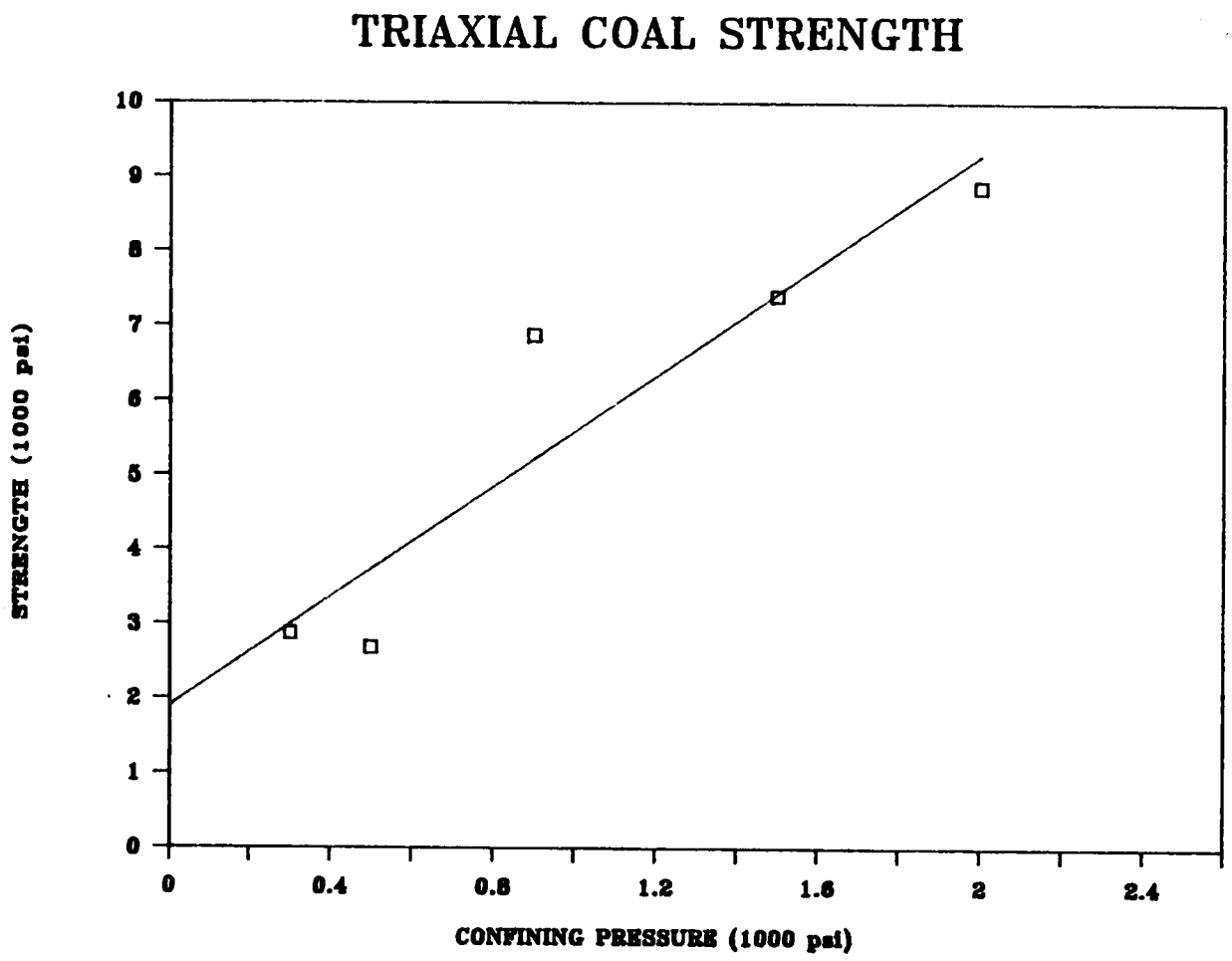


Figure 4.17 Triaxial Coal Strength

constructed as shown in Figure 4.18. The mesh consisted of 417 elements and 491 nodes. In order to better simulate pillar yielding phenomena, smaller elements were used for the yield pillars and for the stable pillar ribs. The coal seam was divided into two layers with each layer being three feet thick. For the yield pillars and the stable pillar ribs, an element size of 2.5 by 3.0 feet was used. The boundary condition on the symmetrical line, which is on the right side of the mesh, was set to allow vertical movement only, as indicated by the rollers in the mesh plotting. Because of the symmetry, no horizontal displacement was assumed to exist on the symmetrical line. Since there was no information available from the mining site about the horizontal stress condition, the horizontal stress was assumed to be one half of the cover load in the simulation. The material properties used in the finite element models are listed in Table 4.2. In the table, the laboratory uniaxial strength of coal has been reduced by a factor of 1/5, and the roof and floor rock 1/2 to 1/5 to accommodate the in-situ conditions. The factor 1/2 has been applied to the uniaxial strength of bolted roof rock, which was considered to be reinforced by the roof bolts. Two different approaches discussed in Chapter 3 for non-linear simulations, namely the successive iteration model (S.I.M) and the elastic-plastic model (E.P.M.), were both used in the modeling. The stresses computed by the two models are presented in Table 4.3 and compared with the observed values. The stresses calculated by the progressive failure method (P.F.M.) are also listed in Table 4.3 for comparison.

These results demonstrate that values derived from both finite element models agreed reasonably well with the observed values. Both models estimated the same yield zone width (7.5 feet), which was close to that estimated by the P.F.M. (8.75 feet). The progressive failure method predicted a yield pillar peak stress of 6,700 psi, which was close to the observed value of 6,100. The S.I.M. model predicted a yield pillar peak stress slightly higher than the E.P.M. model, but both values were lower than those observed.

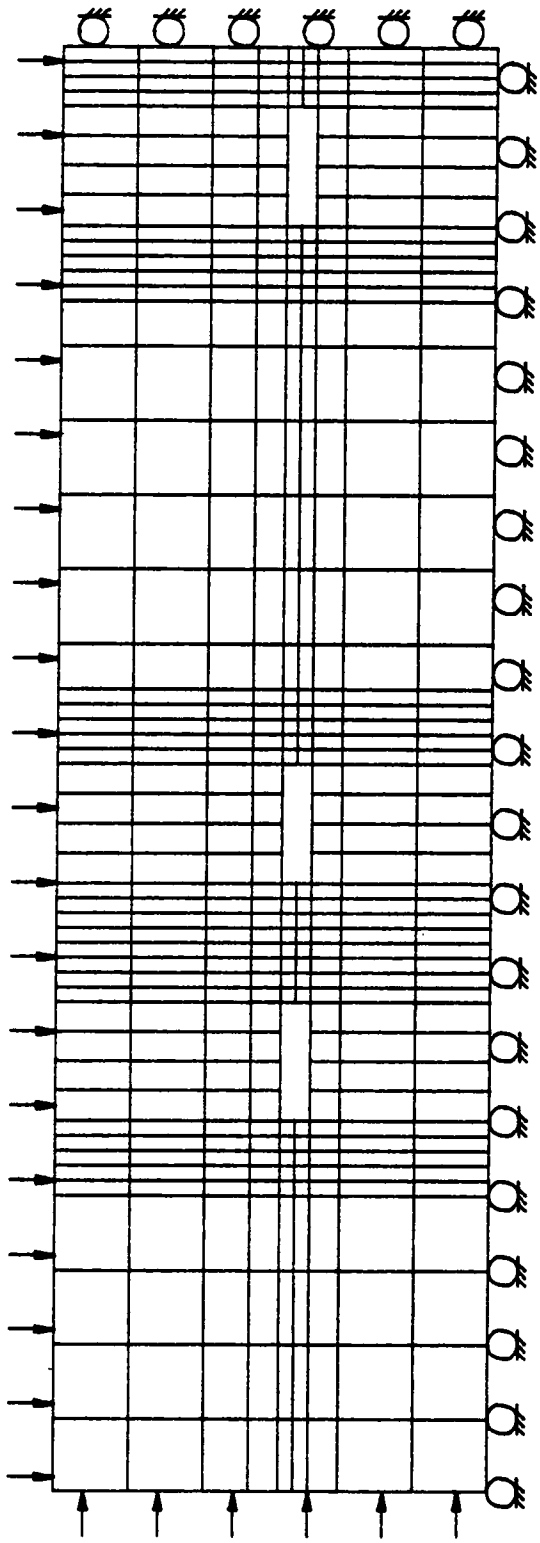

Figure 4.18 Finite Element Mesh for Site 2

**Table 4.2. Material Properties**

| | |
|---|---|
| Elastic Modulus (Coal) | 350,000 psi |
| Elastic Modulus (Roof & Floor) | 4,200,000 psi |
| Uniaxial Strength (Coal) | 370 psi |
| Uniaxial Strength (Roof & Floor) | 3960 psi |
| Uniaxial Strength (Bolted Roof) | 9900 psi |
| Triaxial Factor (Coal) | 3.71 |
| Triaxial Factor (Roof & Floor) | 2.00 |
| Poisson's Ratio (Coal) | 0.34 |
| Poisson's Ratio (Roof & Floor) | 0.20 |

**Table 4.3. Stress Comparison**

| | Measured | P.F.M. | S.I.M. | E.P.M. |
|---|---|---|---|---|
| Width of Yield Zone | -- | 8.75 ft. | 7.50 ft. | 7.50 ft. |
| Yield Pillar Peak Stress (No. 1) | 6100 psi | 6700 psi | 5200 psi | 4600 psi |
| Stable Pillar Peak Stress (No. 3) | 3300 psi | 6700 psi | 3800 psi | 3500 psi |
| Stable Pillar Center Stress (No. 5) | 2050 psi | -- | 2300 psi | 2300 psi |
| Stable Pillar Peak Stress (No. 6) | 2820 psi | 6700 psi | 3700 psi | 3400 psi |
| Yield Pillar Peak Stress (No. 7) | 6600 psi | 6700 psi | 5100 psi | 4500 psi |

The reason may be that the peak stress values from the finite element models were an average of the stress in two elements having a combined length of five feet. If smaller element mesh had been used, higher values could have been expected. The progressive failure method, however, determined the same peak stress value for the stable pillar as for the yield pillar, which was not observed in the field. On the other hand, the stable pillar stress values calculated by the two finite element models at both the rib and the center points are more accurate than that calculated by the progressive failure method. The S.I.M. model predicted a stress value at the stable pillar rib slightly higher than that predicted by the E.P.M. model.

Figures 4.19 and 4.20 display the stress profiles produced by the two finite element models, and compared with the observed values and with the profile generated by the progressive failure method. The stress profile generated by the S.I.M. model was very similar to that by the progressive failure method. The stress profile generated by the E.P.M. model, however, was slightly different, especially as regarded the stress distribution in the yield zone. This will be further discussed in Chapter 6.

The convergences estimated by the elastic-plastic model are listed in Table 4.4 and compared with the values observed in the field. All of the predicted values are obviously higher than those which were observed. This is due to a delayed setting-up of monitoring stations. The stations were able to be installed only after the opening was excavated. By that time, some initial convergence had already occurred. The observed convergence thereafter was evidently smaller than the total convergence. Taking a close look at these values, however, one may notice that the observed values have the same pattern as do the predicted ones. The highest value occurs at the yield pillar side and the lowest at stable pillar side. In addition, the convergence at the entry center is much closer to that

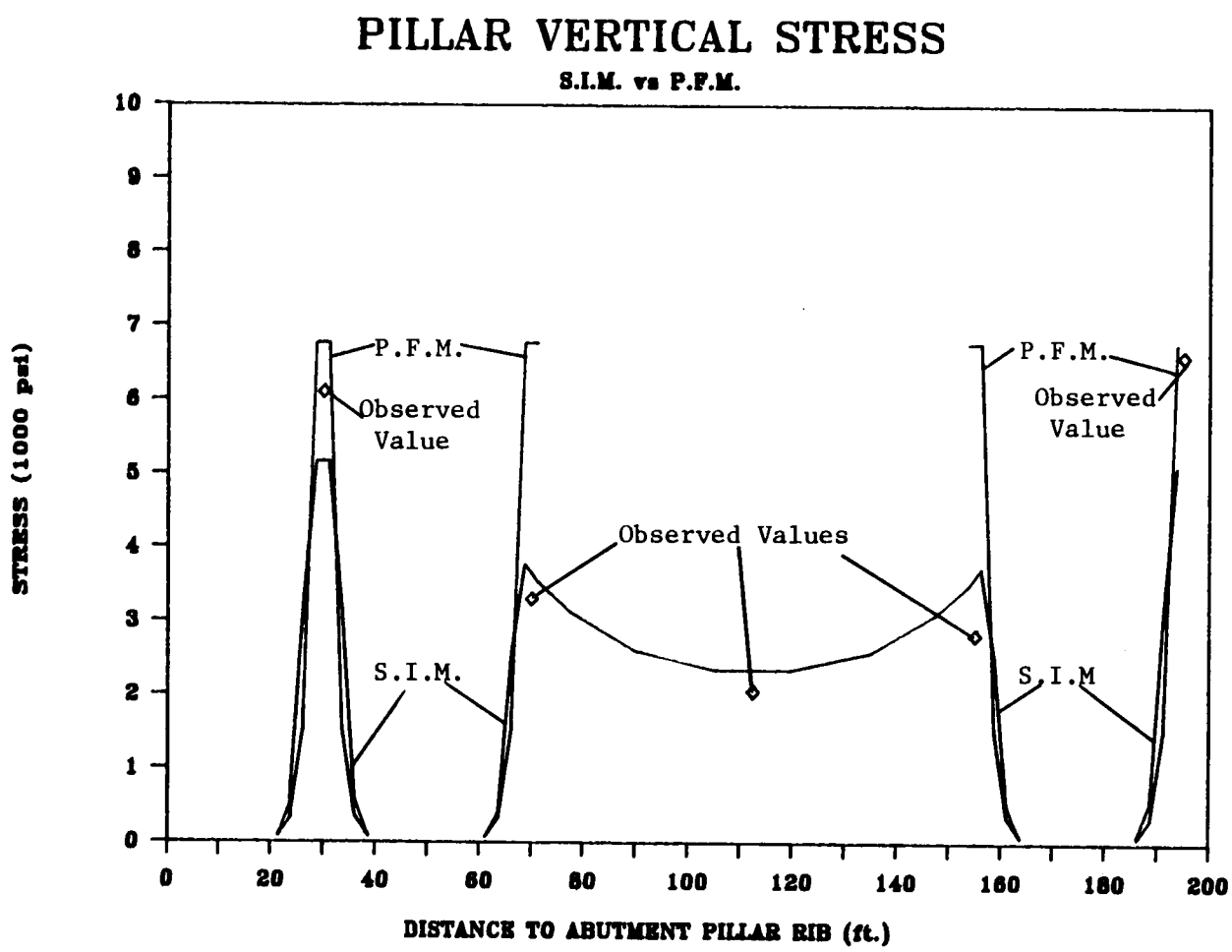


Figure 4.19 Stress Profile Comparison I

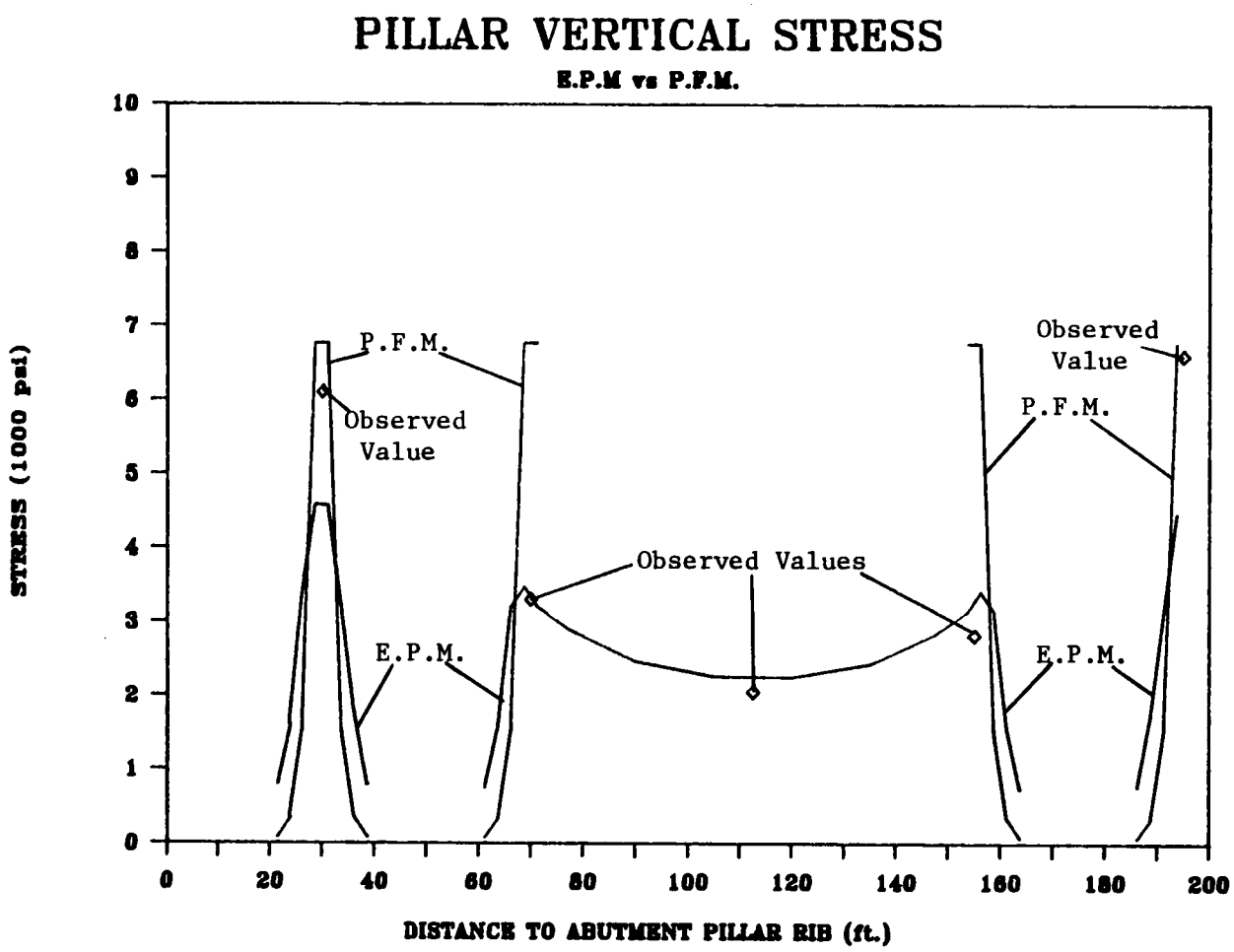


Figure 4.20 Stress Profile Comparison II

**Table 4.4. Convergence Comparison**

| | Measured (in.) | S.I.M. (in.) | E.P.M. (in.) |
|---|---|---|---|
| Stable Pillar Side (Pt. 181) | 0.363 | 0.92 | 0.82 |
| Entry Center (Pt. 180) | 0.502 | 0.97 | 0.86 |
| Yield Pillar Side (Pt. 179) | 0.578 | 0.98 | 0.87 |
| Yield Pillar Side (Pt. 198) | 0.494 | 0.98 | 0.86 |
| Entry Center (Pt. 199) | 0.470 | 0.97 | 0.85 |
| Stable Pillar Side (Pt. 181) | 0.367 | 0.92 | 0.81 |

observed at the stable pillar side. It can be concluded that the elastic-plastic finite element model provides a reasonable estimation of the roof-floor convergences.

In general, the finite element models proved to yield adequate predictions of stresses and displacements around underground openings and coal pillars. Since the elastic-plastic model was considered to simulate continuous mining sequences better, as discussed in Chapter 3, this model was utilized in the investigation of different pillar layouts at different mining stages.

# CHAPTER 5: ANALYSIS OF LONGWALL ENTRY LAYOUTS AND PARAMETRIC STUDIES

## 5.1 Longwall Entry Layout Analysis

In order to investigate the performance of different longwall entry layouts, especially the suitability of yield pillars for longwall entries, three different entry layouts were simulated utilizing the elastic-plastic finite element model developed in Chapter 3. Three and four entry designs, commonly used in practice, were examined in the study and included a yield-stable-yield (y-s-y) four-entry pillar system, a total stable (s-s) three-entry pillar system and a total yield (y-y) three-entry pillar system, as shown in Figure 5.1.

Longwall chain pillars are subject to dynamic loading conditions. As the longwall face advances, an abutment pressure is formed in front of the face and on either side of the longwall panel. The abutment pressure travels along with the longwall face and exerts

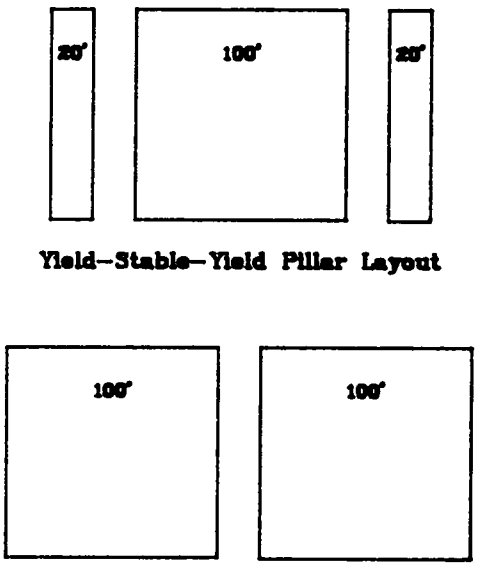


Figure 5.1 Three Pillar Layouts

additional load on the pillars as it progresses. A pillar in the longwall entry is, therefore, affected by different loading stages. To examine the performance of a pillar in the longwall entry, the condition of the pillar has to be tested at different mining stages, i.e. at different distances from the longwall face. In order to accomplish this, a three-dimensional model may seem appropriate. Such modeling, however, is costly and time-consuming. In dealing with yield pillars, it is necessary to observe the yielding process of a pillar, and very dense finite element meshes requiring even more computing time must be constructed. As a result, three-dimensional modeling of yield pillars is rather impractical.

In order to overcome the difficulties in simulating underground mining structures using 3-D models, while still developing the necessary information, a load augment technique was developed by Pariseau and Sorensen (1979) utilizing a 2-D finite element program. The technique is based upon a simple augmentation of forces in a 2-D analysis to produce the same average pillar stress that would occur in a full 3-D analysis. Comparisons were made between 2-D and 3-D models and the augmented loading procedure appeared to be promising as an efficient and cost-reducing technique for mine pillar design.

Based upon the load augmentation principle, 2-D finite element models were constructed to calculate pillar stresses and roof-floor convergences at different mining stages. The input data were based on those from the mine where the underground monitoring was conducted. In order to consider 3-D effects, a 2-D model was first constructed, representing a cross section along the center line of the longwall panel. The finite element mesh is illustrated in Figure 5.2. The abutment pressure was then calculated with this model, which is shown in Figure 5.3. The graph indicates that the maximum peak pressure was

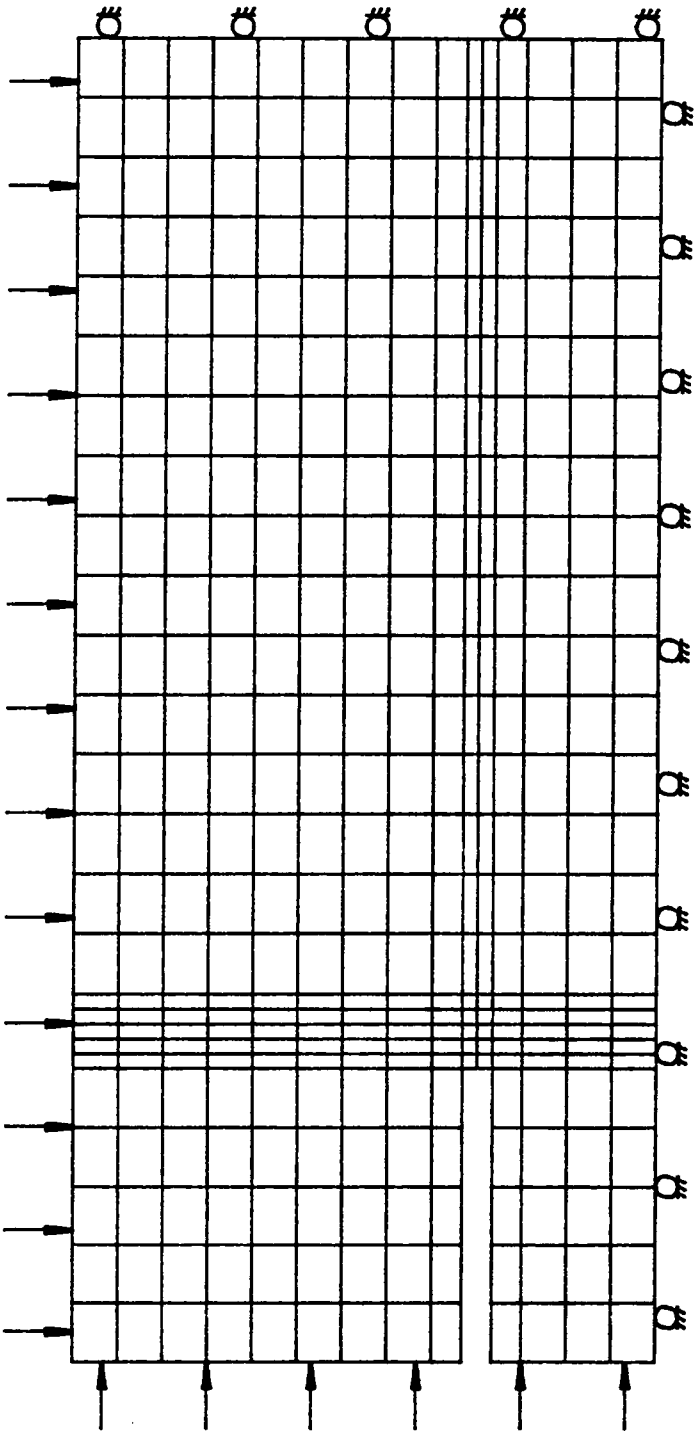

Figure 5.2 Finite Element Mesh for Abutment Pressure Calculation

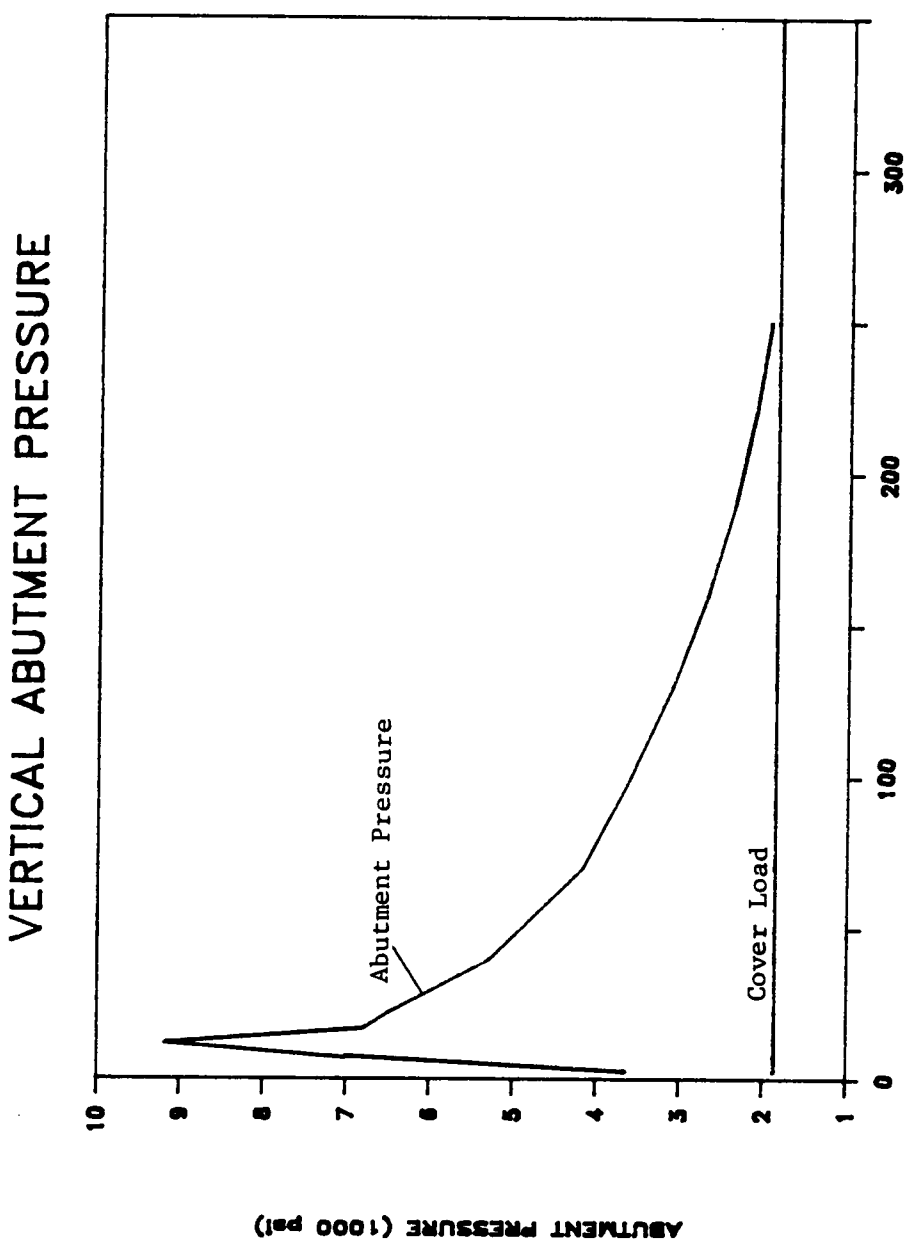


Figure 5.3 Abutment Pressure

about 5 times of the cover load and occurred about 13 feet in front of the face. Typical ranges of abutment pressures have been reported by Peng and Chiang (1984) based on field measurements. Their data indicate the front abutment pressures ranging from 0.2 to 6.4 times the cover load and the maximum pressure occurring from 3 to 20 feet in front of the face. By comparison, the predicted values are well within the empirical ranges.

The stress distribution in and above the coal seam was recorded at three locations, i.e. 200 feet in front of the face, 100 feet in front of the face, and 13 feet in front of the face, the last being where the peak pressure occurred in the seam. The resulting abutment loads were applied to the 2-D models representing three different pillar layouts. Figures 5.4 through 5.6 show the finite element meshs for the y-s-y layout, the s-s layout, and the y-y layout, as well as the corresponding loading conditions. The horizontal stresses in the models were assumed to be one half of the vertical cover load. It can be noticed that, besides the cover load and the initial horizontal stresses, an additional load induced by the abutment pressure was introduced above the longwall panel. The distribution of the stress was arranged according to that calculated by the abutment load model. This additional load varied as the longwall face advanced. At a location 300 feet in front of the face, there was no additional load but only the cover load and the initial horizontal stress. When the face was 200 feet away, additional load was introduced on top of the longwall panel, which increased when the face advanced nearer until the peak stress was reached. The finite element modeling representing each pillar layout was carried out following these sequences. The load was added to the model continuously without re-starting the simulation and the results were recorded after every load addition.

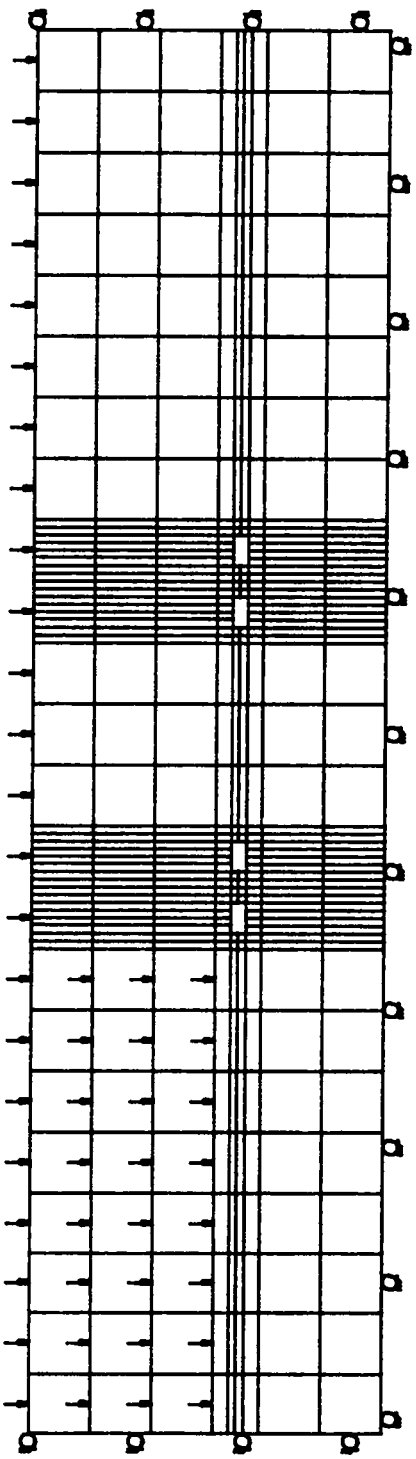

Figure 5.4 Finite Element Mesh for Y-S-Y Layout

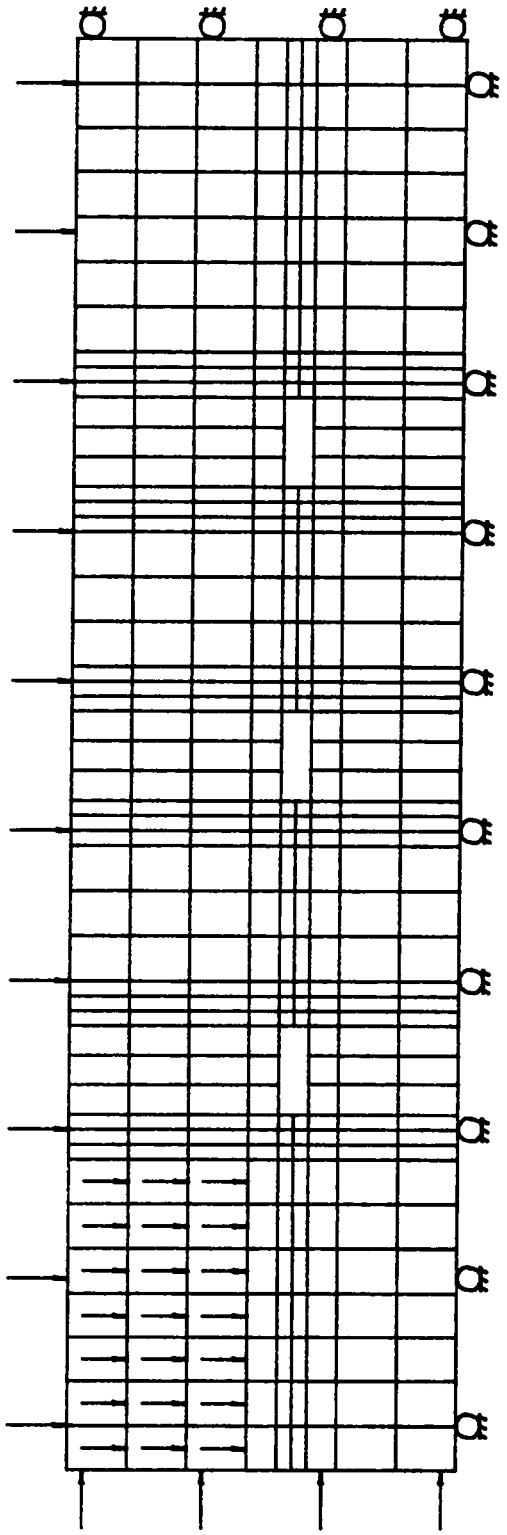

**Figure 5.5 Finite Element Mesh for S-S Layout**

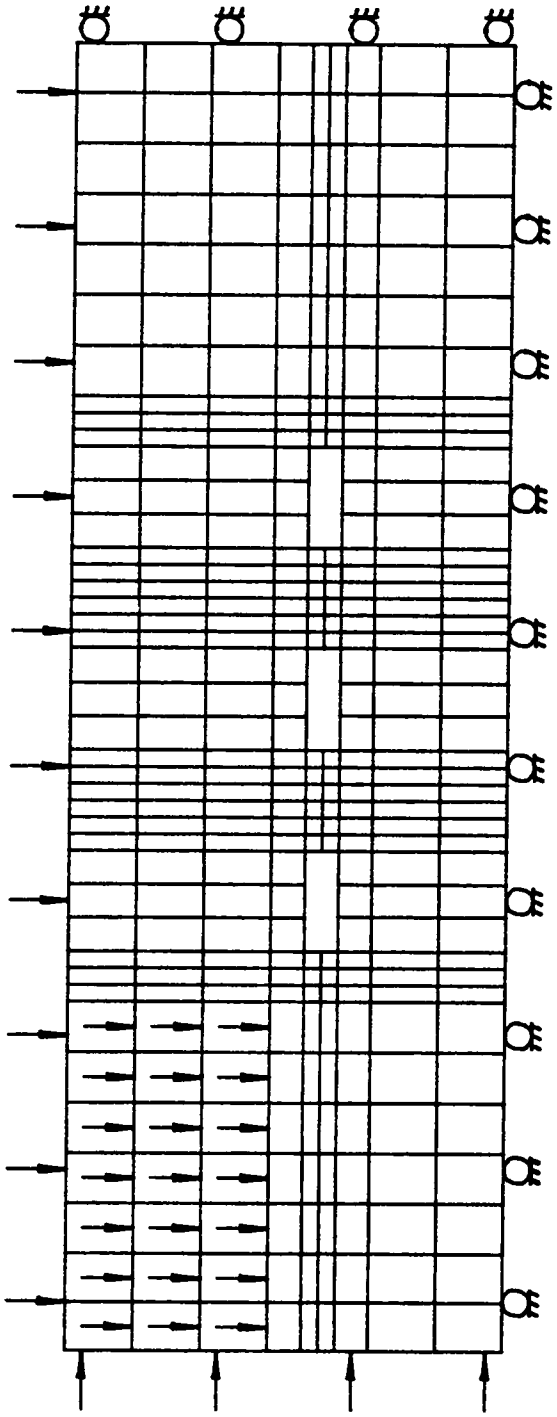

Figure 5.6 Finite Element Mesh for Y-Y Layout

The simulation results indicated that the yield pillars in both the y-s-y layouts and the y-y layout started to yield after they were formed during the excavation period, and that the stable pillars in both the y-s-y and s-s layouts held an elastic core throughout the mining sequence. The calculated vertical stresses in the pillar next to the headgate entry are plotted in Figure 5.7, which reveals that the stresses in the yield pillar layouts were higher than that in the stable pillar layout when there was no influence from abutment pressure. However, the stress in the stable pillar layout increased dramatically when the face approached, producing a high stress concentration. By contrast, the stresses in the yield pillars were kept approximately constant and the high stress was released. Further examination also showed that the pillar stress at the headgate was the lowest when the y-s-y layout was used. The stress in the y-y layout was only slightly higher. However, the modeling results indicated that, in the y-y layout, the roof began to break when the peak abutment stress was reached. On the other hand, when the y-s-y layout was used, roof remained in good condition throughout the mining sequence.

Figure 5.8 illustrates the convergences at the center of headgate entry. The convergences increased as the face advanced. The s-s layout had the lowest value and the y-y layout the highest. The convergence in the y-s-y layout was approximately equal to the average value of the other two.

The vertical stress in the stable pillar of the y-s-y layout is presented in Figure 5.9 and also compared with that of the s-s layout. It demonstrates that the stress in the y-s-y layout was higher when the face was far away. However, the stress in the s-s layout increased more rapidly and exceeded the stress level in the s-y-s layout when the face was passing by.

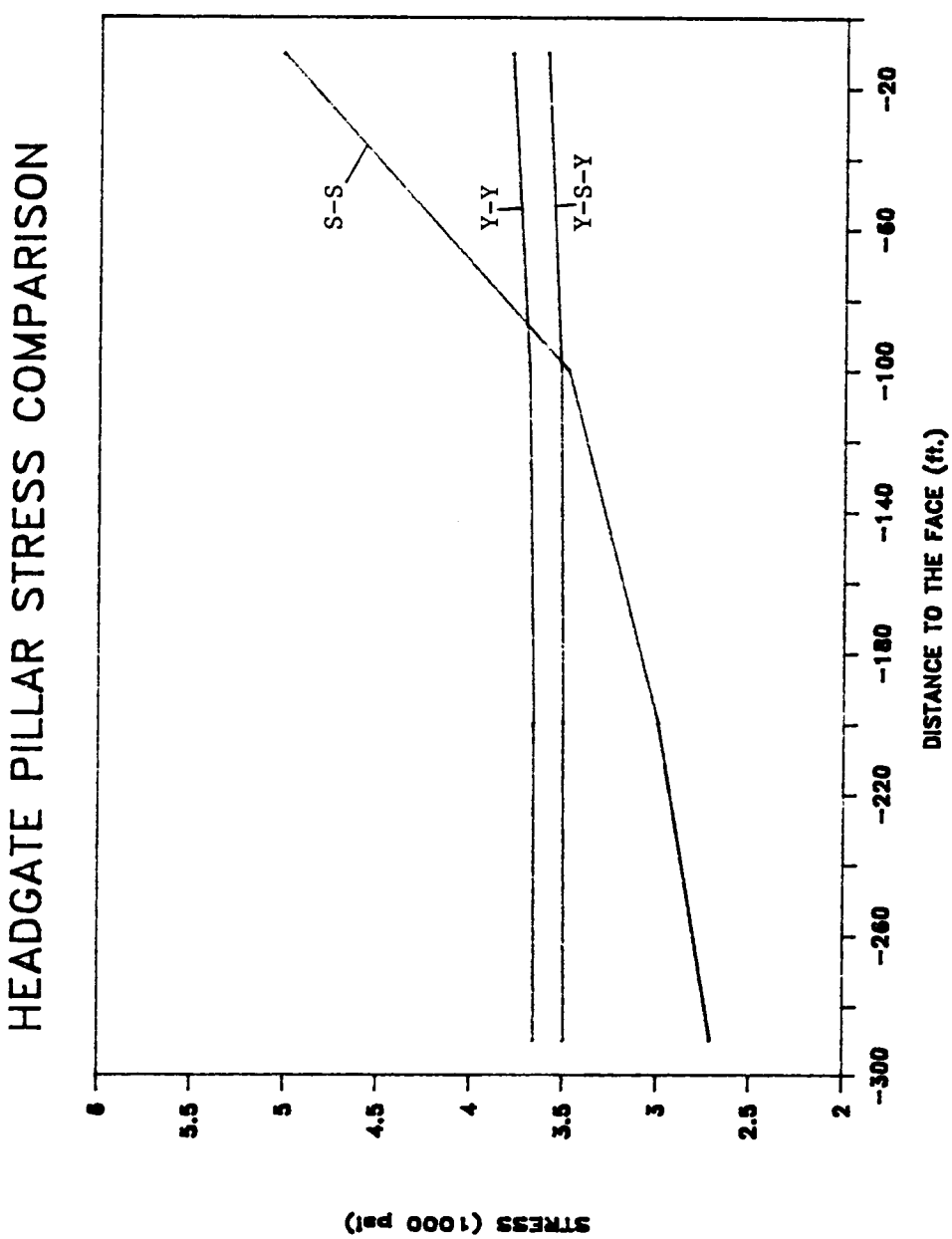


Figure 5.7 Headgate Pillar Vertical Stress Comparison

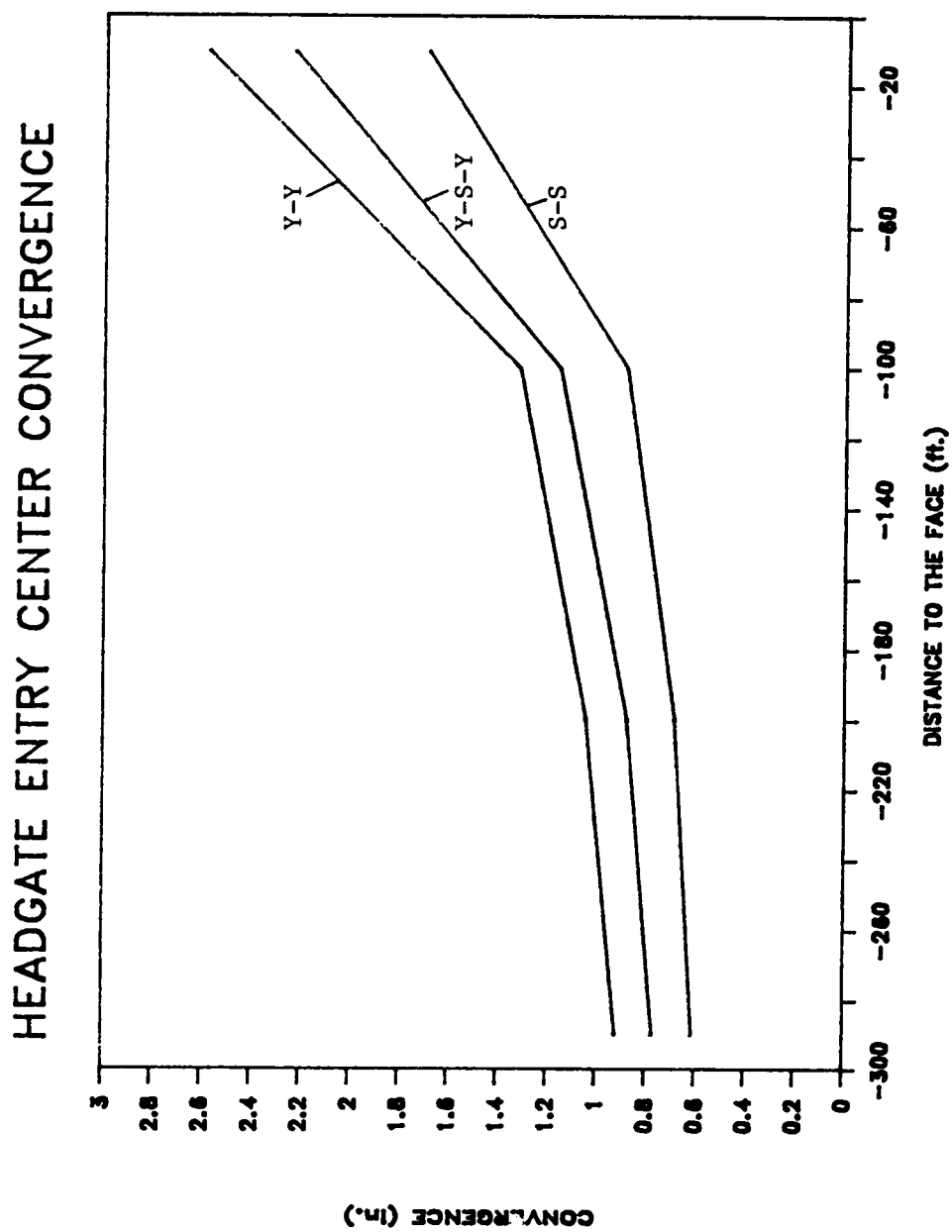


Figure 5.8 Headgate Center Convergence Comparison

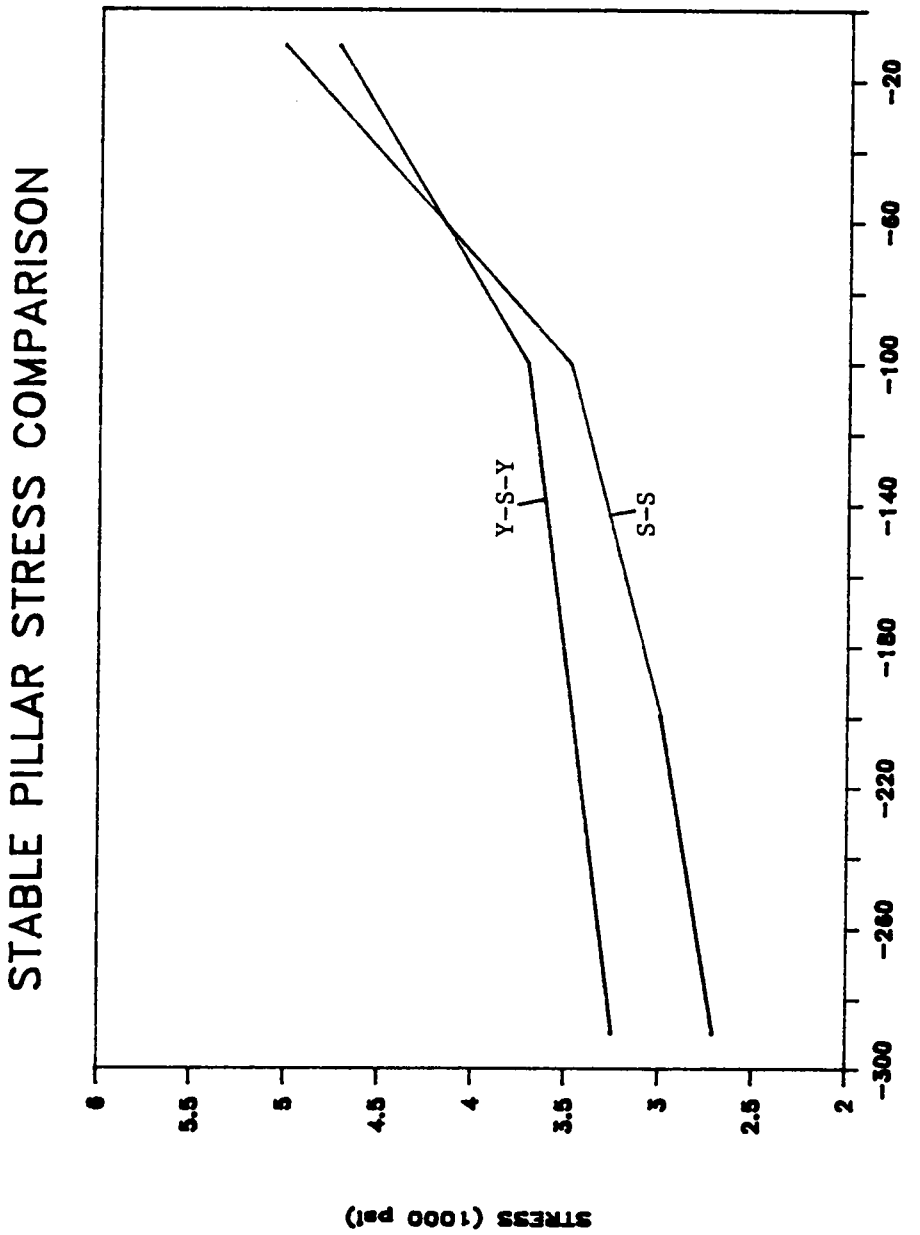


Figure 5.9 Stable Pillar Stress Comparison

By comparing the modeling results of the three pillar layouts, it may be concluded that, under the given conditions, the y-s-y layout may be the most suitable design. It will release high stress concentrations and maintain roof stability.

## 5.2 Parametric Studies

Parametric studies were conducted in order to further explore the mechanism of pillar yielding. For this purpose, a smaller finite element model was constructed as shown in Figure 5.10, concentrating on a single yield pillar. Different parameters affecting pillar yielding were examined. Each parameter was varied over a range of values and tested with the finite element model.

Poisson's ratio and the triaxial factor were found to be the two most influential parameters. Poisson's ratio was varied from 0.32 to 0.36. With the other parameters remained constant, a greater Poisson's ratio resulted in a higher peak vertical stress in the pillar. When the Poisson's ratio was sufficiently great, there was an unyielded elastic core remaining in the pillar and the peak vertical stress was slightly lower than that of critical yielding condition (Figure 5.11). In the case being studied, when Poisson's ratio was greater than 0.35 at a depth of 1,500 feet, there was an unyielded core in the 20 foot pillar. An intuitive explanation of this may be stated as follows. The strength of coal is a function of confining pressure, which is the horizontal stress in this case. A simplified relation between the horizontal stress and the vertical stress may be expressed as follows:

$$\sigma_h = \mu\sigma_v \tag{5.1}$$

where:

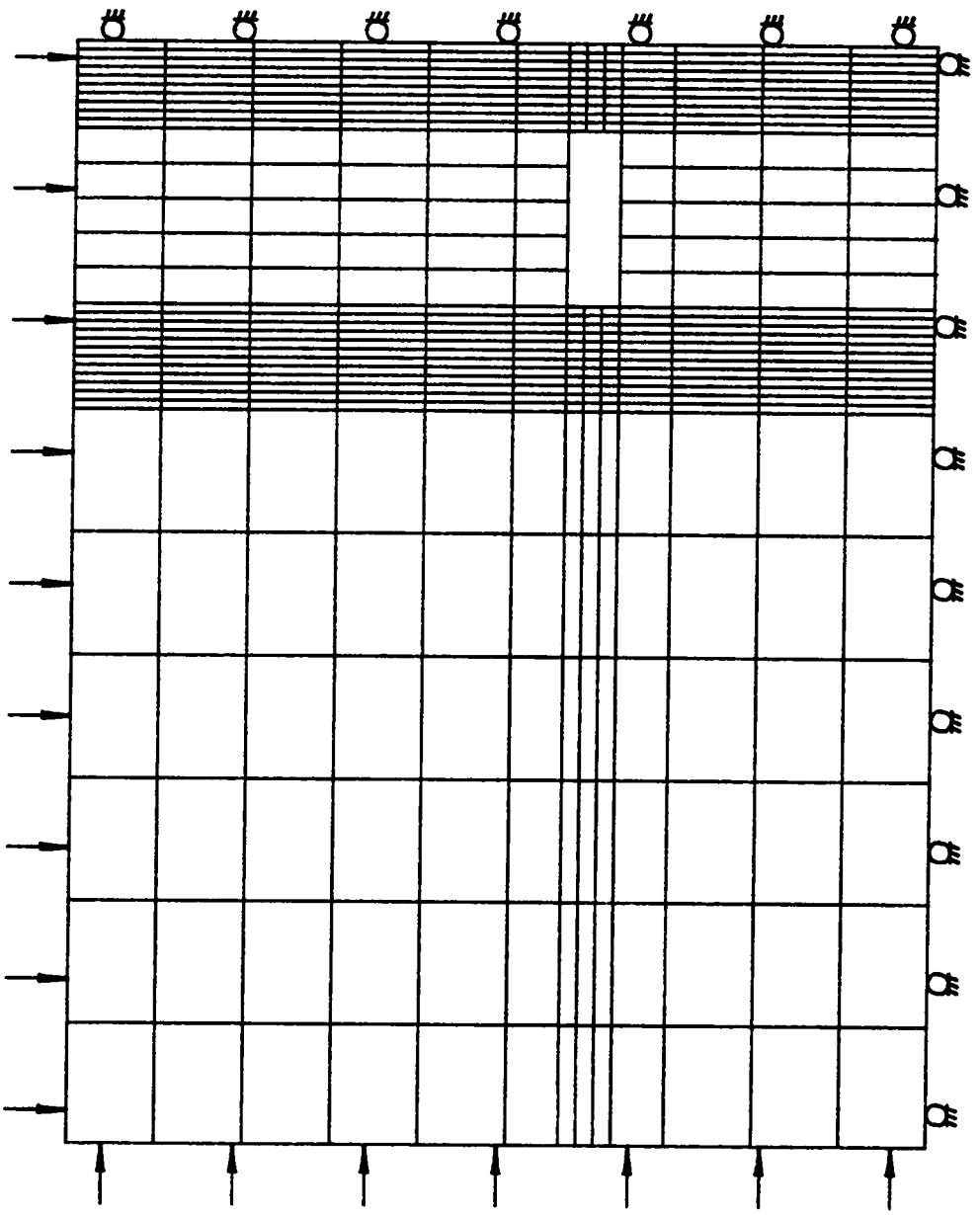

Figure 5.10 Yield Pillar Model

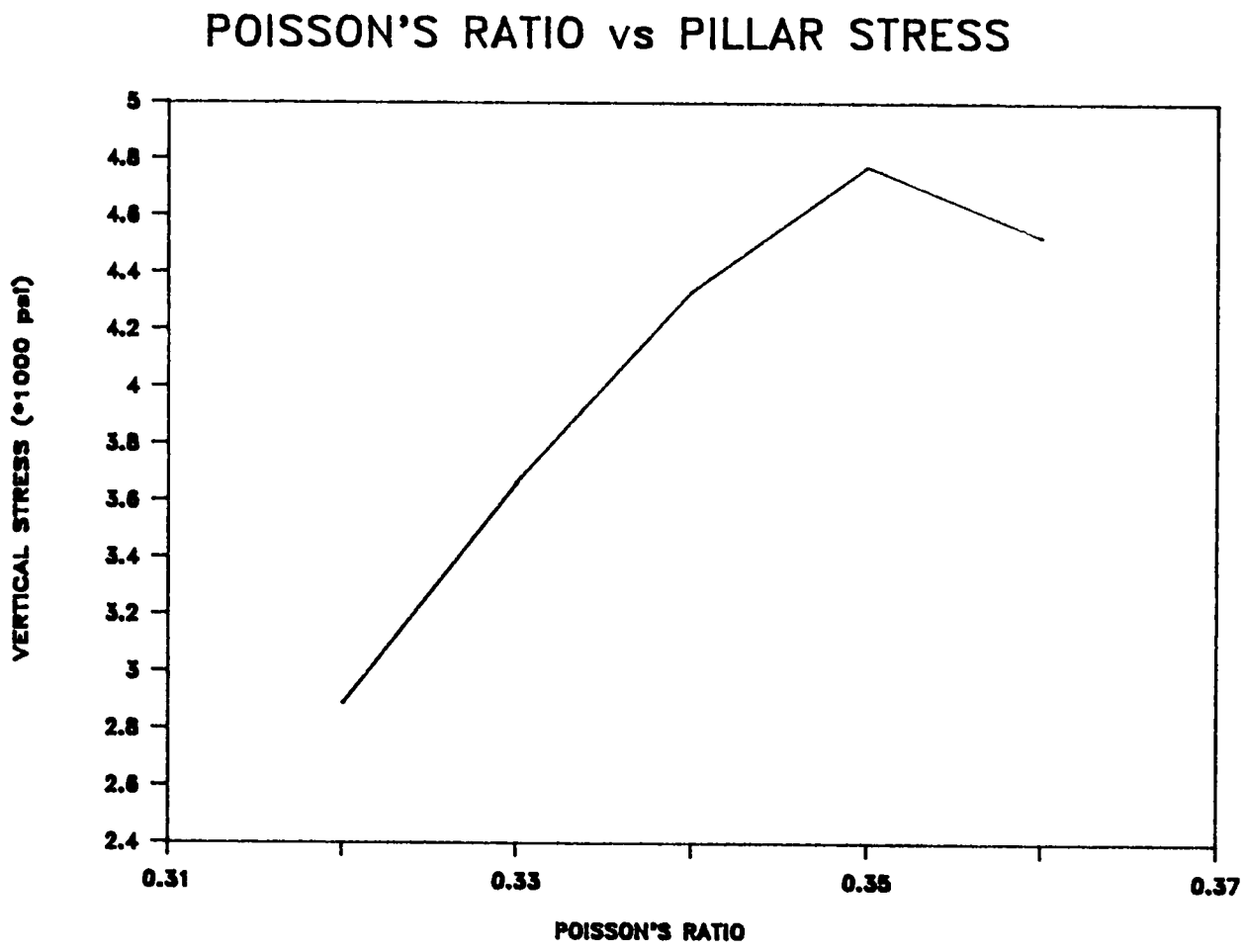


**Figure 5.11 Effect of Poisson's Ratio on Pillar Stress**

$\sigma_h$ = horizontal stress;

$\sigma_v$ = vertical stress; and

$\mu$ = Poisson's ratio.

With the same vertical stress, the horizontal stress is higher if the Poisson's ratio is greater. As the Poisson's ratio increases the horizontal stress increases, which imposes a higher confining pressure on the pillar core and increases the strength of coal. With the greater strength, coal will stand a higher vertical load, producing a higher vertical stress in the pillar. It may be noticed that the effect of Poisson's ratio has not been considered in the progressive failure formulation developed by Wilson (1977, 1981). The pillar stress and the yield zone are not affected by Poisson's ratio in that formulation.

The triaxial factor was varied from 3.7 to 4.5 and a trend similar to that exhibited by Poisson's ratio was found, and is presented in Figure 5.12. With a greater triaxial factor, a higher peak vertical stress occurred in the pillar. When the triaxial factor was sufficiently large, the pillar did not yield completely. Instead, an elastic pillar core remained in the center. This is due to the fact that a larger triaxial factor will result in a greater coal strength, and in turn will induce higher stress in the pillar.

By varying the width of the yield pillar from 10 to 24 feet, it was found that the vertical stress in the yield pillar was strongly related to the yield pillar width. As illustrated in Fig. 5.13, when the pillar size was small, the pillar yielded completely, producing a low vertical stress. As the pillar width increased, the stress increased until the width was great enough to allow for an elastic core in the pillar. While the stress in the yield pillar increased, less and less load was transferred to the abutment pillar. The peak stress in the abutment pillar was, therefore, decreasing. As displayed in Figure 5.13, however, the peak stress change in the abutment was not as significant as was the peak stress change in the yield pillar.

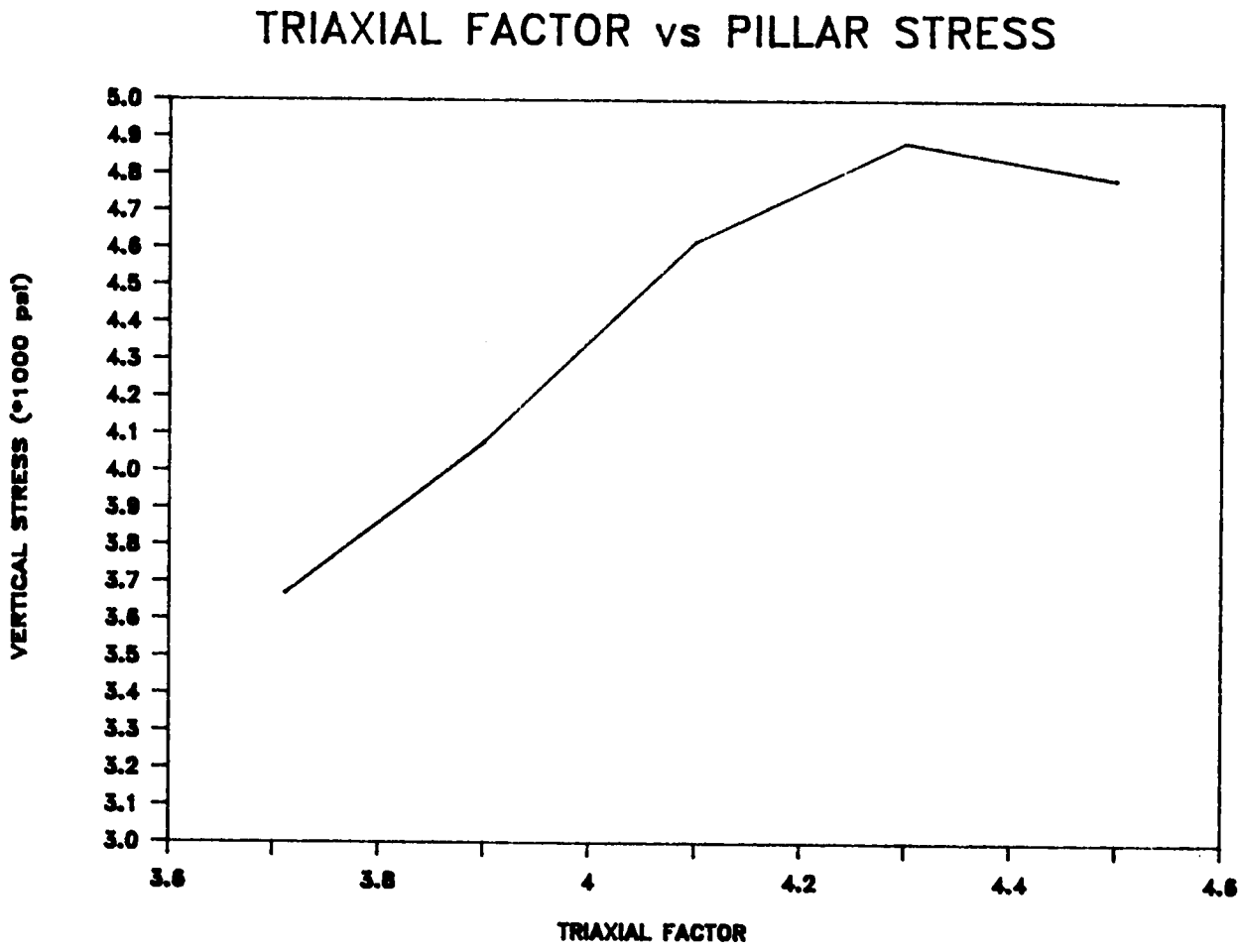


**Figure 5.12 Effect of the Triaxial Factor on Pillar Stress**

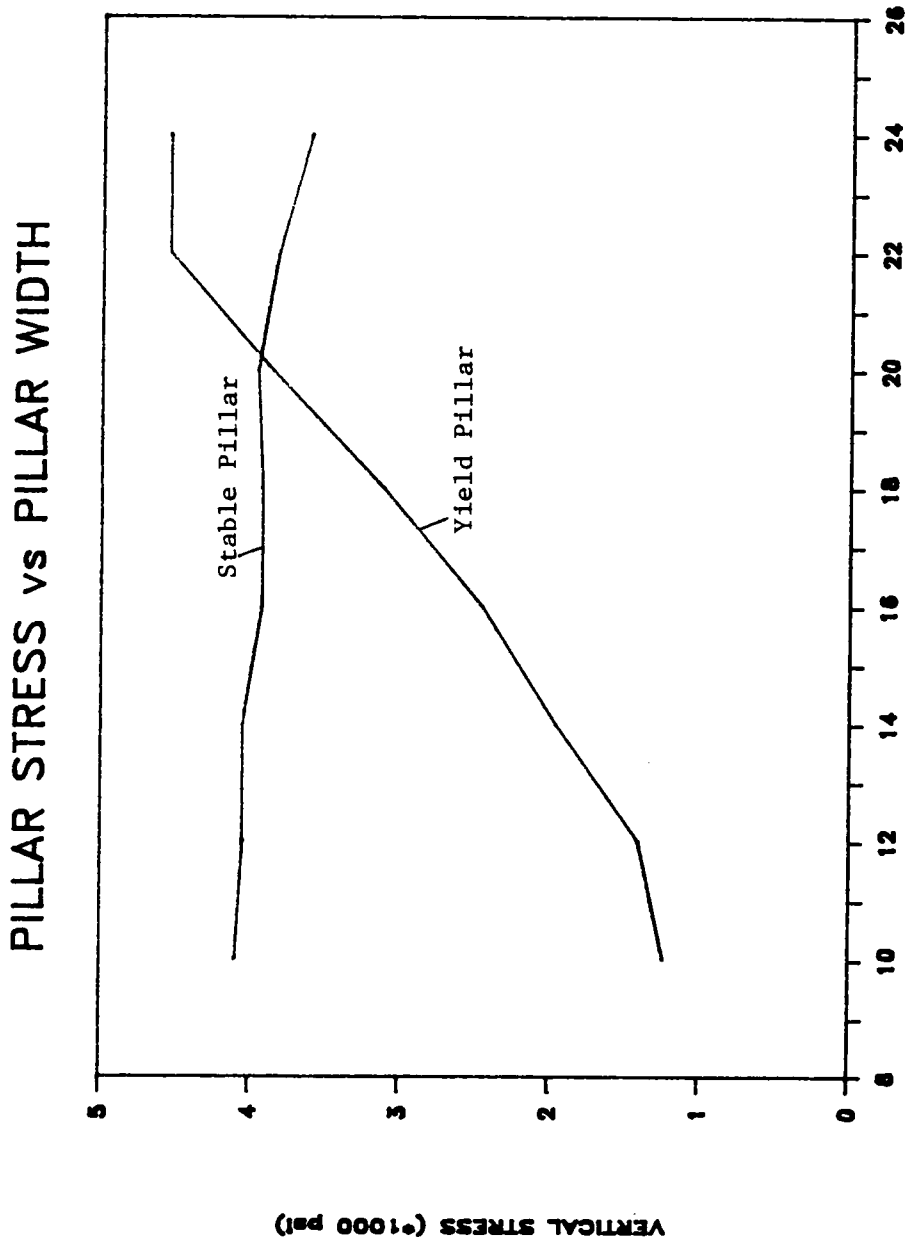


Figure 5.13 Effect of the Pillar Width on Pillar Stress

The width of the opening was tested from 10 to 28 feet, and the relationship between the width of the opening and pillar stress was found as shown in Figure 5.14. It can be observed that the peak vertical stress in the abutment pillar increased, corresponding to an increase in the opening width. Since the yield pillar had yielded, the stress in the yield pillar did not change significantly except for displaying some minor fluctuations which were due to the numerical approximation technique used in the modeling. The yield zone in the abutment pillar, however, did change considerably, from 7.5 feet at an opening width of 10 feet, to 10 feet at an opening width of 22 feet, as shown in Figure 5.15. Again, by contrast, the influence of the opening width upon the pillar stress and the yield zone is not reflected in Wilson's method.

Finally, as might be expected, depth is a major factor affecting the yield zone. As illustrated in Figure 5.16, at a depth of 300 feet the yield zone was around 2.5 feet, and it increased up to 10 feet at a depth of 1,300 feet indicating that the 20 foot yield pillar started to yield as a whole.

In addition, the material Young's modulus was also examined in this study. Within the tested range, however, no significant effects were found with this model.

## 5.3 Summary and Discussion

A modified load augmentation technique was introduced in this chapter, which took into account the abutment effect upon the longwall chain pillars with 2-D finite element models. The technique greatly reduced the cost of computer simulation and made the modeling of yield pillars simpler. Although further testing of the accuracy of the recommended method remains to be conducted, the modeling yielded very reasonable results.

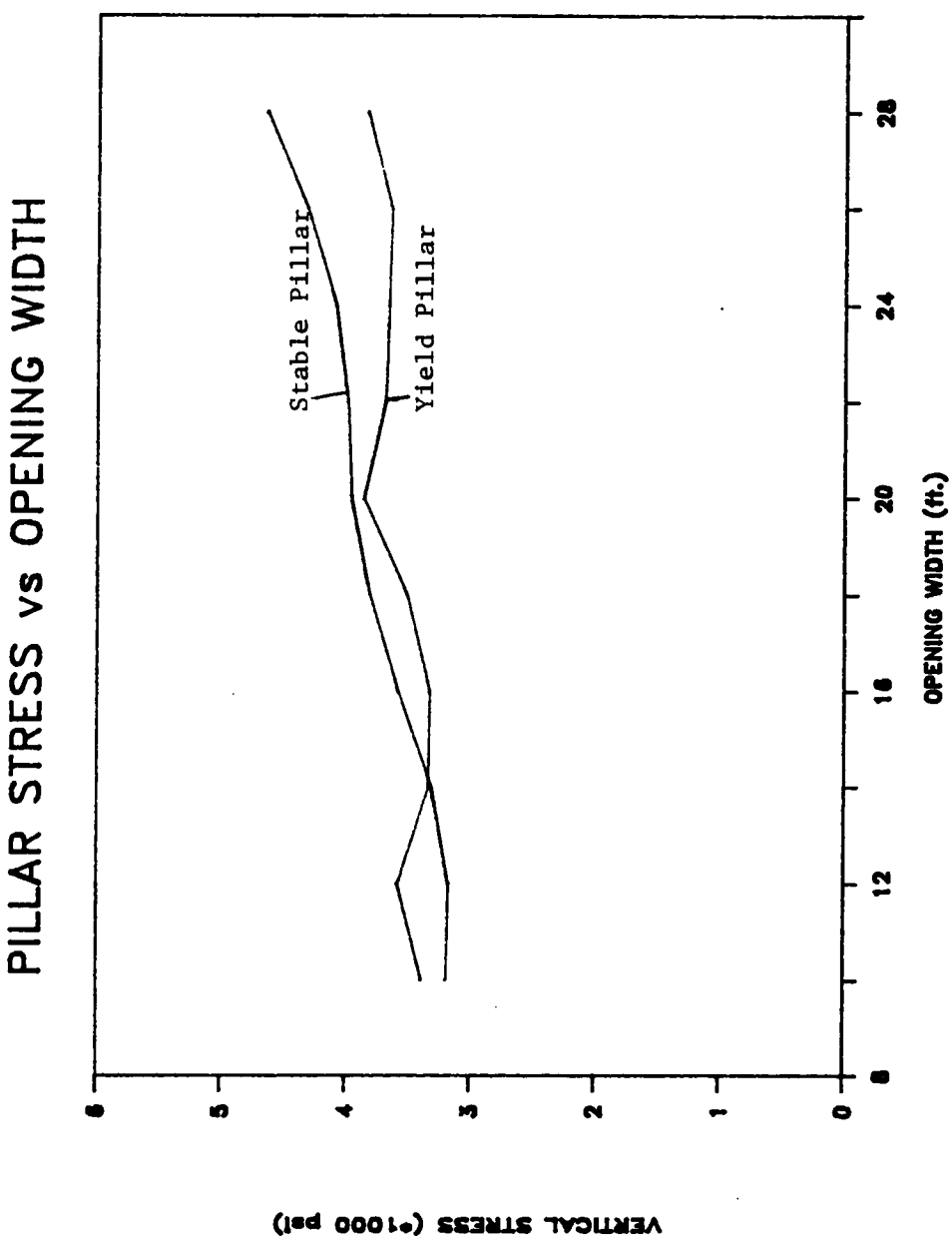


Figure 5.14 Effect of the Opening Width on Pillar Stress

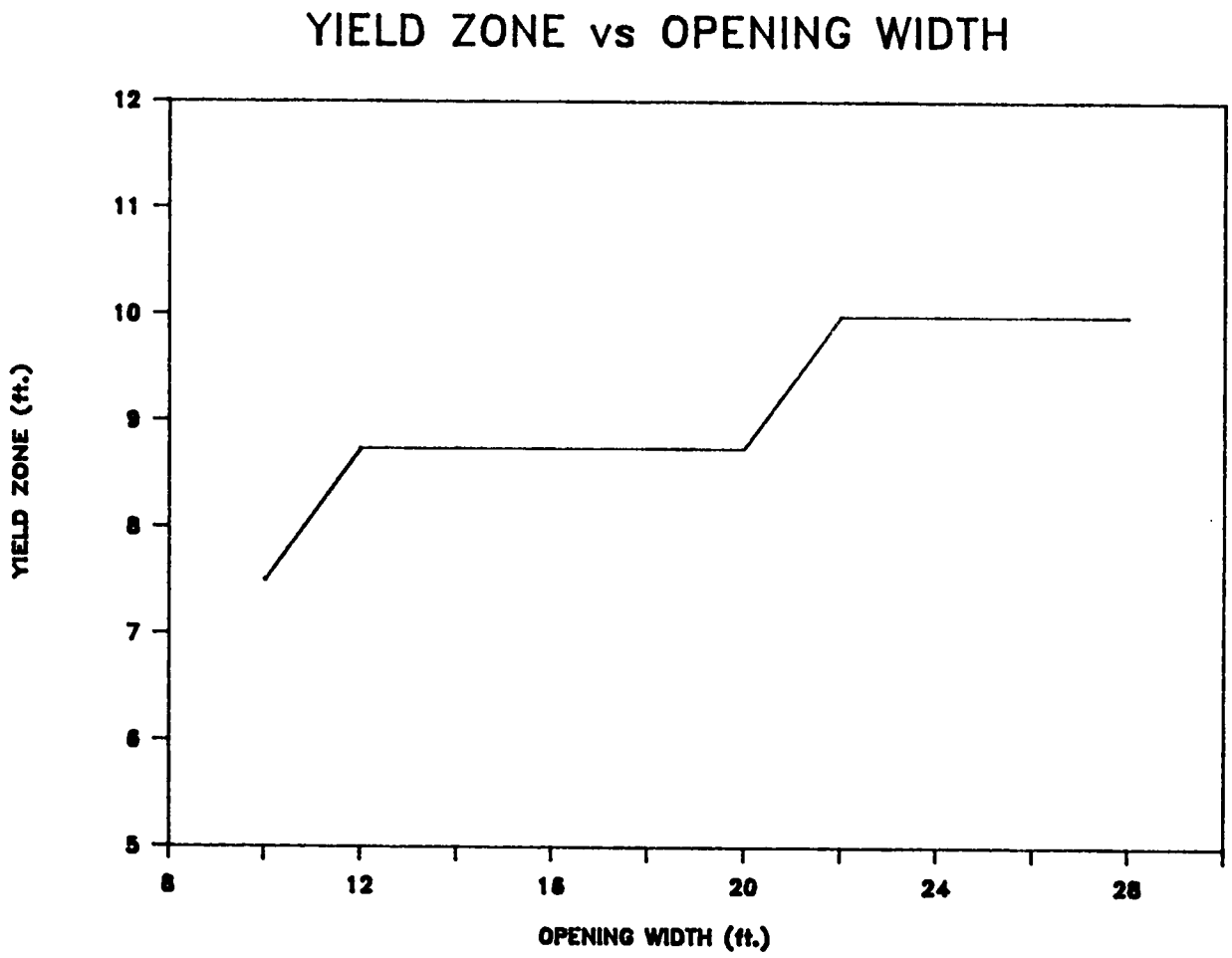


Figure 5.15 Effect of the Opening Width on Pillar Yield Zone

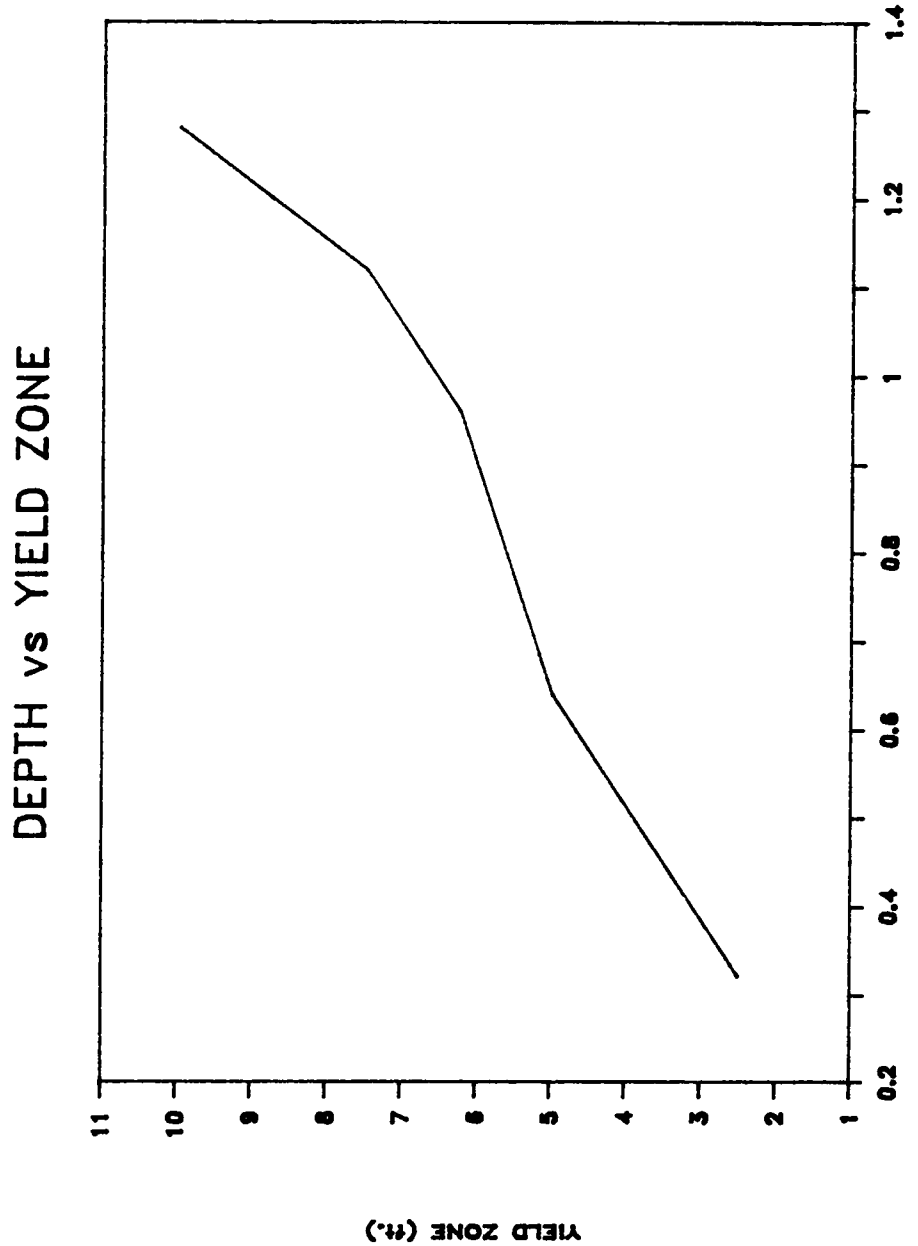


Figure 5.16 Effect of the Mining Depth on Pillar Yield Zone

Three different longwall entry pillar layouts were investigated in this chapter. The results indicated that adopting yield pillars in longwall entries might reduce the high stress concentration significantly. This has the potential to prevent floor heaving problems, to improve ground conditions in multi-seam mining, and to ease some ground control difficulties in general. Among the three pillar systems examined, the yield-stable-yield pillar system was found to be the most suitable design under the given conditions. This coincided with the experience obtained in actual mining operations (Gauna, et al., 1985, and Gauna, et al., 1986), where the yield-stable-yield pillar layout had been found to be the best design and had significantly reduced the floor heave which existed in the regular pillar system.

The parametric analysis performed in this chapter revealed that the yielding condition and the stress distribution in a yield pillar depended on a number factors. Among the material properties, Poisson's ratio and the triaxial factor were found to be the most influential parameters. As the study indicated, the load was transferred from the yield pillar onto adjacent abutment pillars and the stress in the yield pillar was released. The transferred load in the abutment pillars was, however, distributed over a relatively large area. The stress increase in the abutment pillars was, therefore, less significant than the stress decrease in the yield pillar. The final result was then a great peak stress reduction in the yield pillar, with a small stress increase in the abutment pillar. This may significantly release stress concentration in some sensitive areas.

# CHAPTER 6: DEVELOPMENT OF YIELD PILLAR DESIGN GUIDELINES

## 6.1 Introduction

Without a good understanding of the stress distribution in the pillar yield zone, an adequate design of yield pillars is almost impossible. As indicated in Chapter 4, there was some discrepancy between the elastic-plastic finite element modeling and the progressive failure theory as regarded stress distribution in the pillar yield zone. This discrepancy is discussed in detail in this chapter, and the progressive failure theory critically reviewed. Following the review, a mathematical model concerning the yield zone stress distribution, established based on the statistical analysis of finite element simulations, will be presented. It will then be shown how this mathematical model was further developed to estimate the pillar bearing capacity and the width of yield zone. On the basis of the new equations describing the pillar yield zone, yield pillar design concepts will be introduced and nomograms constructed for quick reference presented.

## 6.2 Discussion on the Progressive Failure Theory

Based on the assumption that the strength of coal is a linear function of the confining stress, Wilson in his progressive failure theory was able to obtain a closed-form solution for estimating the stress distribution in the yield zone. A set of formulas was derived for the estimation of the yield zone width and for the calculation of pillar strength.

According to the progressive failure theory, the equilibrium of an element of thickness dx in the broken coal zone of a mine pillar is given by (Figure 6.1):

$$H d\sigma_x = 2v\sigma_y dx \tag{6.1a}$$

or,

$$\frac{d\sigma_x}{dx} = \frac{2v}{H}\sigma_y \tag{6.1b}$$

where

H = mining height;

$v$ = coefficient of internal friction;

$\sigma_x$, $\sigma_y$ = horizontal and vertical stresses; and

x = distance into the pillar .

The equation implies that the horizontal force at any point should be equal to the resistant force induced by the vertical stress due to the internal friction. This equation was further developed in order to obtain the stress distribution in the yield zone. However, closer examination indicated that the right-hand side of Equation 6.1a is the maximum possible resistant force under the vertical stress $\sigma_y$. The resistant force does not have to be the maximum value at all times. Any horizontal force of less than this maximum

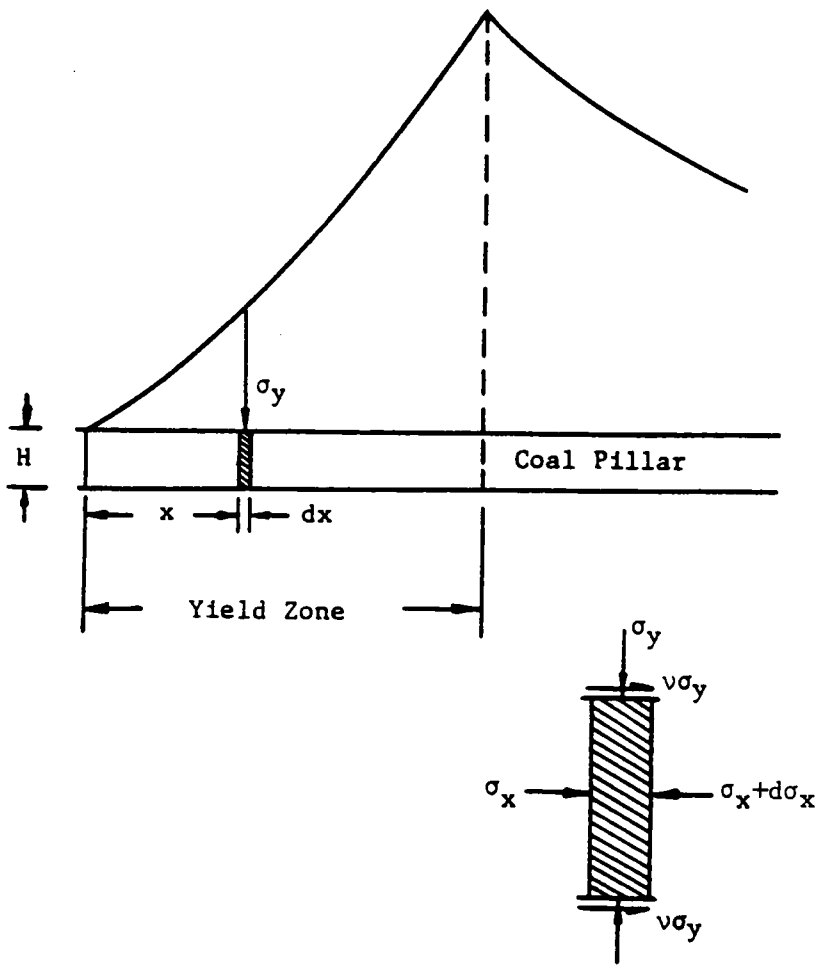


**Figure 6.1 Force Equilibrium in the Yield Zone**

value will be balanced by a matching resistant force. Therefore, equilibrium may be achieved under a less strict condition, that is:

$$Hd\sigma_x \leq 2v\sigma_y dx \tag{6.2a}$$

or,

$$\frac{d\sigma_x}{dx} \leq \frac{2v}{H}\sigma_y \tag{6.2b}$$

Assuming that the linear relation between the coal strength and the confining stress still holds true in the yield zone, that is:

$$\sigma_y = q\sigma_x \tag{6.3}$$

where:

q = triaxial factor.

Equation 6.2b may be rewritten as:

$$\frac{d\sigma_x}{dx} \leq \frac{2qv}{H}\sigma_x \tag{6.4}$$

Therefore, any function $\sigma_x = f(x)$ satisfying the above condition can be a possible horizontal stress distribution in the yield zone. The stress distribution formula obtained in the progressive failure theory illustrates only an extreme case in which the horizontal force is assumed to be the maximum possible resistant force induced by the vertical load through internal friction, which may not be a valid assumption.

In addition, as indicated in the previous chapter, the stress in the yield pillar is also a function of Poisson's ratio. This relation between the pillar stress and Poisson's ratio is

not reflected in the progressive failure formulation. In the following, a formula describing the stress distribution in the yield zone, and developed by statistically analyzing the results of a series of finite element simulations is shown. The formula incorporates the effect of Poisson's ratio, as well as that of the triaxial factor, into the calculation of stress distribution in the yield zone.

## 6.3 Finite Element Modeling and Analysis of the Results

In order to study the behavior of the yield zone, a 2-D finite element mesh was constructed as shown in Figure 6.2, and computer simulations were conducted using this model. From the simulation results, it was found that the stress distribution in the yield zone was not affected by the applying load. As long as the coal yielded, the stress in the yielding zone was irrespective of the magnitude of the load applied to the pillar. In the yield zone, all the materials were assumed to behave plastically. When additional load was applied to the pillar, the materials deformed continuously without increasing the stress, which was indicated by a flat line in the stress-strain curve. The stress in the yield zone can, therefore, be considered to be irrespective of the applied load.

In the simulation, a range of values was used for the input parameters. The triaxial factor covered a range from 3.5 to 4.5 and the Poisson's ratio from 0.3 to 0.4. These ranges were considered to be the common values for most coals. The simulation results were statistically analyzed utilizing several different linear and non-linear procedures, and a simple formula was reached. It was found that the stress in the yield zone of coal pillars was influenced by three parameters: the triaxial factor, the Poisson's ratio, and the distance into the pillar. This can be expressed as follows:

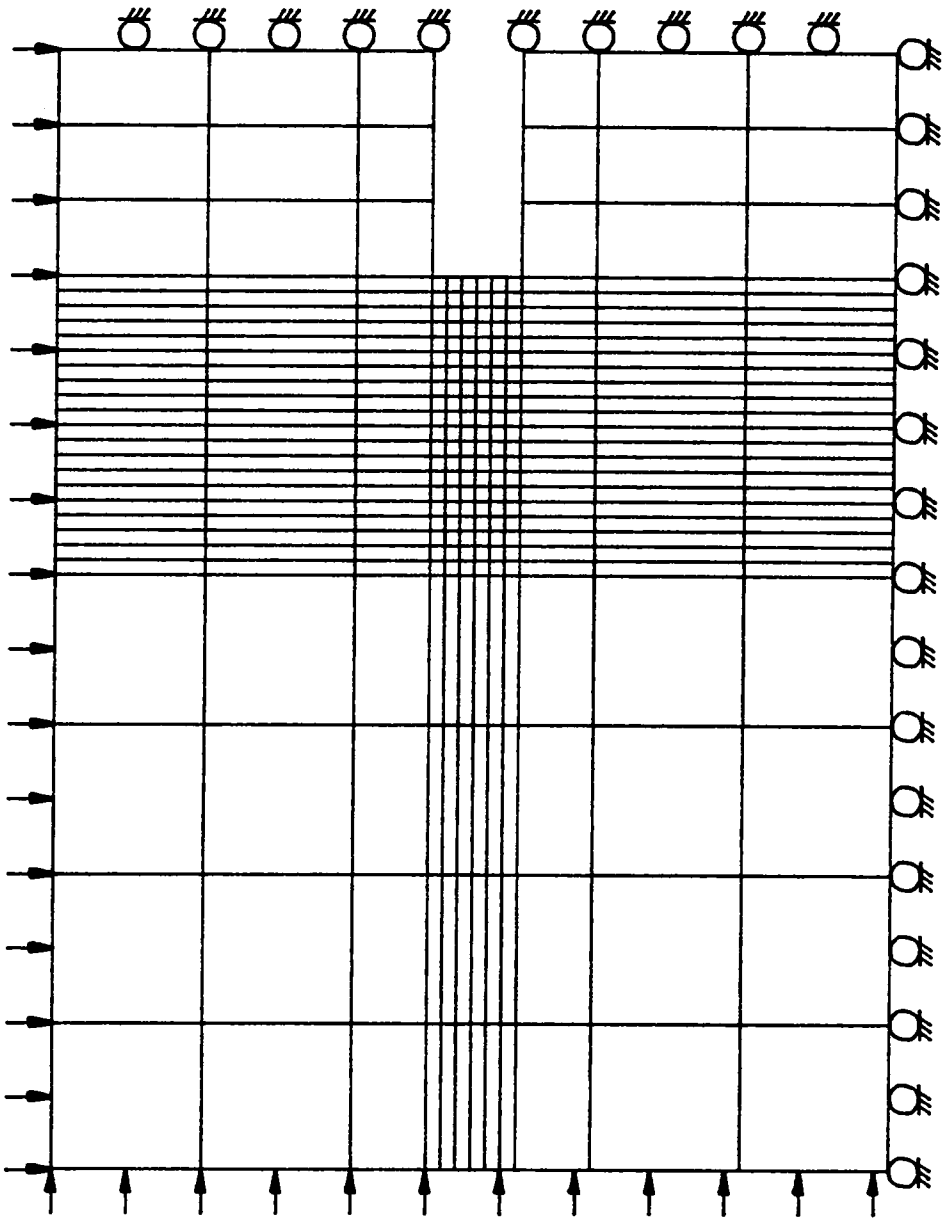

Figure 6.2 Finite Element Model for the Study of the Yield Zone

$$\sigma_x = f(q)\, f(\mu)\, f(\frac{x}{H}) \tag{6.5}$$

where:

$\sigma_x$ = horizontal stress in the yield zone (psi);

q = triaxial factor;

$f(q) = q^{1.7}$ ;

$\mu$ = Poisson's ratio;

$f(\mu) = -0.028 + 0.057\mu + 0.17\mu^2$ ;

x = distance into the pillar;

H = height of the pillar; and

$f(\frac{x}{H}) = 6545(\frac{x}{H})^2 + 454(\frac{x}{H})^3$ .

Assuming that the linear relation between the strength of coal and the confining pressure is valid in the yield zone, the vertical stress was found to be:

$$\sigma_y = q\sigma_x = q\, f(q)\, f(\mu)\, f(\frac{x}{H}) \tag{6.6}$$

A comparison was made between Equation 6.6, the formula proposed by Wilson (1972), and the field data which was used to validate Wilson's model. The comparison is illustrated in Figure 6.3, which shows clearly that the formula developed in this study fits the observed data better than does Wilson's equation. One questionable point about Wilson's equation is that, at a large distance into the yield zone, the stress increases so rapidly that within a very small distance, the difference in stress is excessive. Such a steep increase is unlikely to occur in practice. On the other hand, the formulation presented here produces a smoother and, therefore, more realistic stress increase.

The formula was also tested against Equation 6.4, as shown in Figure 6.4. The figure shows that the inequality condition is satisfied everywhere in the yield zone except at the

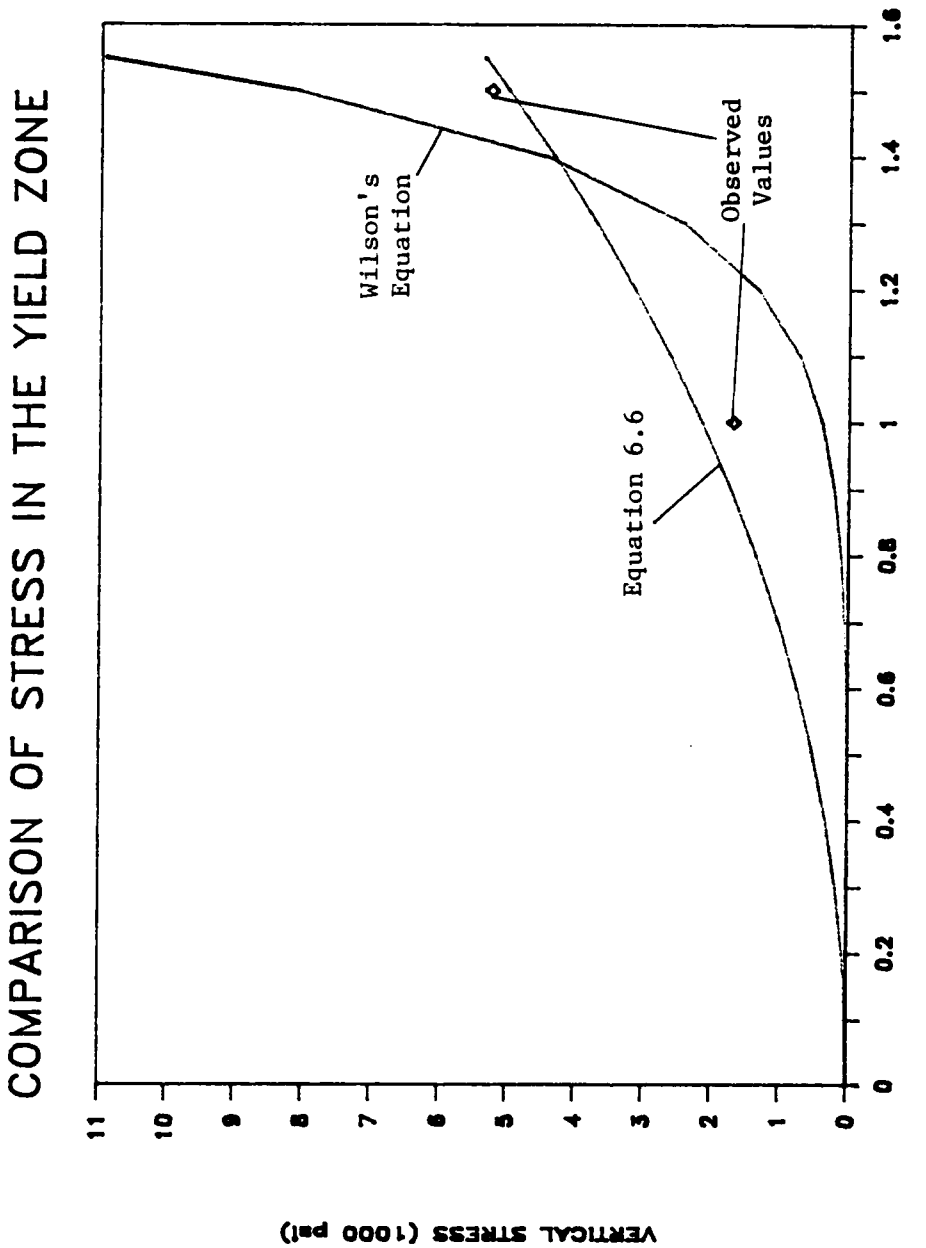


Figure 6.3 Comparison of Stress in the Yield Zone

very edge of the pillar. In the finite element model no constraint was applied on the pillar rib, and the stress at the rib was forced to be zero in the regression procedures. This caused the inequality condition to be unsatisfied at the pillar rib. However, examination indicated that forcing the stress at the pillar rib to be zero had little effect on the accuracy of the equation while simplifying the computation significantly.

Since Equation 6.6 was obtained from statistical analyses, there are certain limitations and, therefore, the equation should be used with caution. In general, the estimated yield zone should be within 5 times the pillar height. The triaxial factor should be between 3.0 and 5.0, and the Poisson's ratio in the range of 0.25 to 0.45. Since these values cover a wide range of mining conditions in most coal seams, the equation developed in this study has a wide application.

Using the same assumption as in the progressive failure theory, the horizontal stress at the inner boundary of the yield zone can be considered equal to the virgin stress, $\gamma h$, that is:

$$\sigma_x = f(q)\, f(\mu)\, f(\frac{x}{H}) = \gamma h \qquad (6.7)$$

The width of the yield zone may be determined by solving for x, i.e.

$$X_b = H\,\{9.61 \times \cos[\,\frac{1}{3}\,\cos^{-1}(\frac{\gamma h \times 10^{-5}}{f(q)\, f(\mu)} - 1)] - 4.8\} \qquad (6.8)$$

where

$X_b$ = width of the yield zone (in.);

$\gamma$ = average overburden density (lb/cubic in.); and

h = depth (in.).

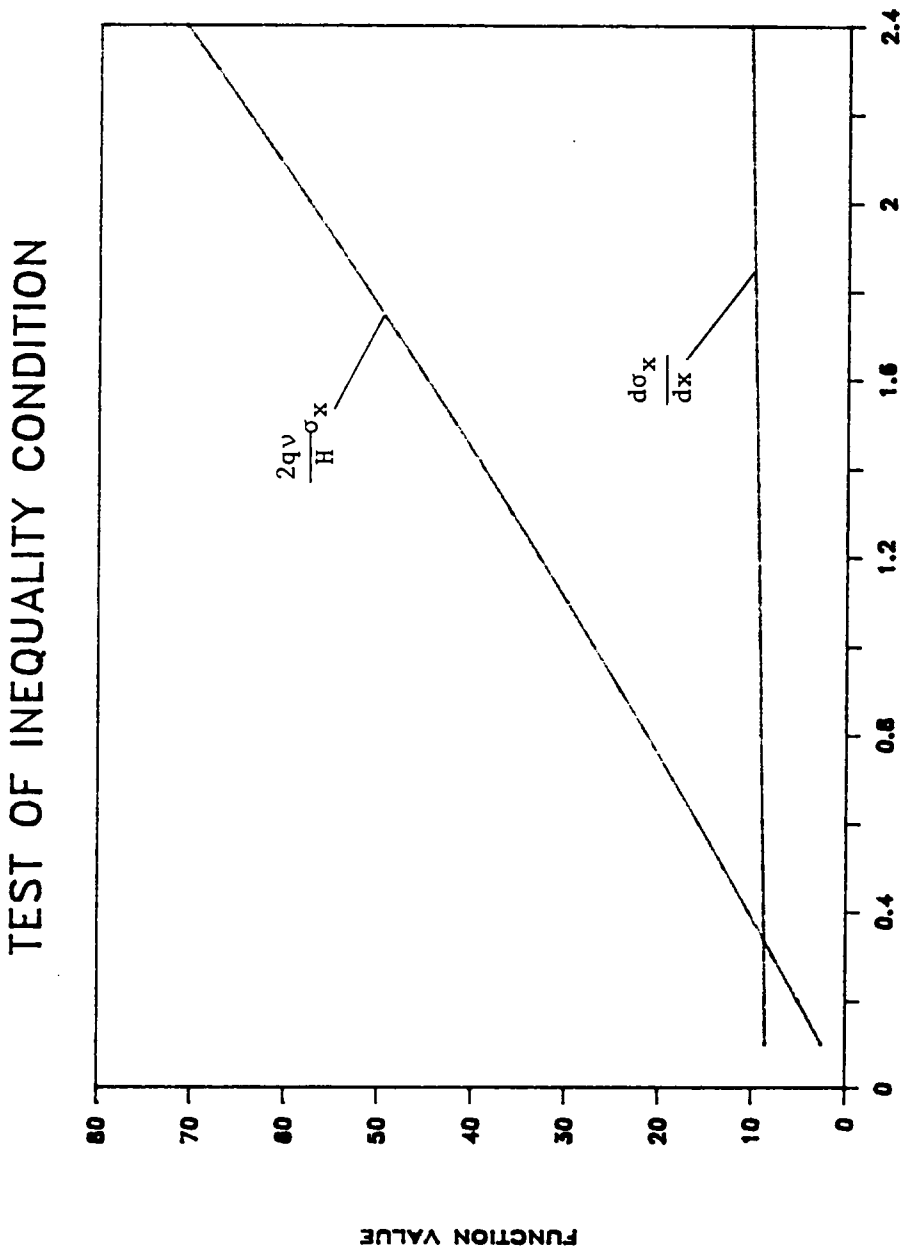


Figure 6.4 Test of Inequality Condition

The width of the yield zone versus mining depth is plotted in Figure 6.5. The curves are also compared with the results obtained from Wilson's original formulas. There are two equations defined by Wilson for the width of the yield zone. In Equation I, it is assumed that the roof and floor have a similar strength as the coal. In Equation II, the roof and floor are assumed to be stronger than the coal. It is interesting to note that, with a small Poisson's ratio, the curve of Equation 6.8 coincides with Wilson's Equation I, and as Poisson's ratio increases, it approaches the curve suggested by Wilson's Equation II. In other words, with different values of Poisson's ratio Equation 6.8 covers the range calculated by the two formulas proposed by Wilson.

Following a similar derivation as that in the progressive failure theory, the equations for the estimation of the pillar bearing capacity P were obtained as follows:

(1) For a square yield pillar in which there is no elastic core:

$$P = q\, f(q)\, f(\mu)\, (273 \frac{W^4}{H^2} + 5.68 \frac{W^5}{H^3}) \tag{6.9}$$

(2) For a rectangular yield pillar in which there is no elastic core:

$$P = q\, f(q)\, f(\mu)\, [273 \frac{W^4}{H^2} + 5.68 \frac{W^5}{H^3} + (L - W)\, (545 \frac{W^3}{H^2} + 14.2 \frac{W^4}{H^3})] \tag{6.10}$$

(3) For a square stable pillar in which there is an elastic core:

$$P = q\, f(q)\, f(\mu)\, [273 \frac{X_b^4}{H^2} + 5.68 \frac{X_b^5}{H^3} + (W - 2X_b)\, (1090 \frac{X_b^3}{H^2} +$$

$$+ 28.4 \frac{X_b^4}{H^3})] + (W - 2X_b)^2 (\sigma_0 + q\gamma h) \tag{6.11}$$

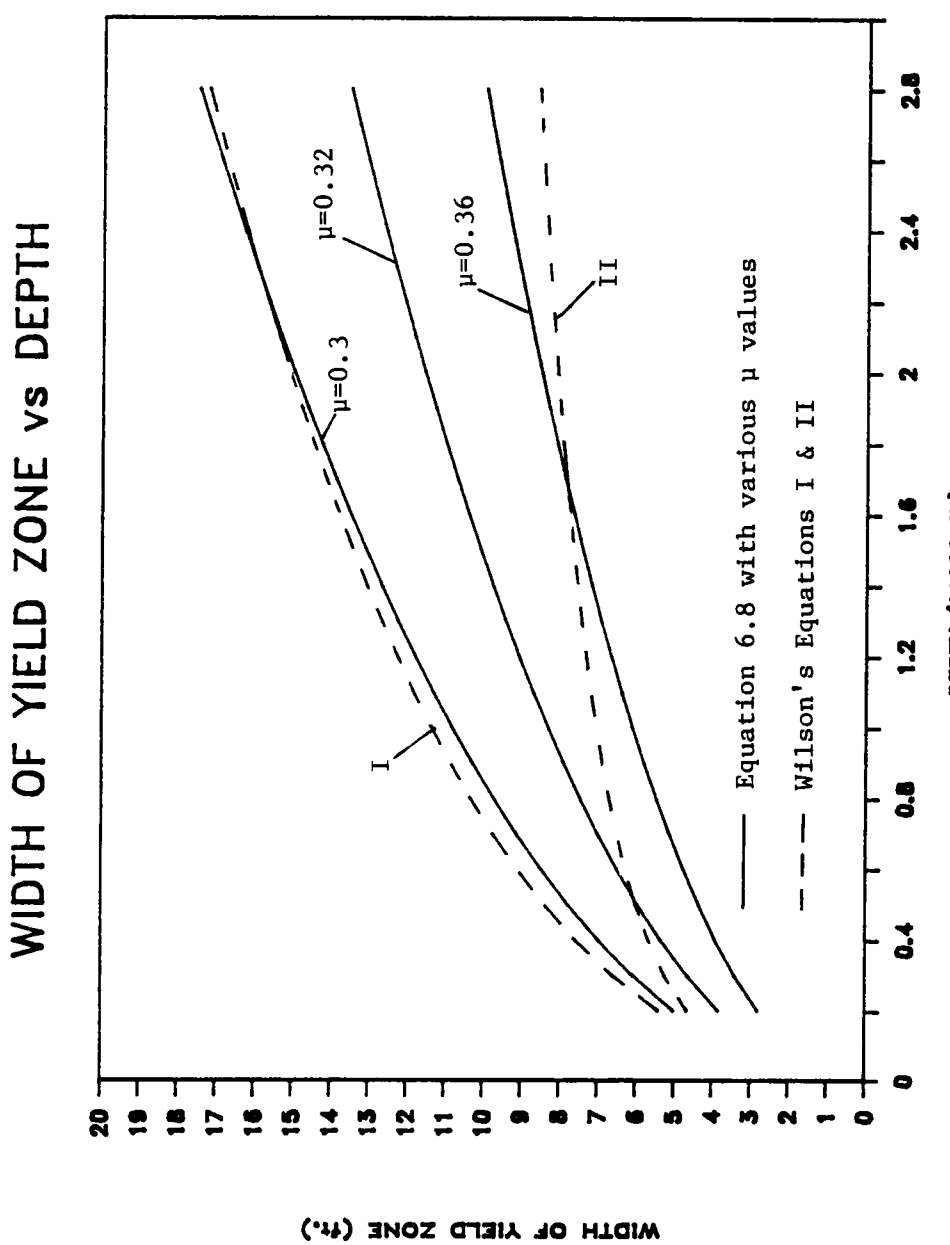


Figure 6.5 Comparison of Yield Zone Width

(4) For a rectangular stable pillar in which there is an elastic core:

$$P = q\, f(q)\, f(\mu)\, [273 \frac{X_b^4}{H^2} + 5.68 \frac{X_b^5}{H^3} + (L + W - 4X_b)\, (545 \frac{X_b^3}{H^2} +$$

$$+ 14.2 \frac{X_b^4}{H^3})] + (W - 2X_b)\, (L - 2X_b)\, (\sigma_0 + q\gamma h) \qquad (6.12)$$

where:

W = pillar width (in.);

L = pillar length (in.); and

$\sigma_0$ = unconfined strength of coal.

In a stable pillar, the strength of the elastic core was assumed to be $\sigma_0 + q\gamma h$ .

## 6.4 Yield Pillar Design Consideration

A yield pillar is defined as one which yields upon isolation from the coal seam (Martin et al., 1985). In order to perform the function of releasing the stress, a yield pillar should not exhibit a elastic core, which would stand a great load and induce a high stress. According to this definition, the yield pillar width may be considered to be twice the width of the yield zone, that is:

$$W = 2\, X_b = 2\, H\, \{9.61 \times \cos[\frac{1}{3} \cos^{-1}(\frac{\gamma h \times 10^{-5}}{f(q)\, f(\mu)} - 1)] - 4.8\} \qquad (6.13)$$

This may be considered the maximum yield pillar width. If the width is greater, an elastic core will appear in the center and the pillar will no longer be classifiable as a yield pillar. Using a triaxial factor of 4.0, a Poisson's ratio of 0.3, and a pillar height of 6 feet, the maximum yield pillar width is plotted against the depth in Figure 6.6.

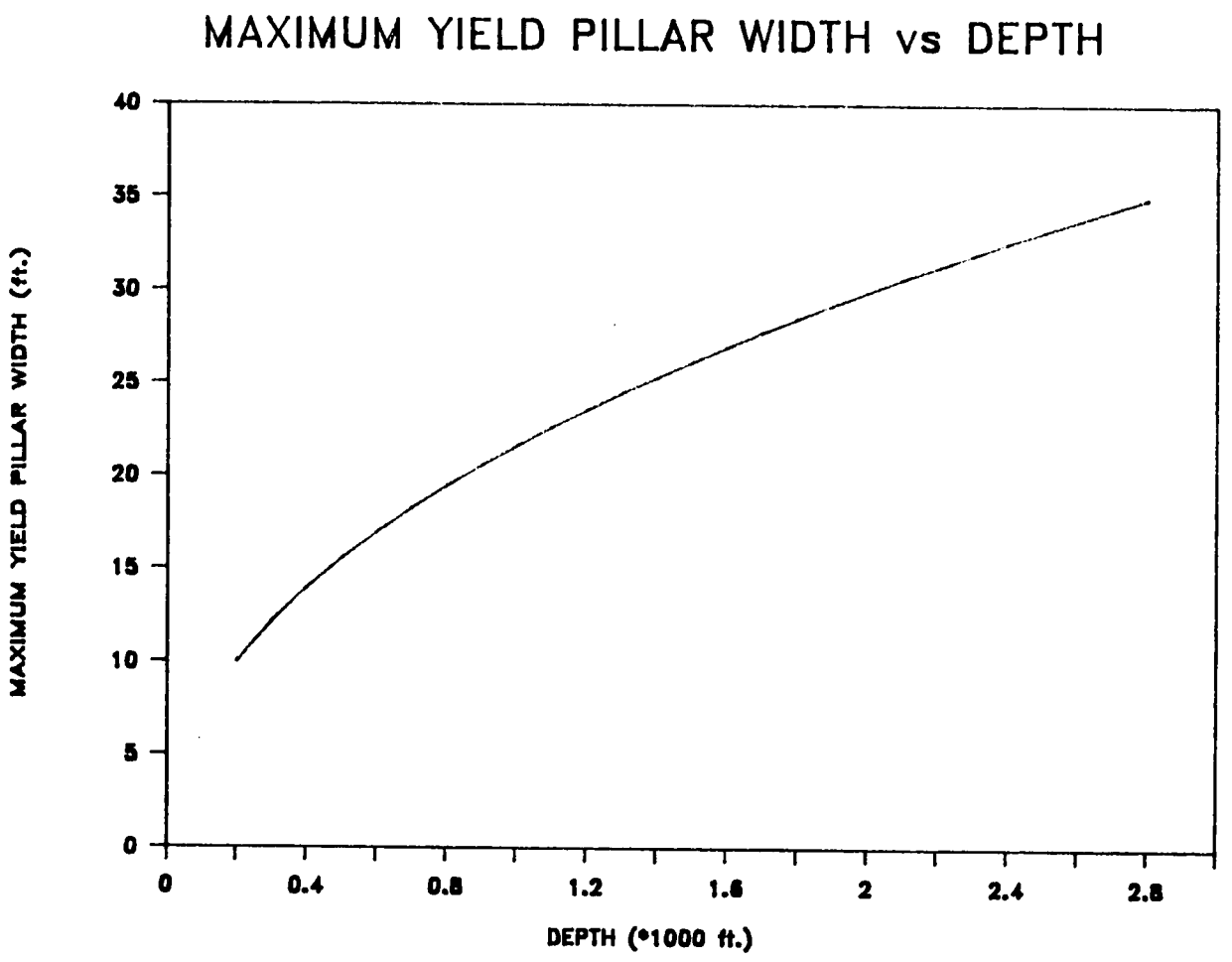


**Figure 6.6 Maximum Yield Pillar Width vs. Depth**

The maximum yield pillar width calculated above is, however, a critical value. Although at this width there is no elastic core in the pillar, a very high stress will occur at the center of the pillar. The peak stress can exceed the cover load by five or six times. In order to avoid this, the pillar width must be reduced. One suggestion is to select a yield pillar such that the peak vertical stress at its center equals the average tributary stress. The average tributary stress may be calculated as:

$$\sigma_T = \frac{\gamma h(W + W_o)(L + W_o)}{W L} \tag{6.14}$$

where:

$\sigma_T$ = average tributary stress (psi);

W = pillar width (in.);

L = pillar length (in.); and

$W_o$ = opening width (in.).

By combining Equations 6.6 and 6.14, the pillar width may be obtained from the following equation:

$$q\, f(q)\, f(\mu)\, f(\frac{W}{2H}) = \sigma_T \tag{6.15}$$

where:

$$f(\frac{W}{2H}) = 6545(\frac{W}{2H})^2 + 454(\frac{W}{2H})^3 .$$

Since $\sigma_T$ is also a function of the pillar width W, both sides of the equation involve the unknown W. A closed-form solution for W is quite complicated. However, utilizing one of the personal computers widely used today in the mining industry, the equation can be solved in a few simple iterations. With a triaxial factor equal to 4.0, a Poisson's ratio equal to 0.3, and a pillar height equal to 6 feet, the recommended yield pillar width versus depth is plotted in Figure 6.7.

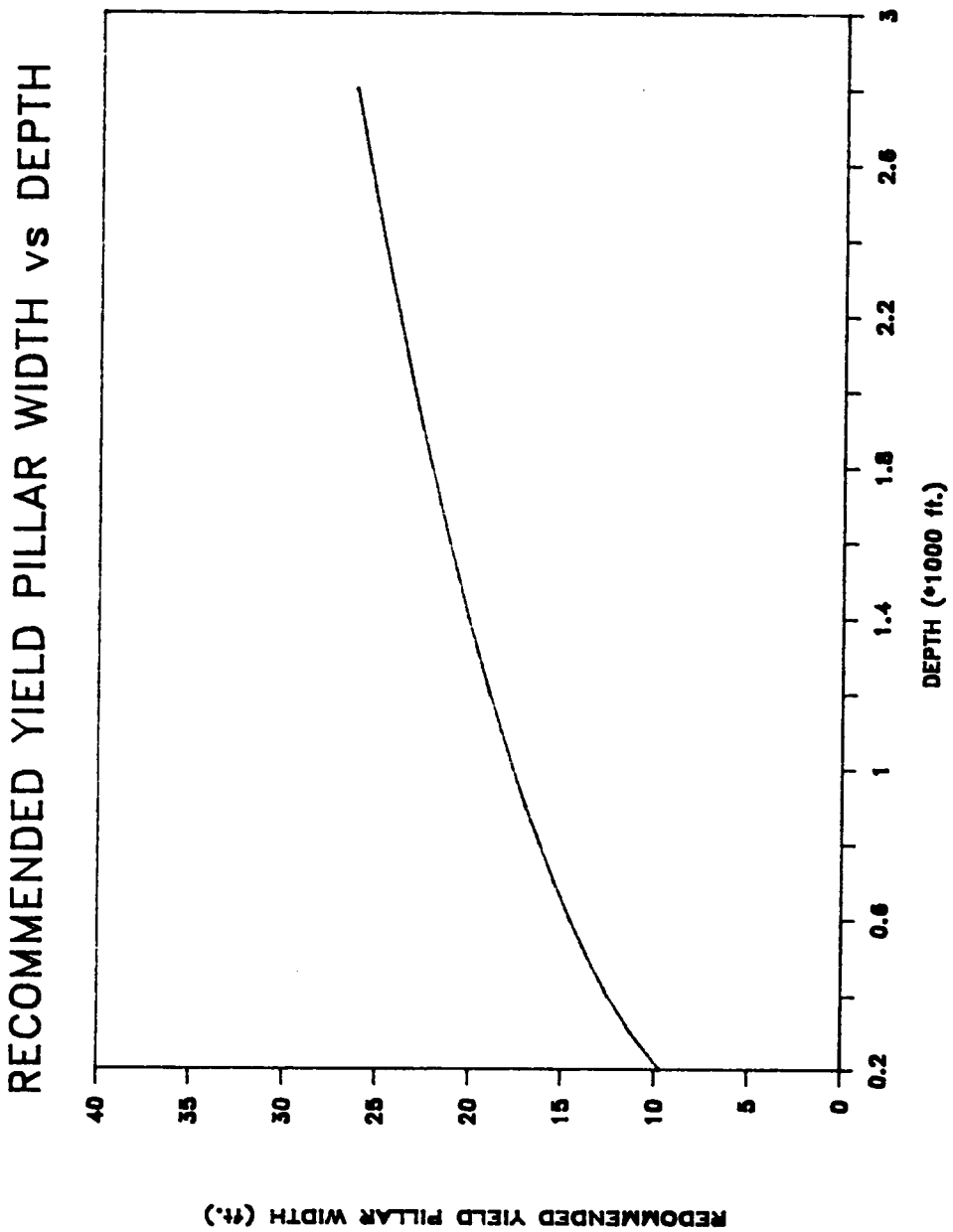


Figure 6.7 Recommended Yield Pillar Width vs. Depth

Practice and theoretical analysis have demonstrated that yield pillars allow a general lowering of the roof and transfer of load onto abutment pillars. This phenomenon can be explained by the pressure arch theory. As a pillar yields, the roof is lowered and a pressure arch is formed above the yield pillar, transferring overburden load to the abutment pillars on either side. As recommended by observations in other coal fields (Holland, 1963), the height of the pressure arch is about twice the opening width. In the case studied here, since the pillar yields, the total opening width $W_T$ will be that of the pillar width plus the opening width on either side of the pillar, that is:

$$W_T = W + 2W_o \tag{6.16}$$

The height of the pressure arch D, therefore, is given by:

$$D = 2W_T = 2\,(W + 2W_o) \tag{6.17}$$

Since the overburden load above the pressure arch is transferred to the abutment pillars, the minimum function of a yield pillar can be assumed only to support the roof strata below the pressure arch. If the pressure arch is considered to have a parabolic shape, the weight of the rock under the arch is:

$$Q = \frac{2}{3}\gamma D W_T\,(L + W_o) \tag{6.18}$$

where:

Q = weight of the rock under the pressure arch (lbs.);

$\gamma$ = average density of the rock (lbs./cubic in.);

D = height of the pressure arch (in.);

$W_T$ = total opening width (in.);

L = pillar length (in.); and

$W_o$ = opening width (in.) .

By equating Q to the loading capacity of yield pillars, the minimum yield pillar width may be obtained. In the case of common rectangularly-shaped pillars (Equation 6.10), the minimum yield pillar width may be determined by the following equation:

$$Q = q\, f(q)\, f(\mu)\, [273 \frac{W^4}{H^2} + 5.68 \frac{W^5}{H^3} + (L - W)\,(545 \frac{W^3}{H^2} + 14.2 \frac{W^4}{H^3})] \qquad (6.19)$$

Again, solving this equation for W is complex, but through a few simple iterations using a personal computer, the minimum yield pillar width can be easily obtained. It may be noticed that neither side of Equation 6.19 involves the depth h. This is because the height of the pressure arch was considered to be twice the total opening width at any depth. The minimum yield pillar width is, therefore, not a function of the mining depth. As long as the pillar is yielded, the minimum pillar width is a fixed value at all depths.

The three yield pillar widths derived above, i.e. the maximum, the recommended, and the minimum, are plotted in Figure 6.8 against mining depth for easy comparison. In the graph, the triaxial factor was taken to be 4.0, Poisson's ratio 0.3, the pillar height 6 feet, and the opening width 20 feet.

As mentioned above, the three equations calculating pillar width can be easily solved by personal computers. For quick reference, three nomograms were also constructed for different values of Poisson's ratios, the triaxial factors, the depths and the pillar heights, which are presented in Figures 6.9 through 6.11. In the nomograms, an average value of 160 lb/ft$^3$ was taken for the overburden density. The opening width was assumed to be 20 feet and the pillar length was taken to be 80 feet, resulting in a combined length of 100 feet which is very common in underground coal mines. Tests using the nomograms indicated that the pillar length was not a very sensitive factor. Within the range of 80$\pm$20% feet, the nomograms provided a reasonable accuracy. As an example

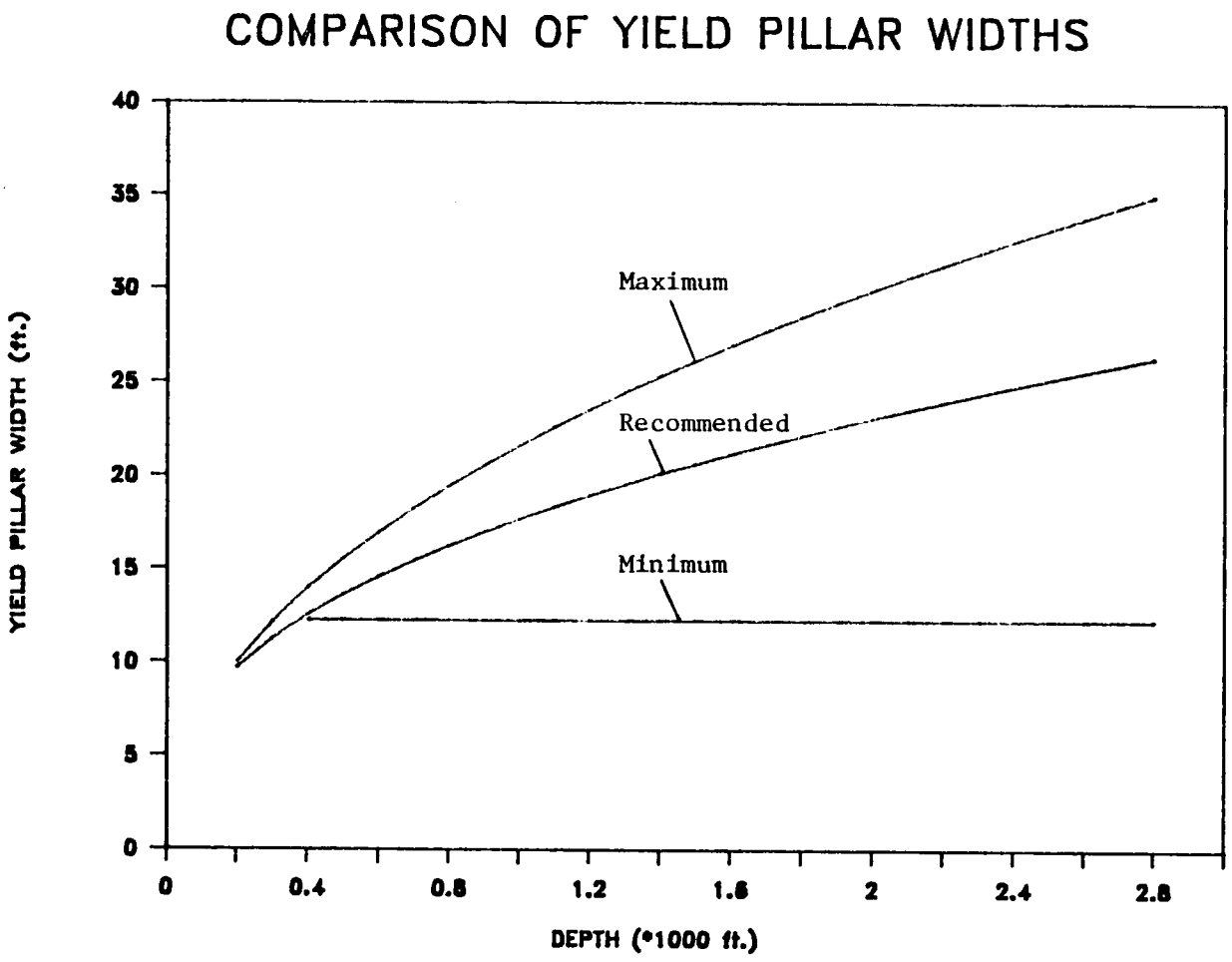


Figure 6.8 Comparison of Yield Pillar Width

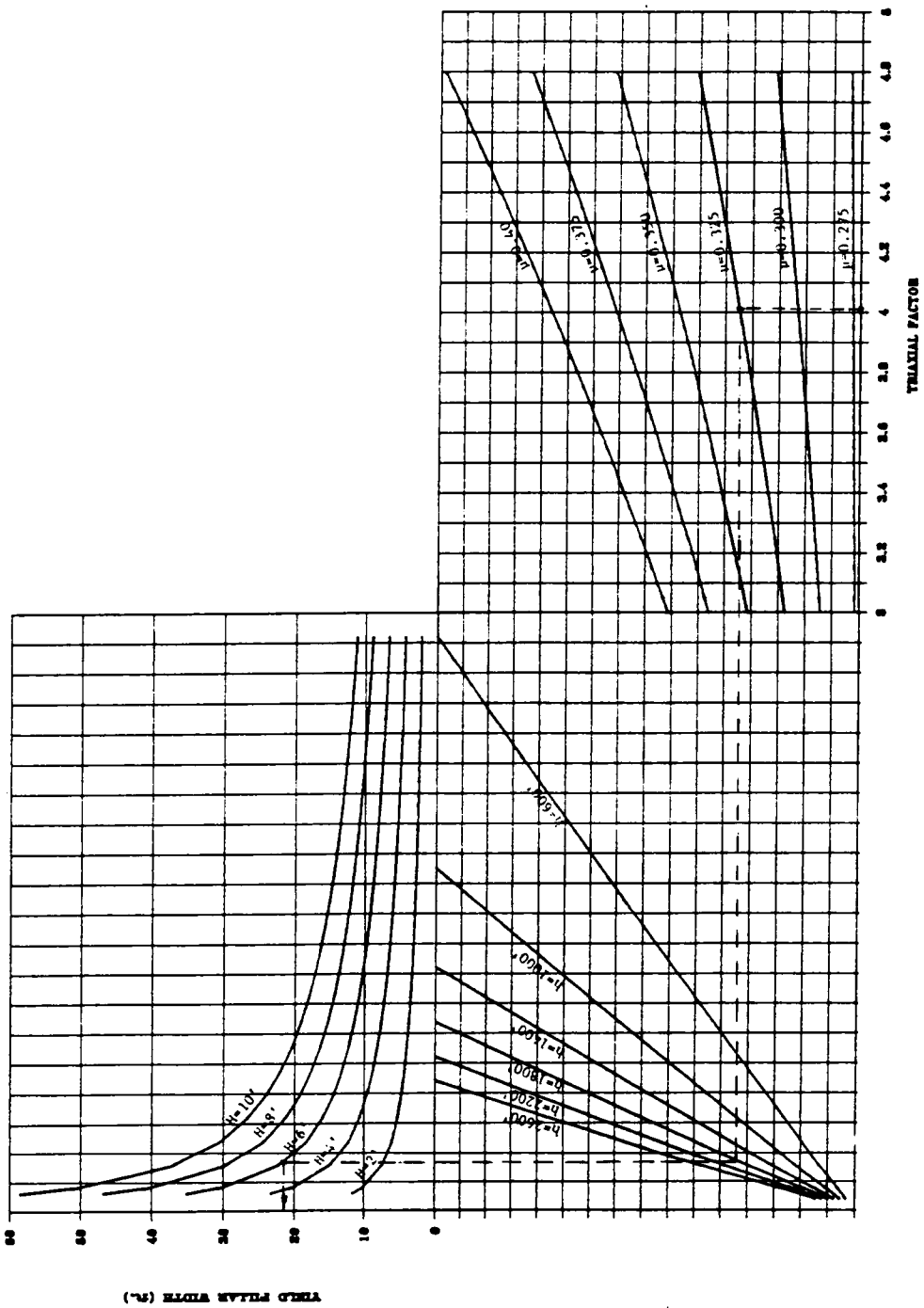


**Figure 6.9** Nomogram for Maximum Yield Pillar Width

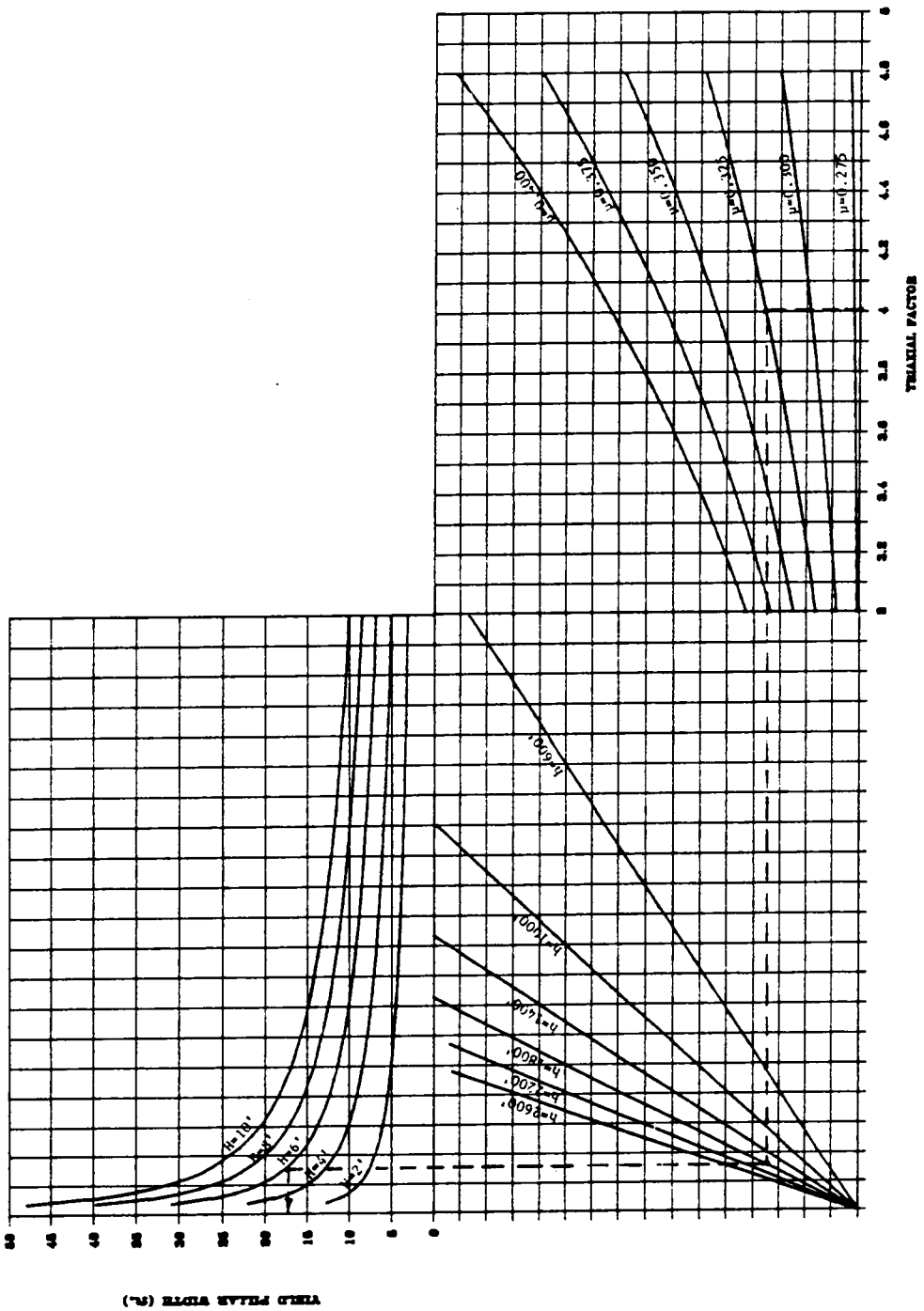


**Figure 6.10 Nomogram for Recommended Yield Pillar Width**

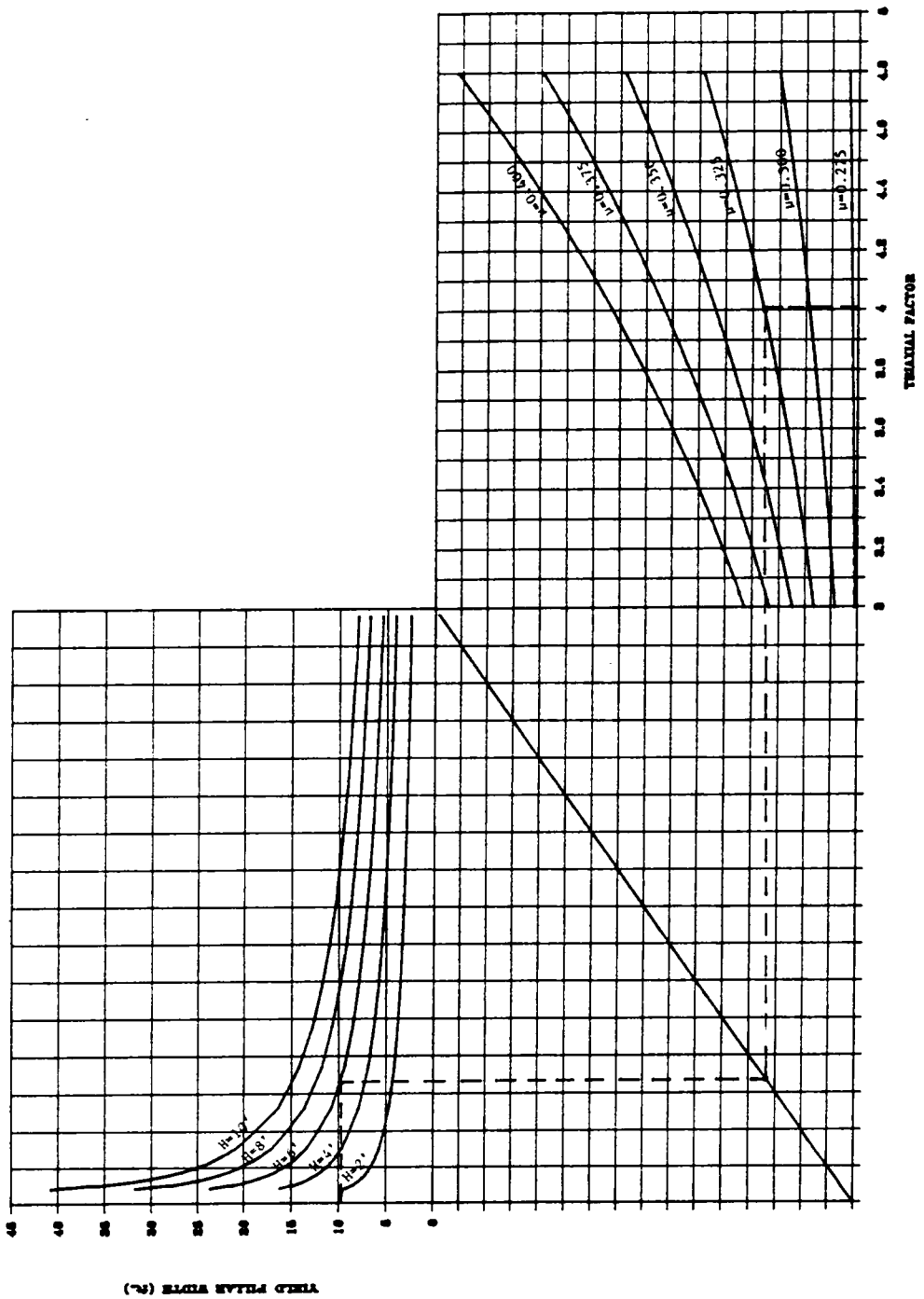


**Figure 6.11 Nomogram for Minimum Yield Pillar Width**

of use of the nomograms, let a triaxial factor of 4.0, a Poisson's ratio 0.325, a depth of 1,800 feet, and a pillar height 6 feet be assumed. Start with the triaxial factor on the nomograms and follow the dotted line. The line intersects the appropriate value of Poisson's ratio, followed by the mining depth and the height of pillar, and finally reaches the required pillar width. For the input parameters given above, the maximum, the recommended, and the minimum yield pillar widths are 21 feet, 17 feet, and 10 feet respectively.

## 6.5 Case Studies

In order to exemplify the equations developed above, two case studies of longwall operations are presented here. In both cases the yield-stable-yield pillar system has been used.

**Case No. 1**: The mine was located in southwestern Virginia and the following input parameters were used to determine appropriate yield pillar sizes:

depth = 1,600 feet
mining height = 6 feet
triaxial factor = 3.71
Poisson's ratio = 0.33
opening width = 20 feet
pillar length = 100 feet

Using Figures 6.9, 6.10, and 6.11, the maximum, the recommended, and the minimum yield pillar sizes were found to be 21 feet, 17 feet, and 10 feet, respectively. The actual

size used in the longwall operation was 20 feet. The stress distribution on those pillars was monitored during a detailed in-situ measurement study at the mine. The results showed that the stress at the center of the pillar increased to a peak of about 6,100 to 6,600 psi, and stayed reasonably constant at that level. This indicated that the pillar was not completely yielding. If the width had been reduced by a few feet, the high stress at the center of the pillar would have been avoided, therefore, the recommended pillar width of 17 feet was shown to be a better choice.

**Case No. 2:** The No.4 Mine of Jim Walter Resources, Inc. located in Alabama adopted yield-stable-yield pillar system in the longwall entries in order to increase the production and to improve ground control conditions (Gauna, et al., 1985 and Gauna, et al., 1986). The yield pillar sizes were determined based upon the following parameters:

depth = 2,000 feet
mining height = 6 feet
triaxial factor = 3.00
Poisson's ratio = 0.33
opening width = 20 feet
pillar length = 100 feet

By using the nomograms, the maximum, the recommended, and the minimum yield pillar sizes were found to be 27 feet, 21 feet, and 12 feet respectively. Two different sizes of yield pillars were tested in the mine, one 25 feet and one 20 feet in width. The 25-foot pillar was found not to yield completely when it was formed, but started to yield when the longwall face came near. The 20-foot pillar yielded immediately after excavation and the mine decided that 20 feet was a more appropriate size for the yield pillars, which was very close to the pillar width recommended here.

## 6.6 Summary and Discussion

A critical review of the progressive failure theory was conducted in this chapter, and it was found that the force equilibrium equation used in the derivation applied only under extreme conditions. The actual conditions might differ. A new equation, describing the stress distribution in the yield zone, was derived by statistically analyzing the results of a series of non-linear finite element simulations. The latter equation fitted the observed field data better than did the original equation, proposed in the progressive failure theory. As indicated above, any function satisfying Equation 6.4 could represent a possible stress distribution in the yield zone. The equation derived in this chapter seemed to be a better one than that proposed in the progressive failure theory. The actual stress distribution in the yield zone, however, might differ from that used in this study. Further studies in this area are certainly needed.

Three possible yield pillar sizes were proposed in this chapter, namely the maximum, the recommended, and the minimum yield pillar widths. The recommended yield pillar width is only a suggestion for reducing the peak stress in the center of the yield pillar. Other possibilities still exist. It should be pointed out that the three yield pillar sizes proposed in this chapter did not take the pillar rib spalling into consideration. In order to account for this effect, an additional factor may be needed, depending on local coal conditions.

# CHAPTER 7: CONCLUSIONS AND RECOMMENDATIONS

## 7.1 Conclusions

An investigation into the mechanism of yield pillars was conducted in this research and yield pillar design formulas were developed. Based on the research results, the following conclusions can be drawn:

1. The literature review conducted in this research reveals that most empirical pillar design formulas only deal with the ultimate strength of coal pillars. No yield zone is considered in those formulas, which makes them difficult to utilize in yield pillar design. On the other hand, the progressive failure theory provides some insight into the pillar yielding mechanism. The theory may be further developed to study the behavior of yield pillars, and may eventually be developed for yield pillar design.

2. Two finite element models were developed in this study, each using a different non-linear approach. The comparisons between the finite element models and the field data demonstrate that both models agree well with the observations of underground monitoring. Both models may be used to predict displacement and stress in coal pillars. The successive iteration non-linear model can be easily adapted from a linear finite element program while the elastic-plastic finite element model needs more computer programming. When adopting the load increment technique, the elastic-plastic model is more suitable for simulating underground excavations.

3. When utilizing the finite element models to study the pillar yielding phenomena, very dense finite element mesh is required. It is extremely costly and time-consuming to perform 3-D finite element modeling with such a dense mesh. The modified load augmentation technique adopted in this study appears to be an economical and efficient way of using 2-D models to simulate yield pillars without losing much of information derived from a 3-D model. Although the accuracy of the suggested technique needs to be further verified by comparison with a 3-D model, the general trend resulting from the 2-D model is very promising.

4. Three longwall entry layouts, namely a yield-stable-yield pillar layout, a stable-stable layout, and a yield-yield layout, were investigated using the elastic-plastic model developed in this research. Of these, the yield-stable-yield pillar layout appears to be the best design for longwall entries. It can release the high stress concentration and maintain the roof stability throughout the mining sequence. This result agrees with the experience obtained in the underground coal mine of the Jim Walter Resources, Inc., where the yield-stable-yield pillar layout was tested and found to be the most suitable design for the mine. The yield-yield layout has a similar stress-

release effect; however, it may encounter some roof instabilities at certain mining stages.

5. A comprehensive parameter analysis performed in this research indicates that, among the material properties, the triaxial factor and Poisson's ratio are the two parameters most influential with regard to pillar yielding. Serious consideration should be given to these factors in designing yield pillars.

6. The progressive failure theory describes pillar yielding phenomena to a certain extent. Critical review of the theory, however, reveals that it ignores the effects of some important factors, such as Poisson's ratio. In addition, in the progressive failure theory, the equation concerning the stress distribution in the yield zone illustrates only an extreme case. The real stress distribution pattern may differ. Further improvements may be needed.

7. On the basis of finite element modeling, a new equation describing the stress distribution in the yield zone was developed by statistically analyzing the modeling results. The new equation appears to fit the field data better than does the equation used in the progressive failure theory.

8. Three formulas for determining yield pillar widths, the maximum, the recommended, and the minimum yield pillar widths, were derived in this study and three nomograms were constructed for quick reference. Case studies conducted in this research demonstrated that the formulas provide reasonably accurate estimation of yield pillar widths.

## 7.2 Recommendations

The studies conducted here also indicates that more research may be needed in the following areas:

1. The computer models established in this study were validated with limited field observations. More extensive in-situ monitoring is certainly needed to further verify the accuracy of the models developed. An important factor in yield pillar design is the stress distribution in the yield zone. In the literature, however, very few case studies concerning the in-situ stress distribution in the yield zone could be found. The in-situ stress in the yield zone should be further investigated in order to have a better understanding of yield pillar behavior.

2. Physical modeling has been effectively performed in rock mechanics research. In the study of yield pillars, it can also serve as a supplemental method to numerical modeling and in-situ monitoring. It may save time and reduce cost, and it has the advantage of easy manipulation compared with in-situ monitoring. Some phenomena which are difficult to observe in the field may be simulated with a physical model, and the results may be used to improve mathematical modeling. Studies of yield pillar behavior using physical models are strongly recommended.

3. The modified load augmentation technique suggested in this study seems to be an economical and efficient way to extract 3-D information from a 2-D finite model. The accuracy of this technique, however, has not been fully tested. A comprehensive 3-D model simulation is needed in order to further verify the load augmentation technique recommended.

4. The factors of pillar rib spalling and fractures in the coal pillar have not been considered in the yield pillar design formulas derived in this study. More studies on these factors are needed. Also, further validation of the yield pillar design formulas through comparison of results with additional case studies is recommended.

# SELECTED BIBLIOGRAPHY


1. Abel, J. F. (1981), "Rock Mechanics Handouts," Introduction to Rock Mechanics, Colorado School of Mines, pp. 28-40.

2. Agapito, J. F. T. and M. P. Hardy (1982), "Induced Horizontal Stress Method of Pillar Design in Oil Shale," ***Proceedings***, 15th Oil Shale Symposium, Denver, Colorado, pp. 179-191.

3. Babcock, C. O. (1986), "Equations for the Analysis of Borehole Pressure Cell Data," ***Proceedings***, 27th U. S. Symposium on Rock Mechanics, pp. 233-240.

4. Barrientos, G. and J. Parker (1974), "Use of the Pressure Arch in Mine Design at White Pine," Transactions of SME, AIME, Vol. 255, pp. 75-82.

5. Barron, K. (1978), "An Air Injection Technique for Investigating the Integrity of Pillars and Ribs in Coal Mines," Int. J. Rock Mech. Min. Sci. & Geomech. Abstr. Vol. 15, pp. 69-76.

6. Benzley, S. E. and R. D Krieg (1982), "A Continuum Finite Element Approach for Rock Failure and Rubble Formation," International Journal for Numerical and Analytical Methods in Geomechanics, Vol. 6, pp. 277-286.

7. Bieniawski, Z. T. (1976), "Rock Mass Classifications in Rock Engineering," ***Proceedings***, Symposium on Exploration for Rock Engineering, pp. 97-106.

8. Bieniawski, Z. T. (1981), "Improved Design of Coal Pillars for U. S. Mining Conditions," ***Proceedings***, 1st Annual Conference on Ground Control in Coal, pp. 13-22.

9. Bieniawski, Z. T. (1987), "Strata Control in Mineral Engineering," John Wiley & Sons, New York, pp. 59-90.

10. Bizier, D. et al. (1986), "Elastomeric Borehole Pressure Cells for Measurement of Stress States and Their Time-Dependent Changes in Salt," ***Proceedings***, 27th U. S. Symposium on Rock Mechanics, pp. 241-247.

11. Carr, F. et al. (1984), "How to Eliminate Roof and Floor Failures with Yield Pillars - Part I," Coal Mining, December, pp. 62-70.

12. Carr, F. et al. (1985), "How to Eliminate Roof and Floor Failures with Yield Pillars - Part II," Coal Mining, January, pp. 44-51.

13. Carr, F. and A. H. Wilson (1982), "A New Approach to the Design of Multi-Entry Developments of Retreat Longwall Mining," 2nd Conference on Ground Control in Mining, West Virginia Univ., pp. 1-21.

14. Chappell, B. A. (1987), "Structural Response and Rock Bolting of a Rock Mass," Mining Science and Technology, Vol. 4, pp. 177-191.

15. Chen, G. et al. (1987), "Yield Pillar Design for Ground Stability," ***Proceedings***, 5th Annual Workshop, Generic Mineral Technology Center, edited by E. Topuz and J. R. Lucas, Univ. of Alabama, pp. 55-66.

16. Chen, G. and M. Karmis (1988), "Computer Modeling of Yield Pillar Behavior Using Post-Failure Criteria," ***Proceedings***, 7th International Conference on Ground Control in Mining, edited by S. S. Peng, West Virginia Univ., pp. 116-125.

17. Coates, D. F. (1981), "Rock Mechanics Principles," Canmet Monograph 874, Canada, pp. 4.1-4.42.

18. Costa, A. M. D. and C. Fairhurst (1985), "Comparison of Numerical Modeling with Predictions from Laboratory Tests and Field Observations of Deformation in a Potash Mine in Sergipe, Brazil," ***Proceedings***, 26th U. S. Symposium on Rock Mechanics, pp. 239-249.

19. Cyrul, T. (1986), "Complex Behaviour of a Coal Sample in a Large Scale In Situ Compression Test," Int. J. Min. & Geol. Eng., Vol. 4, pp.257-271.

20. DeMarco, M. J. et al. (1988), "Characterization of Chain Pillar Stability in a Deep Western Coal Mine - Case Study," Presentation at the SME Annual Meeting, Phoenix, Arizona, 12pp.

21. Drescher, A. and Y. Zhang (1986), "An Approximate Analysis of the Bearing Capacity of Prismatic Rock Pillars," Int. J. Rock Mech. Min. Sci. & Geomech Abstr. Vol. 23, No. 5, pp. 355-362.

22. Drucker, D. C. and W. J. Prager (1952), "Soil Mechanics and Plastic Analysis or Limit Design," Quarterly of Applied Mathematics, Vol. 10, No. 2, pp. 18-23.

23. Elliott, G. M. and E. T. Brown (1986), "Further Development of a Plasticity Approach to Yield in Porous Rock," Int. J. Rock Mech. Min. Sci. & Geomech. Abstr. Vol. 23, No. 2, pp. 151-156.

24. Erer, K. D. and A. Heidarieh-Zadeh (1985), "A Review of In Situ Stress Measurement Techniques with Reference to Coal Measure Rocks," Mining Sci. & Tec. 2, pp. 191-206.

25. Essex, R. J. (1988), "A Non-Linear Confined Core Pillar Design Method," Presentation at the SME Annual Meeting, Phoenix, Arizona, 7pp.

26. Farmer, I. (1985), "Coal Mine Structures," Chapman and Hall, London, pp. 39-76.

27. Gale, W. J. and R. L. Blackwood (1987), "Stress Distributions and Rock Failure Around Coal Mine Roadways," Int. J. Rock Mech. Min. Sci. & Geomech. Abstr. Vol. 24, No. 3, pp. 165-173.

28. Gates, R. H. (1968), "Inelastic Analysis of Slopes by the Finite Element Method," ***Ph. D. Thesis***, Univ. of Ill., Urbana, Ill., 120 pp.

29. Gates, R. H. (1972), "Progressive Failure Model for Clay Shale," ***Proceedings***, Symposium of Applications of the Finite Element Method in Geotechnical Eng., Vicksburg, Mississippi, pp. 327-347.

30. Gauna, M. et al. (1985), "Yield Pillar Usage in Longwall Mining at Depth, No. 4 Mine, Brookwood, Alabama," ***Proceedings***, 26th U. S. Symposium on Rock Mechanics, pp. 695-702.

31. Gauna, M. et al. (1986), "Total Yield Pillar Longwall Development - Experimental Results, No. 4 Mine, Brookwood, Alabama," ***Proceedings***, 27th U. S. Symposium on Rock Mech., Univ. of Alabama, Tuscaloosa, AL., pp. 398-404.

32. Guo, L. B. and S. S. Peng (1984), "Boundary Element Method of Analyzing the Interaction between Roof Strata and Roof Bolts," Mining Science and Technology, Vol. 1, pp. 189-207.

33. Hanna, K. and D. P. Conover (1988), "Design of Coal Mine Entry Intersections," Presentation at the SME Annual Meeting, Phoenix, Arizona, 11pp.

34. Hanna, K. et al. (1985), "Field Investigations of Roof and Pillar Stability in Coal Mine Intersections," ***Proceedings***, 2nd Conference on Ground Control Problem in the Ill. Coal Basin, Southern Ill. Univ., Carbondale, Ill., pp. 76-83.

35. Hanna, K. et al. (1986), "Structural Stability of Coal Mine Entry Intersections - Case Studies," ***Proceedings***, 27th U. S. Symposium on Rock Mechanics.

36. Haramy, K. Y. and M. J. DeMarco (1983), "Use of the Borehole Shear Tester in Pillar Design," ***Proceedings***, 24th U. S. Symposium on Rock Mechanics, pp. 639-644.

37. Haramy, K. Y. and M. J. DeMarco (1985), "Use of the Schmidt Hammer for Rock and Coal Testing," ***Proceedings***, 26th U. S. Symposium on Rock Mechanics, pp. 549-555.

38. Heasley, K. and L. W. Saperstein (1985), "Computer Modeling of the Surface Effects of Subsidence Control Methods," ***Proceedings***, 26th U. S. Symposium on Rock Mechanics, pp. 189-196.

39. Hobbs, D. W. (1970), "The Behaviour of Broken Rock under Triaxial Compression," J. Rock Mech. Min. Sci. Vol. 7, pp. 125-148.

40. Holland, C. T. (1963), "Pressure Arch Techniques," Mechanization, March, pp. 45-48.

41. Holland, C. T. (1964), "The Strength of Coal in Mine Pillars," ***Proceedings***, 6th Symposium on Rock Mechanics, Univ. of Missouri, Rolla, Missouri, pp. 450-456.

42. Hsiung, S. M. and S. S. Peng (1985), "Chain Pillar Design for U. S. Longwall Panels," Mining Sci. & Tech., Vol. 2, pp. 279-305.

43. Hsiung, S. M. and S. S. Peng (1987), "Control of Floor Heave with Proper Mine Design - Three Case Studies," Mining Science and Technology, Vol. 4, pp. 257-272.

44. Karmis, M. et al. (1985), "The Development of Ground Subsidence Above Underground Coal Mines in the Appalachian Coalfield and Its Prediction Using Empirical Techniques," ***Proceedings***, 2nd Conference on Ground Control Problems in the Ill. Coal Basin, Southern Ill. Univ., Carbondale, Ill., pp. 127-137.

45. Karmis, M. and A. Jarosz (1985), "Subsidence Control in the Appalachian Coalfields," ***Proceedings***, 3rd Annual Workshop, Generic Mineral Technology Center, Mine Systems Design and Ground Control, Lexington, Kentucky.

46. Kicker, D. C. and D. W. Park (1986), "Yield Pillar Simulation Using Physical Modeling," ***Proceedings***, 27th U. S. Sym. on Rock Mech., pp. 224-231.

47. Kidybinski, A. and C. O. Babcock (1973), "Stress Distribution and Rock Fracture Zones in the Roof of Longwall Face in a Coal Mine," Rock Mechanics 5, pp. 1-19.

48. Kripakov, N. P. and M. T. Melvin (1983), "A Computer Procedure to Simulate Progressive Rock Failure Around Coal Mine Entries," ***Proceedings***, 1st Conf. on the Use of Computers in the Coal Industry, Y. J. Wang and R. L. Sanford, Editors, West Virginia Univ., Morgantown, WV, pp. 487-502.

49. Kripakov, N. P. (1981), "Finite Element Analysis of Yield-Pillar Stability," Computers & Structures, Vol. 13, pp. 575-593.

50. Logie, C. V. and G. M. Matheson (1982), "A Critical Review of the Current State-of-the-Art Design of Mine Pillars," ***Proceedings***, 1st International Conference on Stability in Underground Mining, Vancouver, Canada, pp. 359-382.

51. Lu, P. H. (1986), "A New Method of Rock Stress Measurement with Hydraulic Borehole Pressure Cells," ***Proceedings*** of the International Symposium on Rock Stress and Rock Stress Measurements, Stockholm, pp. 237-345.

52. Lu, P. H. (1986), "Triaxial Loading Measurement for Mine Pillar Stability Evaluation," ***Proceedings***, 27th U. S. Symposium on Rock Mechanics, pp. 379-385.

53. Maleki, H. N. et al. (1986), "Gate Road Layout Design for Two-Seam Longwall Mining," Int. J. Min. & Geol. Eng., Vol. 4, pp. 111-127.

54. Mark, C. and Z. T. Bieniawski (1986), "An Empirical Method for the Design of Chain Pillars for Longwall Mining," ***Proceedings***, 27th U. S. Sym. on Rock Mech., pp. 415-422.

55. Martin, E. and F. Carr (1984), "Control of Floor Heave in Coal Mines," 2nd International Conference on Stability in Underground Mining, Lexington, Kentucky.

56. Martin, E. et al. (1985), "Yield Pillar Application - Impact on Strata Control and Coal Production," ***Proceedings***, 4th Conference on Ground Control in Mining, West Virginia Univ., pp. 1-20.

57. Mayer, A. D. et al. (1984), "Validation and Error Analysis of a Strata Modelling Technique," International Journal of Mining Engineering, Vol. 2, pp. 305-321.

58. Mayer, A. D. and Isaac (1984), "Stochastic Methods for the Prediction of Strata Behavior," International Journal of Mining Engineering, Vol. 2, pp. 291-304.

59. Newman, D. A. (1985), "The Design of Coal Mine Roof Support and Yielding Pillars for Longwall Mining in the Appalachian Coalfield," ***Ph. D. Thesis***, Pennsylvania State Univ., pp. 135-165.

60. Newman, D. A. (1986), "Evaluation of Yielding in Longwall Chain Pillars - a Case Study," SME nonmeeting paper, 5pp.

61. Newman, D. A. (1988), "Automated Data Acquisition System for Remote Monitoring of Pillar and Roof Deformation on a Longwall Panel," Presentation at the SME Annual Meeting, Phoenix, Arizona, 6pp.

62. Obert, L. and W. I. Duvall (1967), "Rock Mechanics and the Design of Structures in rocks," Wiley, New York, pp. 236-545.

63. Okubo, S. and Y. Nishimatsu (1986), "Computer Modelling of Stochastic Rock Failure During Uniaxial Loading," Int. J. Rock Mech. Min. Sci. & Geomech. Abstr. Vol. 23, No. 5, pp. 363-370.

64. Pariseau, W. G. and I. M. Eitani (1981), "Comparisons Between Finite Element Calculations and Field Measurements of Room Closure and Pillar Stress during

Retreat Mining," Int. J. Rock Mech. Min. Sci. & Geomech. Abstr. Vol. 18, pp. 305-319.

65. Pariseau, W. G. and W. K. Sorensen (1979), "3-D Mine Pillar Design Information from 2-D FEM Analysis," Int. J. for Num. and Anal. Methods in Geomech., Vol. 3, pp. 145-157.

66. Park, D. W. and N. F. Ash (1985), "Stability Analysis of Entries in a Deep Coal Mine Using Finite Element Method," Mining Sci. & Tech., Vol. 3, pp. 11-20.

67. Peng, S. S. (1986), "Coal Mine Ground Control," 2nd edition, John Wiley & Sons, New York, pp. 237-264.

68. Peng, S. S. and H. S. Chiang (1984), "Longwall Mining," John Wiley & Sons, pp. 50-69.

69. Peng, S. S. et al. (1988), "Evaluation of Shield Support Performance by Numerical Analysis," Mining Science and Technology, Vol. 7, pp. 19-30.

70. Peng, S. S. and L. B. Guo (1988), "A Hybrid Boundary Element - Finite Element Method of Stress Analysis for Bolt - Reinforced Inhomogeneous Ground," Mining Science and Technology, Vol. 7, pp. 1-18.

71. Reyes, S. F. (1966), "Elastic-Plastic Analysis of Underground Openings by the Finite Element Method," ***Ph. D. Thesis***, Univ. of Ill. at Urbana, Ill, pp. 18-23.

72. Salamon, M. D. G. and A. H. Munro (1967), "A Study of the Strength of Coal Pillars," Journal of South African Inst. Min. Metall., Vol. 68, pp. 55-67.

73. Schaller, S. and G. M. Savidis (1986), "Chain Pillar and Gateroad Stability in Australian Longwalls Working under Relatively Massive Strata," Mining Science and Technology, Vol. 3, pp. 277-286.

74. Serata, S. (1982), "Stress Control Methods: Quantitative Approach to Stabilizing Mine Openings in Weak Ground," ***Proceedings***, 1st International Conference on Stability in Underground Mining, Vancouver, Canada, pp. 52-98.

75. Sheorey, P. R. (1984), "Use of Rock Classification to Estimate Roof Caving Span in Oblong Workings," Int. J. Min. Eng., Vol. 2., pp. 133-140.

76. Sheorey, P. R. et al. (1982), "A Numerical Procedure for Rock Pressure Problems in Level Seams," ***Proceedings***, Symposium on Strata Mechanism, Amsterdam, pp. 254-259.

77. Sheorey, P. R. et al. (1986), "Pillar Strength Approaches Based on a New Failure Criterion for Coal Seams," Int. J. Min. & Geol. Eng., Vol. 4, pp. 273-290.

78. Sheorey, P. R. et al. (1987), "Coal Pillar Strength Estimation from Failed and Stable Cases," Int. J. Rock Mech. Min. Sci. & Geomech. Abstr. Vol. 24, No. 6, pp. 347-355.

79. Singh, J. G. and P. C. Upadhyay (1986), "Bending of Thick Rock Slabs," Mining Science and Technology, Vol. 3, pp. 255-265.

80. Siriwardane, H. J. (1985), "Numerical Modelling of the Behavior of Overburden Rock Masses Associated with Longwall Mining," ***Proceedings***, 26th U. S. Symposium on Rock Mechanics, pp. 171-177.

81. Su, W. H. and S. S. Peng (1987), "Cutter Roof and Its Causes," Mining Science and Technology, Vol. 4, pp. 113-132.

82. Sugawara, K. and Y. Obara (1986), "Measurement of In Situ Rock Stress by Hemispherical-Ended Borehole Technique," Mining Science and Technology, Vol. 3, pp. 287-300.

83. Szwilski, T. B. (1982), "Sizing of Chain Pillars around Longwall Panels," ***Proceedings***, 1st International Conference on Stability in Underground Mining, pp. 535-558.

84. Tang, D. H. and S. S. Peng (1986), "Causes and Mechanisms of Surface Fractures in a Central West Virginia Coal Mine," Mining Science and Technology, Vol. 4, pp. 41-48.

85. Tang, D. H. and S. S. Peng (1988), "Structure Analysis of Mine Pillars Using Finite Element Method - a Case Study," Mining Engineering, September, pp. 893-897.

86. Unrug, K. and T. B. Szwilski (1982), "Method of Roof Caveability Prediction," ***Proceedings***, International Symposium on Ground Control in Longwall Mining and Mine Subsidence, AIME, Honolulu, pp. 13-29.

87. Wang, F. D. et al. (1974), "Proposed Technique for Improving Coal Mine Roof Stability by Pillar Softening," Transactions, SME, AIME, pp. 59-63.

88. Wang, S. T. (1985), "2-D and 3-D Finite Element Analyses of Room-Pillar Mining Systems with Flat and Rolling Coal Seams," ***Proceedings***, 26th U. S. Symposium on Rock Mechanics, pp. 231-237.

89. Whittaker, B. N. and R. N. Singh (1981), "Stability of Longwall Mining Gate Roadways in Relation to Rib Pillar Size," Int. J. Rock Mech. Min. Sci. & Geomech. Abstr. Vol. 18, pp. 331-334.

90. Whittaker, B. N. and R. N. Singh (1984), "Deformational Behaviour of Longwall Gate Roadways," Mining Science and Technology, Vol. 1, pp. 275-284.

91. Wilson, A. H. (1962), "The Measurement of Rock Stress," Colliery Guardian, January, pp. 1-9.

92. Wilson, A. H. (1977), "The Effect of Yield Zones on the Control of Ground," Sixth International Strata Control Conference, September, Banff Springs, Canada.

93. Wilson, A. H. (1980), "The Stability of Underground Workings in the Soft Rocks of the Coal Measures," Ph. D. Thesis, Univ. of Nottingham, U. K., 204 pp.

94. Wilson, A. H. (1981), "Stress and Stability in Coal Ribsides and Pillars," ***Proceedings***, 1st Conference on Ground Control in Mining, S. S. Peng, editor, West Virginia Univ., pp. 1-12.

95. Wilson, A. H. and D. P. Ashwin (1972), "Research Into the Determination of Pillar Size - Part I, An Hypothesis Concerning Pillar Stability," Mining Engineer, U. K., pp. 409-417.

# APPENDIX A: CALCULATION OF RESIDUAL STRESS CONDITIONS IN THE ELASTIC-PLASTIC MODEL

In the elastic-plastic model, when the stress condition satisfies the yield function, the material yields and the stresses drop down to a residual stress level. The calculation of the new residual stress condition is discussed in the following. As described in Section 3.3, the stress condition is changing along line L in the stress space as shown in Figure 3.7. Assuming that at stress level ($\sigma_{x1}$, $\sigma_{y1}$, $\sigma_{z1}$), the material starts to yield, the equation representing line L is expressed as:

$$\frac{\sigma_x - \sigma_{x1}}{\sigma_m - \sigma_{x1}} = \frac{\sigma_y - \sigma_{y1}}{\sigma_m - \sigma_{y1}} = \frac{\sigma_z - \sigma_{z1}}{\sigma_m - \sigma_{z1}} \qquad \text{(A.1)}$$

where:

$\sigma_m = (\sigma_{x1} + \sigma_{y1} + \sigma_{z1})/3$ ; and

$\sigma_x, \sigma_y, \sigma_z$ = stresses in the stress space.

The equation for the residual stress surface (the smaller cone-shaped yield surface in Figure 3.7) is:

$$\alpha I_1 + (J_2)^{1/2} = 0 \tag{A.2}$$

Explicitly, this equation may be expressed as (for plane strain problems):

$$\alpha(\sigma_x + \sigma_y + \sigma_z) + \{\frac{1}{6}[(\sigma_x - \sigma_y)^2 + (\sigma_y - \sigma_z)^2 + (\sigma_z - \sigma_x)^2] + \tau_{xy}\}^{1/2} = 0$$

where:

$\alpha$ = material constant.

Letting $\sigma_{mx} = \sigma_m - \sigma_{x1}$, $\sigma_{my} = \sigma_m - \sigma_{y1}$, and $\sigma_{mz} = \sigma_m - \sigma_{z1}$ Equation A.1 becomes:

$$\sigma_{my}(\sigma_x - \sigma_{x1}) = \sigma_{mx}(\sigma_y - \sigma_{y1}) \tag{A.3a}$$

$$\sigma_{mz}(\sigma_x - \sigma_{x1}) = \sigma_{mx}(\sigma_z - \sigma_{z1}) \tag{A.3b}$$

Rearranging the equations produces:

$$\sigma_y = \frac{\sigma_{my}}{\sigma_{mx}}(\sigma_x - \sigma_{x1}) + \sigma_{y1} \tag{A.4a}$$

$$\sigma_z = \frac{\sigma_{mz}}{\sigma_{mx}}(\sigma_x - \sigma_{x1}) + \sigma_{z1} \tag{A.4b}$$

Based on the mechanics of material, the shear stress is related to the normal stresses. The relationship may be expressed as:

$$\tau_{xy} = \frac{\tan 2\theta}{2}(\sigma_x - \sigma_y) \tag{A.5}$$

where:

$$\tan 2\theta = \frac{2\tau_{xyl}}{\sigma_{xl} - \sigma_{yl}} .$$

Considering Equation A.5, letting $R_{xy} = \frac{\sigma_{my}}{\sigma_{mx}}$, $R_{xz} = \frac{\sigma_{mz}}{\sigma_{mx}}$, and substituting Equation A.4 into Equation A.2 result in:

$$3\alpha\sigma_m + \{\frac{1}{6}[\sigma_x - R_{xy}(\sigma_x - \sigma_{xl}) - \sigma_{yl}]^2 + [R_{xy}(\sigma_x - \sigma_{xl}) + \sigma_{yl} - R_{xz}(\sigma_x - \sigma_{xl}) - \sigma_{zl}]^2 +$$

$$+ [\sigma_x - R_{xz}(\sigma_x - \sigma_{xl}) - \sigma_{zl}]^2 + \frac{\tan^2 2\theta}{2}[\sigma_x - R_{xy}(\sigma_x - \sigma_{xl}) - \sigma_{yl}]^2\}^{1/2} = 0 \quad (A.6)$$

Rearranging the equation produces:

$$54\alpha^2\sigma_m^2 = [(1 - R_{xy})\sigma_x + (R_{xy}\sigma_{xl} - \sigma_{yl})]^2 + [(R_{xy} - R_{xz})\sigma_x - (R_{xy}\sigma_{xl} -$$

$$- R_{xz}\sigma_{xl} - \sigma_{yl} + \sigma_{zl})]^2 + [(1 - R_{xz})\sigma_x + (R_{xz}\sigma_{xl} - \sigma_{zl})]^2 +$$

$$+ \frac{3}{2}\tan^2 2\theta[(1 - R_{xy})\sigma_x + (R_{xy}\sigma_{xl} - \sigma_{yl})]^2 \quad (A.7)$$

Letting:

$$\beta_1 = 54\alpha^2\sigma_m^2$$

$$\beta_2 = 1 + \frac{3}{2}\tan^2 2\theta$$

$$C_1 = 1 - R_{xy}$$

$$C_2 = 1 - R_{xz}$$

$$C_3 = R_{xy} - R_{xz}$$

$$C_4 = R_{xy}\sigma_{xl} - \sigma_{yl}$$

$$C_5 = R_{xz}\sigma_{xl} - \sigma_{zl}$$

results in:

$$\beta_2(C_1\sigma_x + C_4)^2 + [C_3\sigma_x - (C_4 - C_5)]^2 + (C_2\sigma_x + C_5)^2 - \beta_1 = 0 \quad (A.8)$$

Expanding the equation produces:

$$\beta_2 C_1^2 \sigma_x^2 + 2\beta_2 C_1 C_4 \sigma_x + \beta_2 C_4 + C_3^2 \sigma_x^2 - 2C_3(C_4 - C_5)\sigma_x + (C_4 - C_5)^2 +$$

$$+ C_2^2 \sigma_x^2 + 2C_2 C_5 \sigma_x + C_5^2 - \beta_1 = 0 \qquad \text{(A.9)}$$

Collecting like terms and letting:

$$A = \beta_2 C_1^2 + C_3^2 + C_2^2$$

$$B = 2\beta_2 C_1 C_4 - 2C_3(C_4 - C_5) + 2C_2 C_5$$

$$C = \beta_2 C_4 + (C_4 - C_5)^2 + C_5^2 - \beta_1$$

lead to:

$$A\sigma_x^2 + B\sigma_x + C = 0 \qquad \text{(A.10)}$$

This finally results in:

$$\sigma_x = \frac{-B \pm \sqrt{B^2 - 4AC}}{2A} \qquad \text{(A.11a)}$$

$$\sigma_y = R_{xy}(\sigma_x - \sigma_{x1}) + \sigma_{y1} \qquad \text{(A.11b)}$$

$$\sigma_z = R_{xz}(\sigma_x - \sigma_{x1}) + \sigma_{z1} \qquad \text{(A.11c)}$$

$$\tau_{xy} = \frac{\tan 2\theta}{2}(\sigma_x - \sigma_y) \qquad \text{(A.11d)}$$

These are the two sets of solutions for Equations A.1 and A.2. The one closer to the point ($\sigma_{x1}$, $\sigma_{y1}$, $\sigma_{z1}$) in the stress space was taken as the new stress condition.

# APPENDIX B: EQUATION DERIVATIONS IN CHAPTER 6

## B.1 Width of the Yield Zone

Equation 6.7 presents:

$$f(g)\, f(\mu)\, [6545(\frac{x}{H})^2 + 454(\frac{x}{H})^3] = \gamma h \qquad (B.1)$$

where:

q = triaxial factor;

$f(q) = q^{1.7}$ ;

$\mu$ = Poisson's ratio;

$f(\mu) = -0.028 + 0.057\mu + 0.17\mu^2$ ;

x = distance into the pillar (in.);

H = height of pillar (in.);

$\gamma$ = average overburden density (lbs/cubic inch); and

h = mining depth (in.).

The solution of x to Equation B.1 is the width of the yield zone (refer to Chapter 6). Rearranging Equation B.1 produces:

$$6545(\frac{x}{H})^2 + 454(\frac{x}{H})^3 - \frac{\gamma h}{f(q)\, f(\mu)} = 0 \qquad (B.2)$$

Letting a = 454, b = 6545, $c = -\frac{\gamma h}{f(q)\, f(\mu)}$, and $y - \frac{b}{3a} = \frac{x}{H}$ produces:

$$a(y - \frac{b}{3a})^3 + b(y - \frac{b}{3a})^2 + c = 0 \qquad (B.3)$$

Expanding the equation results in:

$$ay^3 - by^2 + \frac{b^2}{3a}y - \frac{b^3}{27a^2} + by^2 - \frac{2b^2}{3a}y + \frac{b^3}{9a^2} + c = 0 \qquad (B.4)$$

Collecting like terms produces:

$$ay^3 - \frac{b^2}{3a}y + \frac{2b^3}{27a^2} + c = 0 \qquad (B.5)$$

Dividing both sides by a produces:

$$y^3 - \frac{b^2}{3a^2}y + \frac{2b^3}{27a^3} + \frac{c}{a} = 0 \qquad (B.6)$$

Letting $p = -\frac{b^2}{3a^2}$, and $q = \frac{2b^3}{27a^3} + \frac{c}{a}$ produces:

$$y^3 + py + q = 0 \qquad (B.7)$$

There are three solutions to Equation B.7. For the case being studied in this research, the standard solution is:

$$y = 2\sqrt{-\frac{p}{3}}\ \cos[\frac{1}{3}\ \cos^{-1}(-\frac{q}{2\sqrt{-(\frac{p}{3})^3}})] \qquad (B.8)$$

Substituting variables into the equation produces:

$$\frac{x}{H} = 9.61 \times \cos[\frac{1}{3}\ \cos^{-1}(\frac{\gamma h \times 10^{-5}}{f(q)\, f(\mu)} - 1)] - 4.8 \qquad (B.9)$$

The width of the yield zone, $X_b$, can then be explicitly expressed as:

$$X_b = H\ \{9.61 \times \cos[\frac{1}{3}\cos^{-1}(\frac{\gamma h \times 10^{-5}}{f(q)\, f(\mu)} - 1)] - 4.8\} \qquad (B.10)$$

## B.2 Pillar Bearing Capacity

### 1. Derivation of Equation 6.9 - Square Yield Pillar:

The bearing capacity of one quarter of a square yield pillar is (refer to Figure B.1):

$$P_{1/4} = 2(\frac{W}{2}\int_0^{\frac{W}{2}} \sigma_v dx - \int_0^{\frac{W}{2}}\int_0^{x} \sigma_v dy dx) \qquad (B.11)$$

where:

$P_{1/4}$ = bearing capacity of one quarter of a square yield pillar (lbs);

W = pillar width (in.);

x = distance into the pillar (in.);

$\sigma_v$ = pillar vertical stress (psi); and

$\sigma_v = q\ f(q)\ f(\mu)\ f(\frac{x}{H})$ .

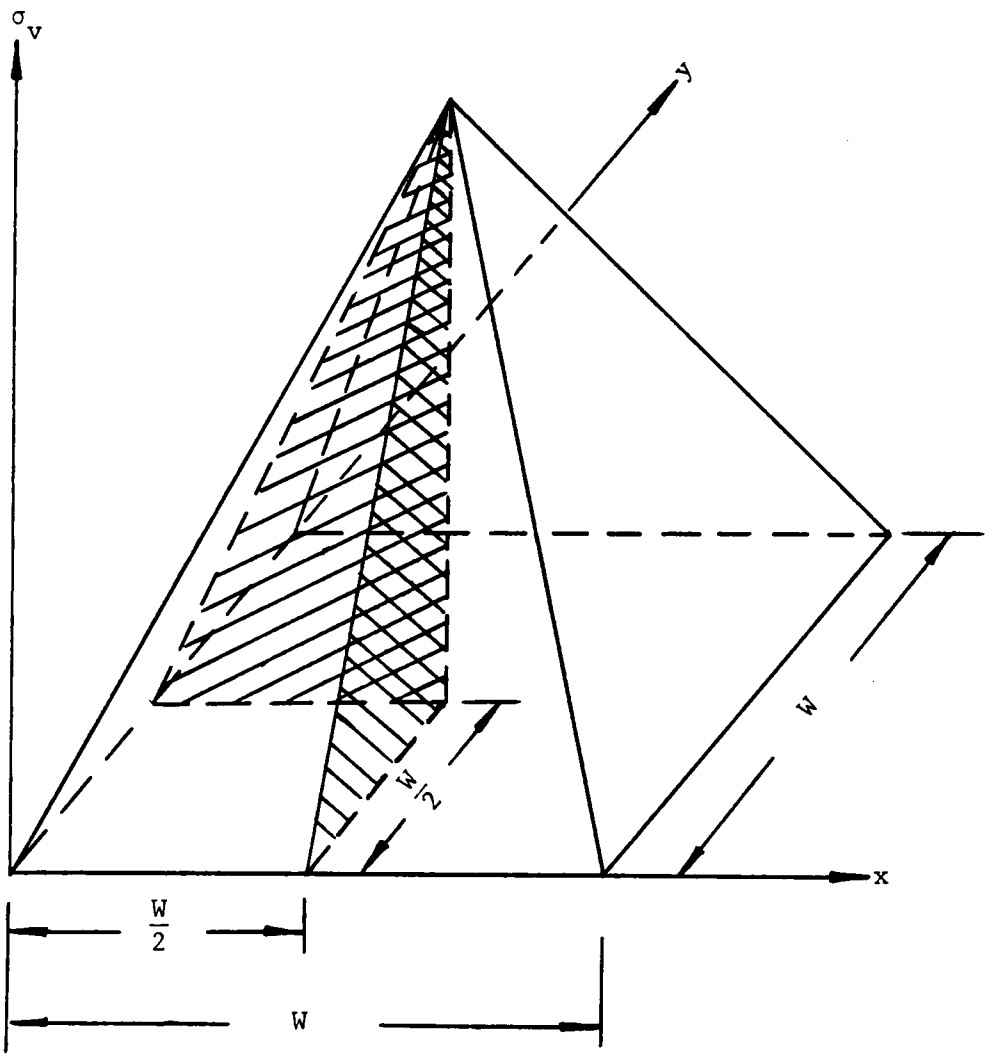


**Figure B.1 Load on a Square Yield Pillar**

Substituting the expression for $\sigma_v$ into Equation B.11 and taking the integration produce:

$$P_{1/4} = q\, f(q)\, f(\mu)\, (68.2 \frac{W^4}{H^2} + 1.42 \frac{W^5}{H^3}) \qquad (B.12)$$

The bearing capacity of a square yield pillar is:

$$P_{sy} = 4P_{1/4} = q\, f(q)\, f(\mu)\, (273 \frac{W^4}{H^2} + 5.68 \frac{W^5}{H^3}) \qquad (B.13)$$

**2. Derivation of Equation 6.10 - Rectangular Yield Pillar:**

As shown in Figure B.2, the bearing capacity of a rectangular yield pillar may be calculated by the following equation:

$$P_{ry} = 4P_{1/4} + 2(L - W)\int_0^{\frac{W}{2}} \sigma_v dx \qquad (B.14)$$

This leads to:

$$P_{ry} = q\, f(q)\, f(\mu)\, [273 \frac{W^4}{H^2} + 5.68(L - W)(545 \frac{W^3}{H^2} + 14.2 \frac{W^4}{H^3})] \qquad (B.15)$$

**3. Derivation of Equation 6.11 - Square Stable Pillar:**

The bearing capacity of a square stable pillar may be calculated by the following equation:

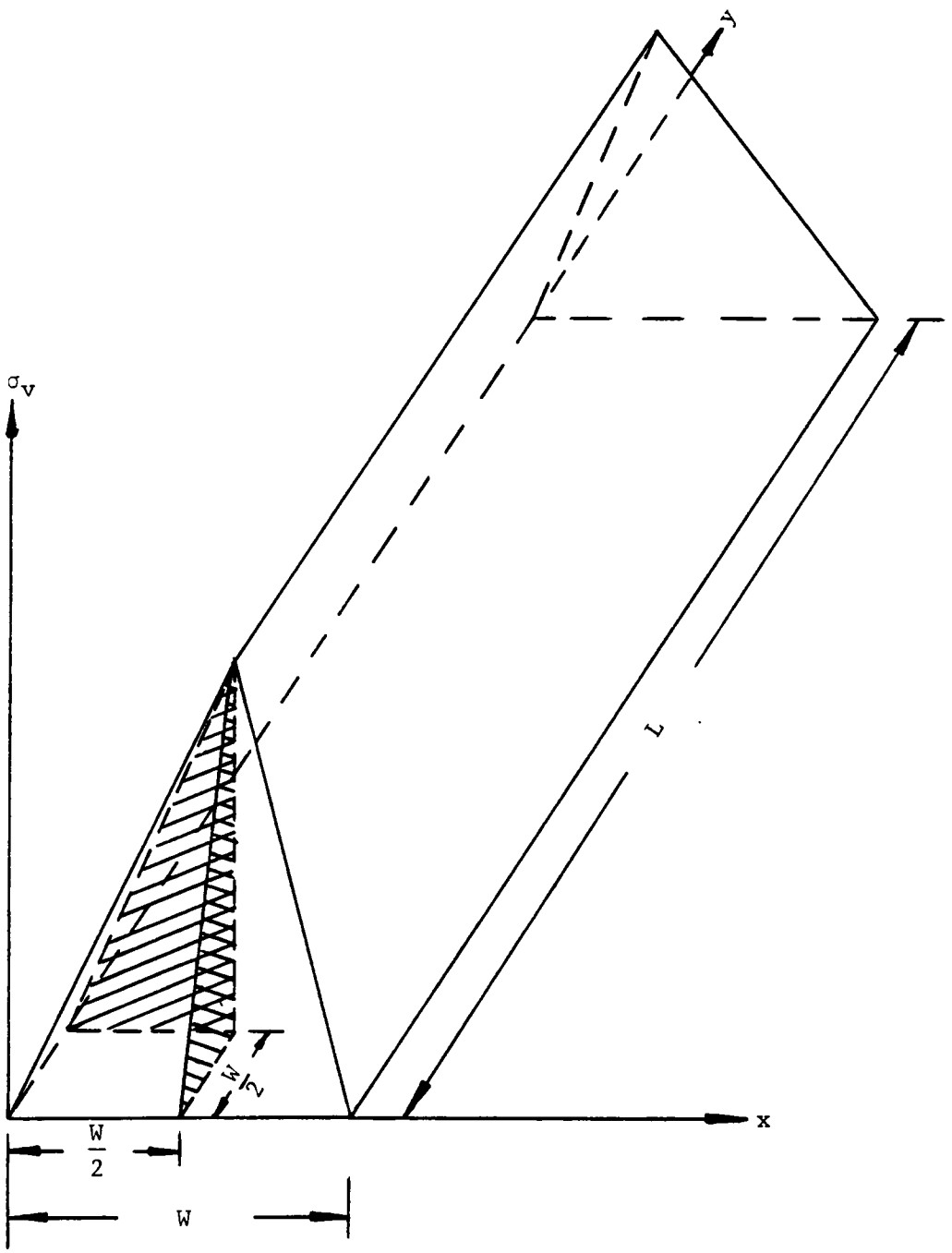


**Figure B.2 Load on a Rectangular Yield Pillar**

$$P_{ss} = 4P_{1/4} + 4(W - 2X_b)\int_0^{X_b} \sigma_v dx + (W - 2X_b)^2(\sigma_0 + q\gamma h) \qquad (B.16)$$

Note that the variable $\frac{W}{2}$ in calculating $P_{1/4}$ should be replaced by $X_b$ in this equation. The calculation finally leads to:

$$P_{ss} = q\, f(q)\, f(\mu)\, [273\frac{X_b^4}{H^2} + 5.68\frac{X_b^5}{H^3} + (W - 2X_b)\,(1090\frac{X_b^3}{H^2} +$$

$$+ 28.4\frac{X_b^4}{H^3})] + (W - 2X_b)^2(\sigma_0 + q\gamma h) \qquad (B.17)$$

**4. Derivation of Equation 6.12 - Rectangular Stable Pillar:**

The bearing capacity of a rectangular stable pillar is expressed as follows:

$$P_{rs} = 4P_{1/4} + 2(L + W - 4X_b)\int_0^{X_b} \sigma_v dx + (W - 2X_b)\,(L - 2X_b)\,(\sigma_0 + q\gamma h) \qquad (B.18)$$

Similarly, the variable $\frac{W}{2}$ in calculating $P_{1/4}$ should be replaced by $X_b$. The result of Equation B.18 is:

$$P_{rs} = q\, f(q)\, f(\mu)\, [273\frac{X_b^4}{H^2} + 5.68\frac{X_b^5}{H^3} + (L + W - 4X_b)\,(545\frac{X_b^3}{H^2} +$$

$$+ 14.2\frac{X_b^4}{H^3})] + (W - 2X_b)\,(L - 2X_b)\,(\sigma_0 + q\gamma h) \qquad (B.19)$$

where:

L = pillar length (in.); and

$\sigma_0$ = unconfined strength of coal (psi).

The vita has been removed from the scanned document